TAMPEREEN TEKNILLINEN YLIOPISTO
TAMPERE UNIVERSITY OF TECHNOLOGY

TAYGUN ERDEN

DESIGN AND IMPLEMENTATION OF ROTATIONAL DEGREES OF FREEDOM INTO MICROROBOTICS PLATFORM

Master of Science Thesis

Examiner: Professor Pasi Kallio
Examiner and topic approved by the Council of the Faculty of Engineering Sciences on 04.06.2014

ABSTRACT

TAMPERE UNIVERSITY OF TECHNOLOGY
Master's Degree Programme in Machine Automation
TAYGUN ERDEN: Design and Implementation of Rotational Degrees of Freedom into Microrobotics Platform
Master of Science Thesis, 74 pages, 14 Appendix pages
August 2014
Major: Mechatronics and Micromachines
Examiner: Professor Pasi Kallio
Keywords: Micromanipulation, Microrobotics, Individual Paper Fiber Bond, Rotational degrees of freedom

The strength of the individual paper fiber bonds (IPFB) is the key parameter which determines the mechanical quality of paper hand sheets. Currently, most of the strength measurements are still done on hand-sheet level because of the absence of high throughput IPFB strength measurement tools. Micro and Nanosystems research group of Tampere University of Technology recognized the demand for an IPFB characterization system and built a microrobotics platform. However, the current configuration of the platform is not able to rotate the microgripper which limits the measurements such as Z-directional bond breaking and shear mode bond breaking. Moreover, this configuration is not capable of dealing with twisted fibers. This thesis addresses these problems and introduces addition of two more degrees of rotation to the current platform. This modification of microrobotic platform will enable the bond strength measurement of IPFBs in desired pure modes which will enhance the paper fiber scientist`s understanding of IPFBs breaking process.

Bond strength measurement with the current platform provides data that is a combination of normal and shear forces which is not desired. After the modifications provided by this thesis, the microrobotic platform will be able to separate the shear force and the normal force during shear mode bond breaking.

In the Z-directional bond strength measurement, it is essential to know which fiber is on the top whereas the platform does not fulfill this requirement. The rotation of the microgripper and thus, the fibers will reveal the orientation of the IPFBs.

Moreover, the rotation of the microgripper enables the user to untwist the twisted fibers by rotating from one end while the other end is fixed with another microgripper.

Forward kinematics of the modified system is calculated through Matlab and compared with the real system. The errors between the ideal system and real system are reduced significantly by modifying the parameters in the overall transformation matrix which ensures that the modified microrobotic platform is now capable of solving all three problems discussed above. Maximum errors are decreased 90.65% (from 107 micrometers to 10 micrometers) at the X-axis, 82.47% (from 97 micrometers to 17 micrometers) at the Y-axis and 87.17% (from 195 micrometers to 25 micrometers) at the Z-axis.

PREFACE

This thesis work was carried out in the Micro and Nano System Research Group at Tampere University of Technology between January 2014 and June 2014.

I would like to express my deepest gratitude to my supervisor Prof. Pasi Kallio for his excellent guidance, suggestions and patience from the beginning to the completion of this thesis.

Pooya`s support, criticism, and suggestions during this work are greatly appreciated. I am indebted to Kourosh, Mathias and Juha who were always open for stimulating discussions and enlightening help. I am also grateful to my colleagues for the pleasant and friendly working environment.

Special thanks to Ali for his editorial contribution to this thesis.

Last but never least, a special thanks goes to my brother for his invaluable encouragement. A heartfelt thanks goes out to my girlfriend for all her love and endless support throughout my studies. I also wish to thank my parents who have always been there for me. This thesis is most warmly dedicated to them.

TABLE OF CONTENTS

Abstract i
Preface ii
List of symbols v
List of abbreviations vii
1. Introduction 1
    1.1 Powerbonds and Fibam Projects Overview 2
    1.2 Goal of the Study 3
    1.3 Thesis Outline 3
2. Application Background 4
    2.1 Wood Fiber Properties 4
    2.2 Previous Studies 7
        2.2.1 Indirect Measurements 7
        2.2.2 Direct Measurements 8
    2.3 Summary 15
3. Microrobotic Platform 16
    3.1 Platform Design 16
    3.2 Bond Making 22
    3.3 Bond Strength in Shear Mode 23
    3.4 Z-Directional Bond Strength Measurement 25
    3.5 Summary 26
4. Design Process 27
    4.1 Engineering Design Process 27
    4.2 Define the Problem 29
        4.2.1 Improving Shear Mode Bond Strength Measurement 29
        4.2.2 Facilitating the Z-Directional Bond Strength Measurement 30
        4.2.3 Untwisting the Twisted Fibers 31
        4.2.4 Theoretical Solution 31
        4.2.5 Technical Requirements 34
    4.3 Gather Information 35
        4.3.1 Spherical Actuators 36
        4.3.2 Rotary Positioners 39
        4.3.3 Pre-made Microrobot 40
        4.3.4 Conclusion 41
    4.4 Generate Multiple Solutions 41
        4.4.1 Attocube 42
        4.4.2 Micronix 44
        4.4.3 Smaract 45
    4.5 Analyze and Select a Solution 47
    4.6 Test and Implement Solution 48
    4.7 Summary 52

5. Demonstration of Completed System 53
5.1 Forward Kinematics 53
5.2 Comparison of Ideal system and Real system 59
5.2.1 Image Processing 59
5.2.2 Measurements 60
5.3 Discussion 65
6. Summary, Conclusions and Future Work 66
6.1 Summary 66
6.2 Conclusion 67
6.3 Future Work and Development Proposals 67
References 68
a.Appendix- COMPARISION WITH IDEAL VALUES 75
b.Appendix- COMPARISION WITH MODİFİED VALUES 82

LIST OF SYMBOLS

Fr	Force on X-axis
Fz	Force on Z-axis
Mr	Torque around X-axis
Mz	Torque around Z-axis
θ_1	Angle between x_{i-1} and x_i about z_{i-1} for roll link
θ_2	Angle between x_{i-1} and x_i about z_{i-1} for pitch link
α_1	Angle from z_{i-1} to z_i about x_i for roll link
α_2	Angle from z_{i-1} to z_i about x_i for pitch link
a_1	Distance from z_{i-1} to z_i along x_i for roll link
a_2	Distance from z_{i-1} to z_i along x_i for pitch link
d_1	Distance from origin (i-1) to x_i along z_{i-1} for roll link
d_2	Distance from origin (i-1) to x_i along z_{i-1} for pitch link
x	Distance from center point of pitch rotation to end mid-point of gripper jaw at X-axis
y	Distance from center point of pitch rotation to end mid-point of gripper jaw at Y-axis
z	Distance from center point of pitch rotation to end mid-point of gripper jaw at Z-axis
ϑ_1	Angle of rotation of the system around X-axis
ϑ_2	Angle of rotation of the system around Y-axis
ϑ_3	Angle of rotation of the system around Z-axis

${}^{Mz}R$	Matrix for rotation of the system around Z-axis for proper orientation in Matlab
${}^{My}R$	Matrix for rotation of the system around Y-axis for proper orientation in Matlab
${}^{x}R$	Matrix for rotation of the system around X-axis
${}^{y}R$	Matrix for rotation of the system around Y-axis
${}^{Z}R$	Matrix for rotation of the system around Z-axis
${}^{Base}T$	Base transformation matrix
${}^{Gripper}T$	Gripper transformation matrix
${}^{Overall}T$	Overall transformation matrix
${}^{Pitch}T$	Pitch rotation transformation matrix
${}^{Roll}T$	Roll rotation transformation matrix

LIST OF ABBREVIATIONS

DOF	Degrees Of Freedom
DH	Denavit-Hartenberg
EDP	Engineering Design Process
F1	Sample Storage Function
F2	Micromanipulation Function
F3	Force Sensing Function
F4	Visualization Function
F5	Dispensing Function
F6	Control Function
G	Microgripper
D	Dispenser Positioner
PP	Passive Probe
IF	Individual Fiber
IPF	Individual Paper Fiber
IPFB	Individual Paper Fiber Bonds
MCS	Modular Control System
MST	Micro System Technology
ML	Middle Lamella
MP1	Microrobotic Platform 1
MP2	Microrobotic Platform 2

P	Primary Wall
PF	Paper Fiber
PM	Permanent Magnet
PVDF	Ploy vinylidenefluoride
RBA	Relative Bond Area
TMP	Thermomechanical pulp
TUT	Tampere University of Technology

1. INTRODUCTION

Paper is a vital product that has sustained the advancement of technology and culture for centuries by providing the exchange of information [1]. Etymologically, the word “paper” comes from the Latin word “papyrus” which was a writing material in ancient Egypt [2] [3]. Paper can be described as a thin material which is produced by amalgamation of fibers, typically cellulose derived from plants, which are bounded to each other by hydrogen bonding [1] [3] [4]. Although wood pulp (hardwoods and softwoods such as birch and pine) serves as the main source of fibers; linen, hemp and cotton are also used. Moreover, apart from natural sources, synthetic fibers such as polyethylene or polypropylene are also used to procure special properties to paper [3]. The fibers in the wood cell walls are separated from each other by so called pulping (mechanically, chemically or by combination of two) in order to reach to cellulose. The dimensions of fibers can vary between values of 0.8-4.5mm in length and 16-70 μm in diameter subject to their type [5]. “Mechanical properties of individual fibre-fibre bonds provide significant insight into the key processes governing paper's mechanical behavior” [1].

Mainly, there are five significant properties of fiber network that are used to characterize the papers which are fiber length, fiber-fiber bond strength, bond area, fiber dimensions and fiber cross-section [3]. Especially the interfiber bond area (contact zone) and bond strength play a crucial role in terms of paper strength [1] [3] [6] [7] [8] [9]. Since 1844, several studies have been carried out in order to understand the relationship between these five properties and the strength of paper. Numerous models about microscale properties of pulp and paper have been proposed whereas none of them was able to answer all of the questions [10]. Every new study in the matter of paper strength reveals new facts and contributes to the development of paper quality as well as reducing costs in papermaking. Among the properties of paper given above, shear bond strength is the essential property that determines the paper strength. There are numerous ongoing studies to measure the shear strength but there is no widely accepted method that is proven to measure it with high accuracy. The shear strength measurements can be divided into two categories such as direct and indirect measurements. Indirect measurement methods are normally based on average parameters which reveal more about the fiber network than the relevant fiber properties whereas the direct measurement methods provide prediction of individual papermaking fiber properties [4] [6] [11].

Microrobotics technology has been developing for over the last decade in order to succeed in high positioning resolution, repeatability and accuracy for micro-scaled applications [12] [13]. Recent advancements in microrobotics made notable contributions “to the expansion of scientific and technological frontiers” [12] in several sectors and

microrobots are expected to “open up new fields of applications” [13] thanks to their high reliability. Nowadays, microrobotics is used in various applications such as medical instruments, medicine, material science and many others. Moreover, the achievements of microrobotics in terms of micro-manipulation, micro-injection, micro-assembly and micro-positioning are verified by many studies [14] [15] [16] [17] [18]. Although microrobotics is utilized by many applications, paper and pulp researchers still cannot benefit from it efficiently. The usage of microrobotics can provide extensive measurement data which will deliver further insight and reveal the substantial properties of paper.

Micro and Nanosystem Research Group of Tampere University of Technology has developed a microrobotics platform in order to achieve mechanical characterization of individual fibers with high throughput. The microrobotic platform is capable of carrying out individual fiber flexibility measurements as well as forming, manipulating, breaking and measuring individual paper fibers (IPFs) and individual paper fiber bonds (IPFBs). In addition, fiber samples can also be prepared for other laboratory equipments such as scanning electron microscopes. Furthermore it can also reveal the contact angles of supplied chemical on a fiber [43]. Currently, Micro and Nanosystem Research Group of TUT has two microrobotic platforms: one for teleoperated operations and another for automated operations.

1.1 Powerbonds and Fibam Projects Overview

This thesis is a part of projects “Powerbonds” and “Fibam” which are carried out in Tampere University of Technology. The main goal of project Powerbonds is to decide and utilize the right combination of technologies to realize the factors that have an effect on paper strength. It covers the measurement of individual paper fiber bond characteristics with also modeling and simulation on the purpose of revealing the paper strength properties and contributing to papermaking technology [19].

The outcomes of this project are intended to increase the competitiveness of pulp and paper industry in three ways. Firstly, developing the effectiveness of paper machines and rate of yield of raw material will notably decrease the production costs . Secondly, increasing the profit margin of fiber based products will facilitate fibers in terms of competing with other materials. Finally, lowering water and raw material depletion will reduce carbon and water footprint of pulp and paper industry [19].

The duration of the project is 1.1.2012-31.12.2014 with a volume of 2.1 million euros. There are five university partners, seven companies and three research organizations which are present in project`s consortium [19].

Fibam project intends to gain a better understanding of properties of wood derived fibers. This project utilizes microrobotics platform for accurate manipulation of microscopic fibers. Fibam project is more concerned with the platform itself whereas Powerbonds is more related with the measurement results. Fibam`s main goal is to install an “autonomous microrobotic system for manipulation, stimulation and characteri-

zation of Fibrous Materials" [20]. Automation plays a crucial role in this research since numerous samples must be examined to ensure the reliability of results.

1.2 Goal of the Study

The goal of this thesis is to implement an addition of two rotational degrees of freedom into the microrobotics platform which is used for various applications such as fiber flexibility measurement, IPFB breaking and characterization of individual fibers. This thesis is intended to develop the microrobotics platform that is built by the Micro and Nanosystems Research Group of the Department of Automation Science and Engineering by implementing a forward kinematics model of the real system. The versatile improvement method that will develop the microrobotics platform is aimed to facilitate in applications like shear bond strength measurement, Z-directional bond breaking and untwisting the twisted fibers.

The new configuration of the system will provide remarkable information concerning microscale paper structure. The outcome of this study will contribute in three paper fiber applications;

- IPFB shear bond strength measurement by allowing pure measurement.
- Z-directional IPFB bond measurement by revealing which fiber is on top.
- Untwisting the twisted IPF.

The tasks of this thesis can be categorised as deciding and designing a solution for fulfilling requirements, validating the selected modification through simulation, installing the new components, implementing new measurement experiments to validate if the requirements are fulfilled and finally comparing simulation results with the real system.

1.3 Thesis Outline

This thesis is divided into six chapters. Chapter 2 goes through previous studies and examines wood fiber properties to enhance the motivation of this thesis. Chapter 3 explains the previous configuration of the microrobotic platform. Chapter 4 first analyses the objectives to accomplish and then proposes a proper design according to end user requirements. Chapter 5 elucidates the experiment results and discusses their significance. Finally, Chapter 6 encompasses the conclusions and future work.

2. APPLICATION BACKGROUND

This chapter contains the application background of the topic. Section 2.1 elucidates the wood fiber properties. Section 2.2 includes the previous studies on direct and indirect fiber bond shear strength measurements and finally Section 2.3 encompasses the summary regarding this chapter.

2.1 Wood Fiber Properties

Wood is the major substance of the trunk of a tree which is a hard fibrous material [29]. Wood is a heterogeneous material and separate parts of tree stem include different fibers and exhibit different properties [30]. There are different layers in wood stem which are heartwood, sapwood, cambium and bark. Heartwood is the innermost layer which mostly consists of the dead cells. It can be identified easily thanks to its dark color. Heartwood has no functional usage in a tree apart from supporting. Sapwood comes after the heartwood which in contrast has a lighter color. It is not only used for supporting but also for storing nutrients and transporting water. Between sapwood and bark there is cambium which is a thin layer. The cambium layer produces new cells for both bark and sapwood. The amount of cell production varies among seasons. For instance, in the first part of growing season, earlywood and in the latter part, latewood is formed. The last layer, bark can be divided into 2 separate layers as the inner bark (phloem) and the outer bark. The outer bark consists of dead cells and this layer is used to protect the tree. It includes a high percentage of extractives. The phloem is thinner than the outer bark and it consists of living cells that are used to transport sap [34] [35]. The structure of wood with layers can be seen in Figure 2.1.

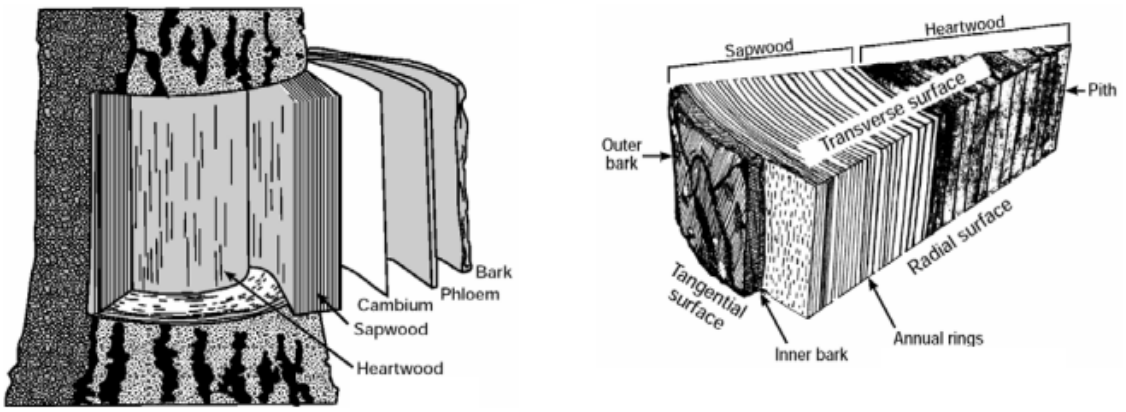

Figure 2.1 *The layers in wood stem [35]*

Wood cell or fiber is the basic element needed for production of paper. It is tubular shaped and contains cellulose as the major material. The properties of fibers have direct relationship with the mechanical properties of paper [36]. The fibers of the outer annual rings are longer than the ones situated in the center. Also younger woods contain shorter fibers which means reduced paper strength. As stated before, earlywood is formed in spring. Its fibers are both thinner and shorter than the latewood fibers. The difference between earlywood and latewood fibers can be observed by examining the cross section of wood stem. Basically the annual rings of trees are formed due to the difference of earlywood and latewood fibers [30] [35] [37] [38]. In Figure 2.2 there is cross section of spruce wood. The light fibers are earlywood fibers and darker area stands for latewood fibers which have fibers with thicker walls.

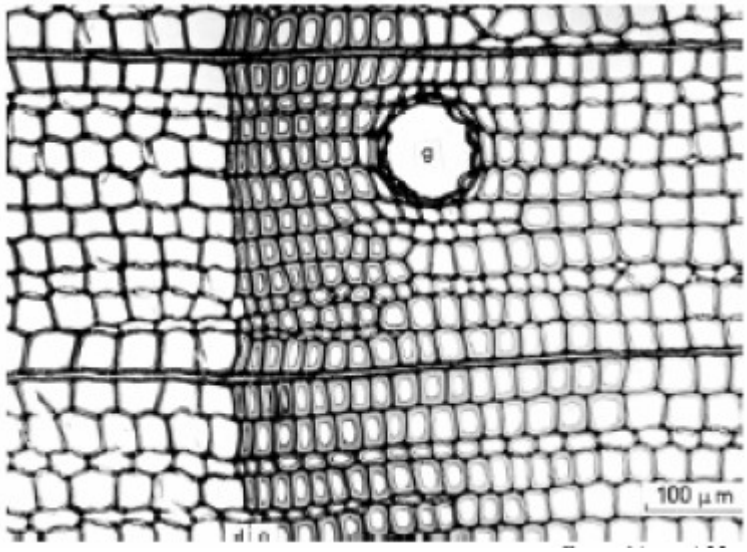

Figure 2.2 *Cross section of wood stem [39]*

Wood fibers can be divided into two groups such as softwood and hardwood fibers. Hardwood means the wood of angiosperms and the softwood means the wood of gymnosperms. These names can be misleading since there is no necessity of a wood to be hard for being hardwood. For instance, Ochroma is a hardwood whereas it is very soft [11]. Softwoods are comprised of tracheid and ray cells where ray cells are just 5-10% of the softwood fibers [40]. In terms of papermaking, long tracheid fibers are the most favorable materials since they provide better paper properties [35] [38]. Hardwoods on the other hand are more complex than softwoods. Fibers of hardwoods are shorter than softwood fibers. One important feature of hardwoods is, they contain vessel elements which are short in length and large in diameter that are used for sap transformation. Considering hardwoods, fibers in the longitudinal direction are significant since they enhance the optical properties. Moreover, the dimensions can change within the same species and same tree. Several factors such as genetics, age, growth rate and environment cause these variations [30] [35] [37] [39]. The average length and width of fibers among different material types are shown in Table 2.1.

Table 2.1 *Fiber dimensions [11]*

	Length (mm)	Diameter (μm)
Hardwood	0.8 - 1.6	16 - 25
Softwood	2 - 4.5	20 - 70

Figure 2.3 shows the structure of fiber. The cell wall is divided into 3 layers which are primary wall, secondary wall and middle lamella. Middle lamella holds two cells together thanks to its high proportion of amorphous material [40]. Secondary cell wall consists of 3 layers which are S1, S2 and S3. The whole secondary wall is comprised of microfibrils and the angles of microfibrils are different in different layers. Microfibrils are important since they are the elements that form the cell wall. They are composed of cellulose molecules. Just like fiber length, microfibrils angle also change with respect to not only different species but also between different layers [35] [37] [39] [41].

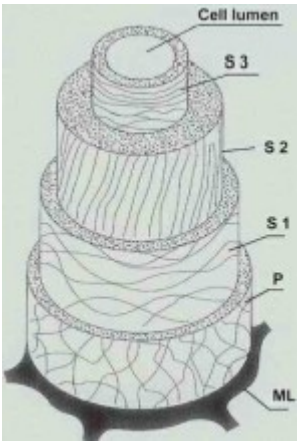

Figure 2.3 *The structure of fiber [42]*

Considering the chemical structure, the main constituents that built up wood are cellulose, hemicellulose, lignin and extractives. Although the chemical composition also changes for different species, still the average composition of hardwood includes more hemicellulose than softwoods whereas softwoods are richer in terms of lignin and extractives. Thus, each component affects the fiber properties and ultimately determines the paper properties [39] [40].

2.2 Previous Studies

The inside structure of the paper is impossible to reveal without understanding the bond strength whereas still there are not enough studies in this area. The main reason for this issue can be the difficulty and complexity of measuring bond strength. Moreover, the need for a vast number of experiments may also contribute. It is not surprising that much more studies have been carried out on the field of materials engineering and composites thanks to high rate of usage of polymer composites in sectors such as aerospace and automotive [3]. On the other hand, although the studies among paper are getting more extensive by benefiting from new technology, the number of published papers seems to be constant since 1960s. The number of published papers related to the shear strength measurement is given in the graph below.

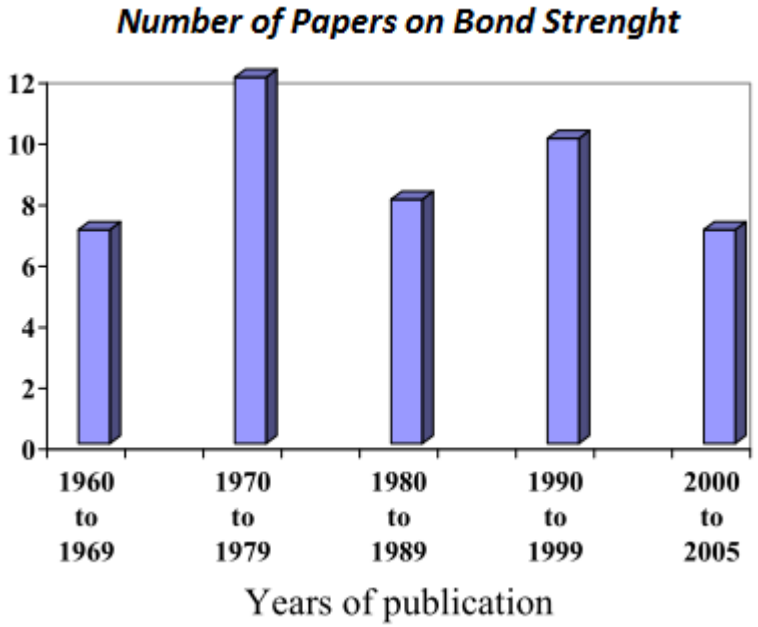

Figure 2.4 *Published papers since 1960 [3]*

Although it was believed that the properties of polymer structures may also apply to paper networks, later Page [21] claimed that the paper bond strength properties are different in many ways due to curls, crimps, kinks and microcompressions. Shear strength measurements can be divided into two categories such as direct and indirect measurements. The rest of this section will go through some of those measurement methods.

2.2.1 Indirect Measurements

The measurement of mechanical properties of fibers is called indirect measurement when the measurement is carried out on the whole sheet rather than individual fibers. Indirect measurements utilize the measured values of whole sheet in order to calculate IPFB strength [22]. Indirect measurement is favored since numerous fiber bonds are examined simultaneously and it provides average data at the end. Moreover, since the

whole sheet is measured, it is certain that the fibers are at the desired condition and orientation.

Indirect measurements also have some important drawbacks. For instance, they are based on straining the sheets and observing the scattering of light caused by fiber bond breakage whereas observed energy dissipation is also highly depended on the inter fiber breakage. Furthermore, properties such as sheet density, fiber interlocking, Z-directional entanglement as well as the mode of loading are not considered. Because of these reasons, indirect measurement is not suitable for comparing different types of pulps. There are also other problems about indirect measurements such as measured bond strength is two- three order of magnitude higher than, the theoretically calculated value [6].

2.2.2 Direct Measurements

In direct measurements, intently prepared IPFBs are measured. The specimens are prepared by bonding a fiber to a shive, to a cellophane strip or to another fiber. When bonding a fiber with another fiber is achieved, both ends of one fiber are fixed to a static frame and just one end of the other fiber is fixed to a frame that will move. The direction of loading is usually selected as the direction of fiber axis of the loaded fiber in order to obtain the maximum shear force [6]. The drawbacks of this method are, IPFBs are too fragile and it is not easy to manipulate without damaging. Moreover, some researchers argue that results are not clear for interpretation since the morphology of fibers and structure of bonds highly affect the results [22]. For instance, fibers can twist and cause different types of loading. The direct measurements also include the studies among the fracture surface of IPFBs. The investigations showed that stronger bond strength means the fracture is deeper [6]**.**

There are several studies where direct measurements are used and some of them are explained briefly in terms of bond making, bond breaking and measurement results. A novel method of making and breaking IPFBs is presented by Saketi and Kallio where microrobotics platform is used. Since this microrobotics platform is at the center of this thesis topic it will be explained in detail in Chapter 3.

Loading Modes

There are four loading modes that are mostly considered for IPFBs which are shear mode (sliding mode), Z-directional mode (opening mode), torsional mode (tearing mode) and peeling mode. These different modes of loading for fiber bonds are shown in Figure 2.5 [49].

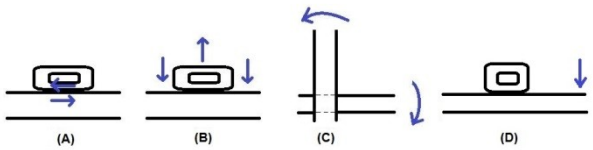

Figure 2.5 *Different modes of loading for fiber bonds. A; Shear mode, B; Z-directional mode, C; Torsional mode, D) Peeling mode [49]*

Bond Making

There are several different processes for making bonds which can be fiber-fiber or fiber-cellophane bonds.

McIntosh and Leopold [3, see 31] bonded individual paper fibers (IPF) on cellophane or shives placed radially in order to measure IPFB shear strength. The preparation of bonds included the following steps. Firstly, they placed a wet fiber shive onto the foil wrapped glass slide and dripped a water droplet to the shive. Then a wet pine fiber was placed with 90 degrees angle with great care. This part also foiled by wrapped glass slide. Then they were placed into the oven with 90°C and 300 grams on top for one night. In the morning, they glued one end of cellophane to paper tab and the other end was glued with the end of shives which contained the fiber bond. The structure of method is shown in Figure 2.6.

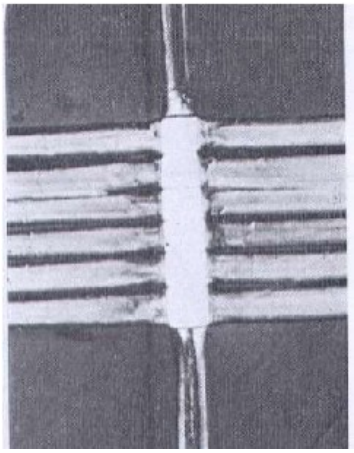

Figure 2.6 *McIntosh experiment structure [3, see 31]*

Thorpe, Mark, Eusufzai and Perkins [3, see 33] also used somewhat the same bond preparation method as McIntosh and Leopold did, apart from the temperature that the bonds were created. They preferred to apply 110-115°C or at 210°C with pressure of around 0.15857 MPa rather than 90°C. When the bond was formed, it was glued on testing assembly by Epon 907 which is an epoxy adhesive. The structure is shown in Figure 2.7.

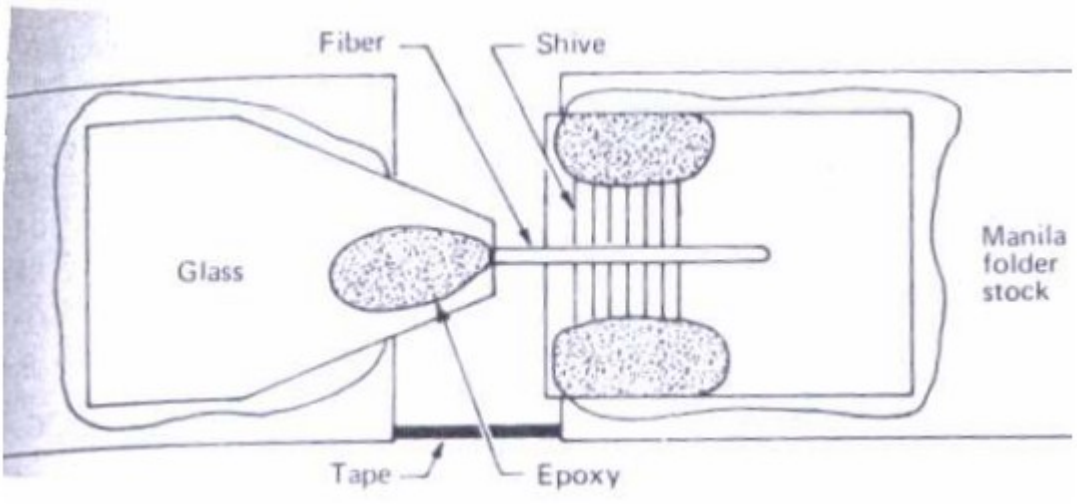

Figure 2.7 *The prepared bond [3, see 33]*

Button`s [3, see 28] sample preparation included chemical treatment at different phases. Ethyl alcohol, distilled water and carbon tetrachloride were selected for this purpose. In order to find the optimum bonding of fibers, several experiments were done and finally bonds were selected to be formed with the following procedure; first the cellophane films were prepared by guillotine-type cutter. Then each cellophane strip was cleaned by washing with various chemicals. After that ready strips were attached to 3 layers of membrane filters. The fibers were sandwiched between 20 layers of filter papers. Then the whole structure was placed between steel plates. The plates had parallel and horizontal holes along them which provided moisture equilibrium of lap joints assemblies. 0.6894 MPa pressure was applied for 24 hours. Once pressing, drying and separation was done the lap joints kept for 24 hours for equilibration before carrying out experiments.

These methods of bond making described above are mainly used to make bonds between fiber and cellophane or shive, thus they do not provide much information regarding the fiber networks which consist of fiber-fiber bonds. Fiber-fiber bonds are also prepared with different processes by different studies and two of them are explained below in order to have a brief idea.

Magnusson and Ostlund [27] dried some fibers in a steel press which had surface covered with Teflon in order to form fiber bonds. 2-10 fibers were placed in depolarized water droplet in order to prevent premature drying. Once drying process was complete, they recognized the fiber bonds on the plates by a stereo microscope.

Stratton and Colson [8] used a dyed and undyed fiber and placed them with the desired angles on top of each other on a Teflon-faced silicone rubber disc under water. Then another disc was positioned on top of the fibers. After that, this structure was placed in oven at 105°C under compressive load of 0.12 MPa for one hour. Then they took the fiber bond out of the oven.

Bond Breaking and Strength Measurement

As bond making methods differ between different research groups, bond breaking and measurement methods also vary.

Fischer, Hirn, Bauer and Schennach [22] introduced a method for measuring fiber bond strength and claimed that their novel technique allows them to examine two unstudied sides of IPFB measurement which are the geometry of deformed fiber and the biaxial loading of the fiber bond. Biaxial loading basically means they can apply force on both of the fibers of fiber bond. They also approached the fiber bond shear strength by distinguishing loading situations such as opening mode, shear mode and tear mode.

During the experiments once dried, unrefined, unbleached softwood kraft pulp, a mixture of spruce and pine wood are used. The setup equipment used for testing can apply preload which allows the determination of effect of biaxial load on fiber bond strength. The setup also included a filming camera that was integrated with a microscope in order to provide the geometry and deformation structure of fibers during failure. The investigation of geometry, deformation and resolution of forces enabled Fischer to make stronger predictions on fiber bond mechanical behaviors. The experiment procedure was divided into four steps. Firstly, IPFB was fixed on the sample holder by glue which was nail polish. Secondly, Fischer melted the bridges (see Figure 2.8) by soldering which fixes the upper and lower parts (part1 and part 2 in Figure 2.8) of sample holder. Melting of the bridges separated the upper and lower parts and left the fiber bond as the only connection between them. Thirdly, the upper and lower parts were forced to move on opposite directions in order to achieve preload of fiber. Lastly, the individual fiber bond was broken by moving the part 3. The whole process is depicted in Figure 2.8 [22].

The force was measured through two strain gauge based load cells with 0.5 mN resolution. The movements were performed by two linear tables where one of them used for preloading and the other one to break the IPFB.

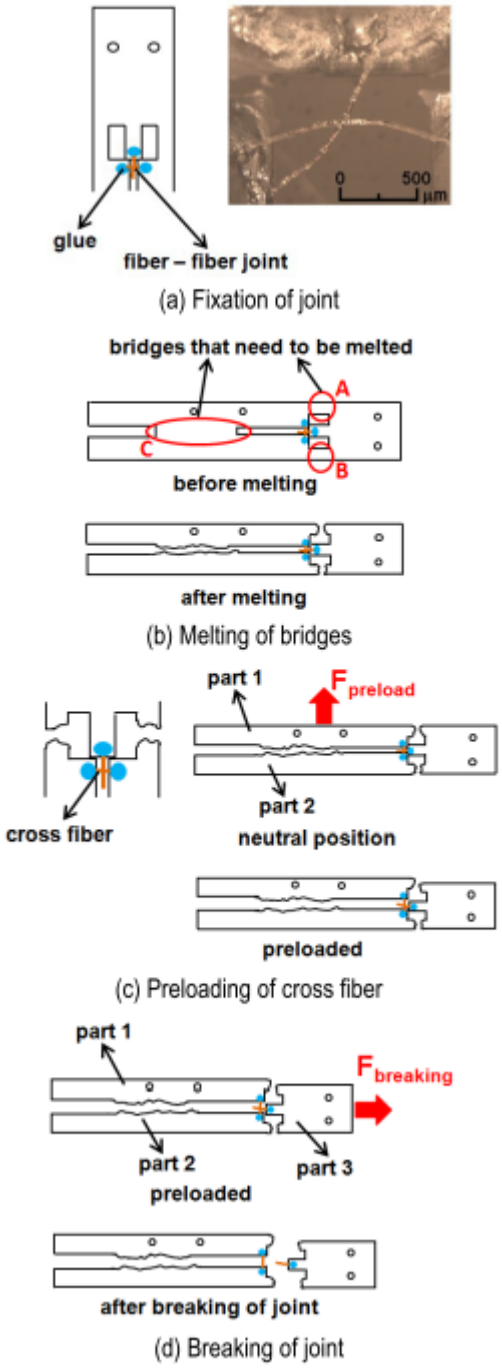

Figure 2.8 *Fischer`s experiment process [22]*

Button utilized the linear elastic model in order to make accurate predictions among shear strength of fiber bonds. In his PhD thesis, he mainly concentrated on fiber bonds and tried to apply linear elastic model to them. Although he used several materials such as holocellulose loblolly pine tracheid, cellophane and loblolly pine fibers, he preferred to work more on cellophane fiber bonds. He also conducted his experiments on both latewood and earlywood fibers [3, see 28]. The bonds were attached to metal pins and then “pins were pushed close together to give desired amount of overlap” [28]. The experiment was done with 0.35 g/sec of loading with fiber load/elongation recorder.

Magnusson and Ostlund`s [27] study included modified and non-modified kraft pulp fibers. They also concentrated on different states of loading such as shear and normal components at the moment when failure occured. They used their observations of different modes of failure to understand the mechanical behavior of fiber bonds when they are forced to break. Basically end of one fiber was attached to some fixture and load was applied on the other fiber which was bonded (desirably with an angle of 90 degrees) on the first one. They selected the fiber bonds and positioned them by using tweezers onto a steel specimen holder. The arrangement of measurement setup and specimen holder is shown in Figure 2.9 where red lines represent fibers and shapes at the ends of fibers stands for glue.

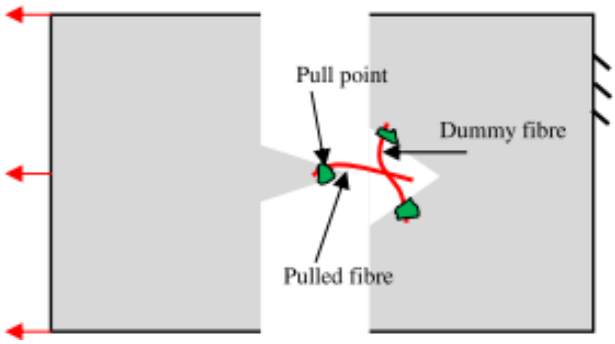

Figure 2.9 *Fiber bond attached to a specimen holder [27]*

The bond strength measurement was done by Instron ElectroPulse E1000 which is an electrodynamic tensile testing machine.

Unlike Magnusson and Ostlund, Stratton and Colson [8] used FLER2 which is a fiber load elongation recorder in order to measure the bond breaking load. They placed the fiber bond on a Mylar mount. The end points of the fiber were glued to the mount by Epon 907. After that the Mylar mount was attached to the FLER2. Load was applied and increased until the failure of the bond. These experiments were carried out in a controlled room with 23°C and 50% RH. The structure of the Mylar mount is shown in Figure 2.10.

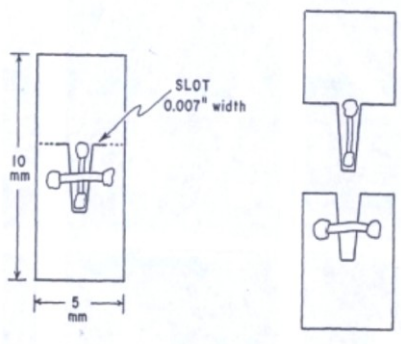

Figure 2.10 *The structure of the Mylar mount [3, see 8]*

Measurement Results

Although it was not discussed in detail, McIntosh and Leopold continued their work and conducted experiments on bond strength after preparing the bonds. They measured the bond strength of springwood fiber and shive bond as 2.7 MPa and bond strength of summerwood fiber and shive bond as 7.1 MPa [3, see 32].

Thorpe, Mark, Eusufzai and Perkins [3, see 33] thought that the straightness of the fiber does not have an important effect in terms of determining the mechanical properties of fiber. Thus, they focused more on the bonded area and tried to find an explanation or a theory that would fit with the experiment results. In their experiments, they measured the average shear bond strength of holocellulose bond as 4 MPa. Thermomechanical pulp (TMP) bond formed at 110°C as 2.86 MPa and TMP bond formed at 210°C as 8.16 MPa.

Button`s results are shown in Table 2.2. These results showed that the area of the bond has almost no effect on the load that is needed for breaking the bond due to the stress concentrations in the bond.

Table 2.2 *Experiment results [3, see 28]*

Type of fiber	Average breaking load(g)	Average Bond Area(sq. micrometers	Average Shear Bond strength (MPa)
Latewood	7.862	11048.4	13.908
Earlywood	5.494	6128.2	8.954

Fischer, Hirn, Bauer and Schennach [22] measured the shear strength of fiber bonds of unbleached softwood kraft pulp fibers and calculated the mean values of breaking forces as 6.54 mN for shear mode and 1.057 mN for tearing mode. According to these results, they concluded that the shear mode shear strength is 84% larger than the tearing mode shear strength and it significantly decreases the bond strength.

Stratton and Colson [8] measured the bond strength of fiber-fiber bonds as 2.1 MPa for earlywood and 6.4 MPa for latewood which are mean values for 40 to 50 tested bonds. Stratton and Colson concluded that the earlywood fibers are weaker than the latewood fibers. Since the fibers are attached only from end points, the bonded area could rotate freely which constraint them from measuring pure shear force. What they measured was a combination of peeling component and shear force.

Magnusson and Ostlund`s [27] measurement results were in the same range as in the literature considering direct fiber-fiber bond measurement experiments. The results that are given above are summarized in Table 2.3.

Table 2.3 *Summary of bond strength measurement results reported in literature [3] [8] [22] [28] [31] [33]*

Researchers	Type of fiber	(E) for Earlywood, and (L) for Latewood or other parameter	Bond strength value
McIntosh and Leopold	Loblolly Pine	E	2.7 MPa
		L	7.1 MPa
Thorpe, Mark, Eusufzai and Perkins	-	TMP (110°C)	2.86 MPa
		TMP (210°C)	8.16 MPa
Button	Loblolly Pine	E	8.9 MPa
		L	13.9 MPa
Fischer, Hirn, Bauer and Schennach	Softwood Kraft Pulp Fibers	Shear mode	6.54 mN
		Tear mode	1.057 mN
Stratton and Colson	Loblolly	E	2.1 MPa
		L	6.4 MPa
Magnusson and Ostlund	Kraft Pulp	Drying Pressure; 2.9 kPa	11.8 MPa

2.3 Summary

Previous studies related to application background have been explained briefly. Both indirect and direct measurements are covered and the main differences between them are clarified. Wood fibers are also investigated in broad sense and their structure and properties are discussed.

There are four loading modes that are mostly considered for IPFBs which are shear mode (sliding mode), Z-directional mode (opening mode), torsional mode (tearing mode) and peeling mode.

Indirect measurement of mechanical properties of fibers is carried out on the whole sheet rather than individual fibers whereas in direct measurements, intently prepared IPFBs are measured. There are several methods for measuring the shear strength of IPFBs. Most of the direct measurement methods fix the IPFB on sample holders by glue and wait for curing of the glue. Once the fixing of IPFB on sample holder is achieved, the bond is broken and a force sensor records the force required to break the bond.

3. MICROROBOTIC PLATFORM

This chapter explains and presents the microrobotic platforms developed at TUT. Section 3.1 introduces the microrobotic platform, while Section 3.2 describes the bond making procedure. Section 3.3 and Section 3.4 examine bond strength measurements as performed with the platform. Section 3.3 discusses the IPFB shear strength measurement and Section 3.4 elucidates the Z-directional bond strength measurement. Finally, Section 3.5 summarizes the chapter.

3.1 Platform Design

Currently there are two microrobotic platforms, Microrobotic platform 1 (MP1) is used for teleoperation and Microrobotic Platform 2 (MP2) is used for automated operations. In this chapter, just one microrobotic platform will be examined and discussed since the systems have too much in common. A photo of MP1 is shown in Figure 3.1.

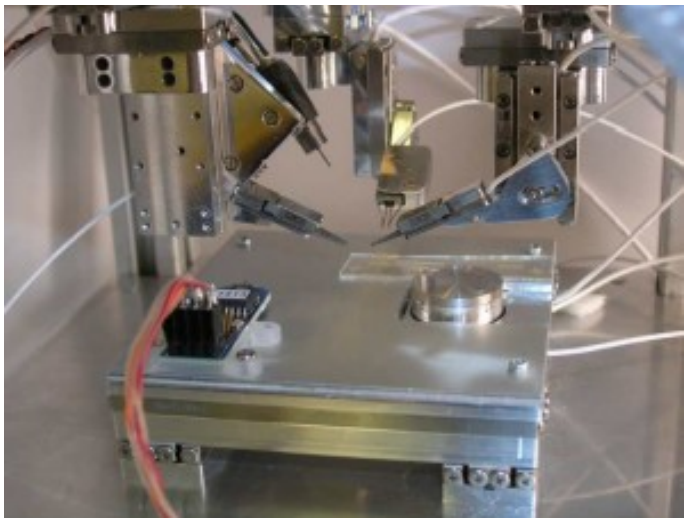

Figure 3.1 *Microrobotic platform [43]*

There are 6 main functions that the platform presents which are shown in Figure 3.2.

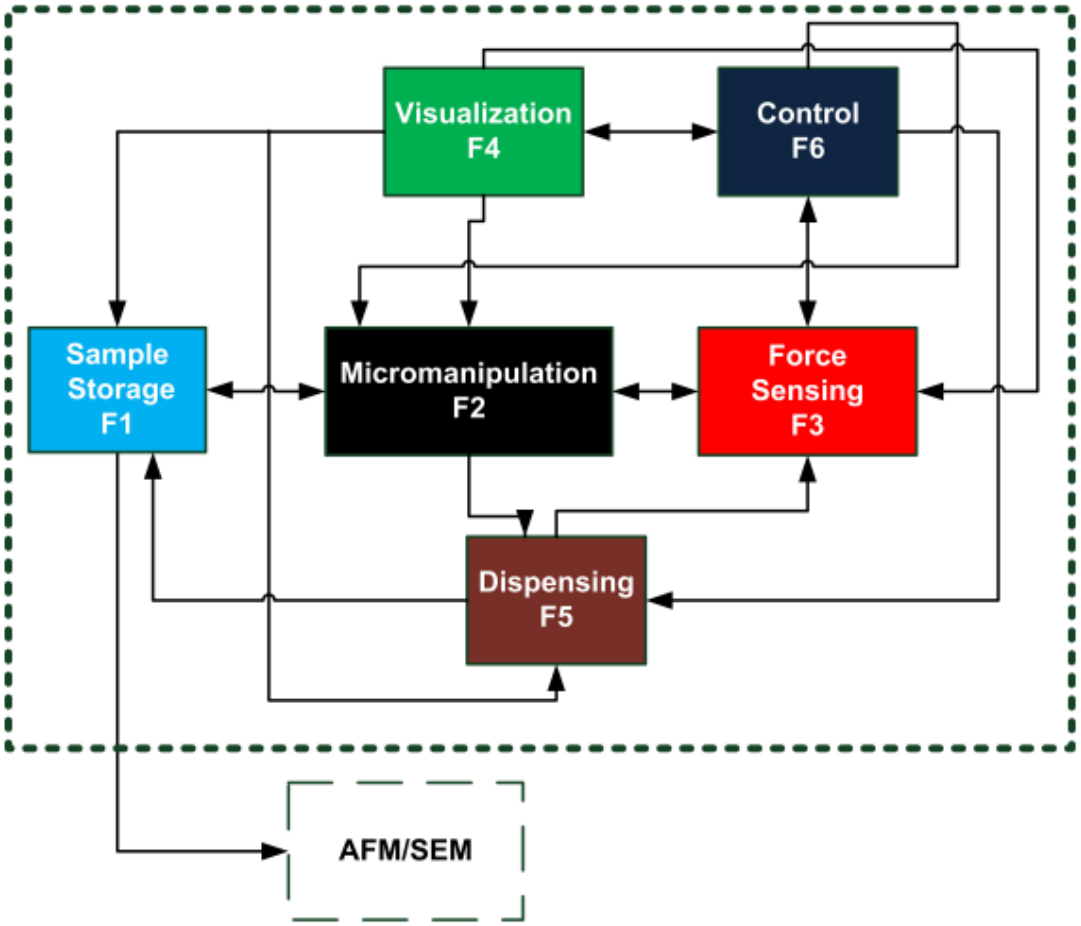

Figure 3.2 *Main functions [11]*

Figure 3.2 shows these six functions and their interaction with each other. Each function is also divided into sub-functions [44].

Sample storage (F1) has three sub-functions which are suspension storage, dry storage and frame fixture. The dry pulp is disintegrated and the fibers are allowed to float in water so that IPFs can be separated and manipulated. Then IPFs are dried and collected in fiber bank. The IPFs are stored in the fiber bank are also sorted according to their type, length and treatment and their coordinates are saved. The samples that the microrobotic platform prepares can also be used by atomic force microscope or scanning electron microscope as can be seen in Figure 3.2.

Micromanipulation (F2) also has three main functions which are micropositioning, micro-orienting and microgripping. Micropositioning sub-function locates the fiber bank, rotary table or force sensor in a position where microgrippers can work on them. Micro-orienting sub-function provides the desired orientation of IPFs, for instance it rotates the fibers on rotary table so that microgrippers can grab them. Microgripping

sub-function is used for picking and handling of fibers. Micromanipulation function is also in charge for moving a dispenser (Function F5) so that it can dispense and apply certain chemical treatments on fibers.

Force sensing function (F3) is utilized when flexibility or bond strength measurement is performed. It measures the magnitude of force that is generated during bending of IPF or the force that is required to break IPFB. It also accepts and utilizes information such as length of fiber from visualization function to determine the flexibility of fibers.

Visualization function (F4) encompasses four sub-functions which are imaging, magnification, illumination and signal analysis. The visual information provided by visualization function is then used by control function as feedback. Suitable magnification with proper illumination is crucial since dimensions of IPFs are very small. Moreover, signal analysis sub-function is required in order to succeed pattern recognition and image analysis in a short span of time.

Dispensing function (F5) contains two sub-functions which are preparatory-chemical treatment and instant chemical treatment. Preparatory chemical treatment is used in the sample storage function whereas instant chemical treatment is used before flexibility measurement.

Control function (F6) encapsulates six sub-functions. Micromanipulation control sub-function is responsible from controlling micropositioning, micro-orienting and microgripping. Visualization control sub-function adjusts focus and zooming. Dispensing control sub-function arranges the desired droplet volume and dispenses it. Measurement algorithm sub-function performs calculations to provide data for the end-user. Finally, user interface sub-function is used to provide control of all sub-function by a human operator [44].

The microrobotic platform includes three micromanipulators (Items 1, 2 and 3 in Figure 3.3), a rotary table (Item 4) and an XY table (Item 5) to perform the micromanipulation functions (F2).

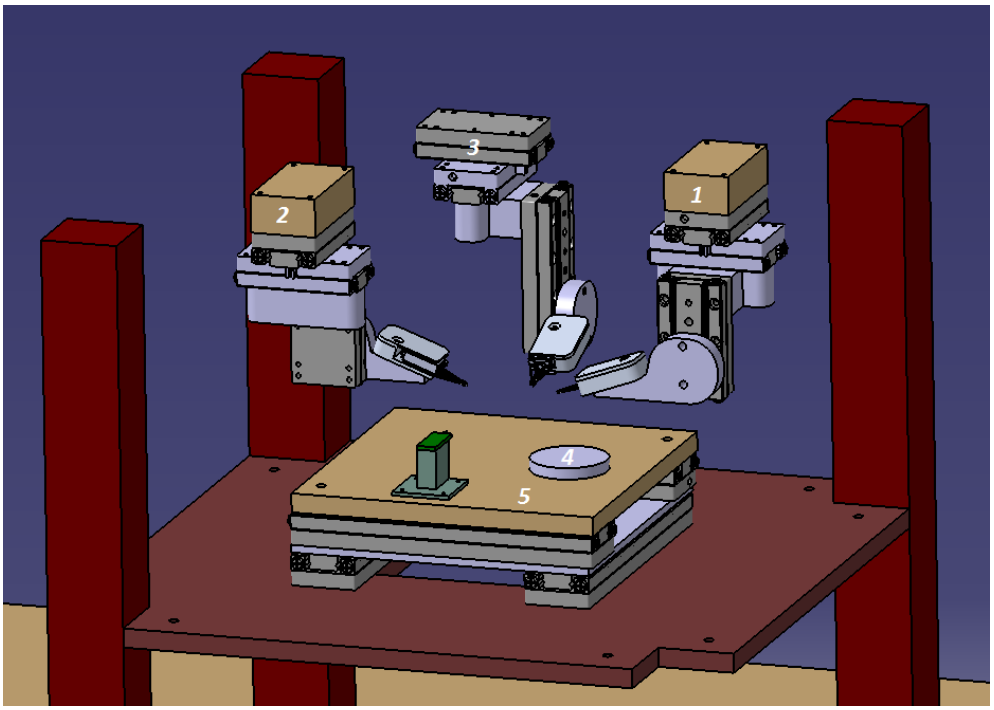

Figure 3.3 *Microrobotic platform before modification*

At the beginning of the thesis work, each micromanipulator consisted of three orthogonal linear micro positioners organized in a stacked gantry crane configuration since it provides compact design [45]. Three linear micro positioners allow traveling at X, Y and Z directions. All of the positioners used in the microrobotic platform are produced by SmarAct GmbH (Oldenburg, Germany). The linear micro positioners (SLC-1730) provide 100 nm resolution, ± 10 µm absolute accuracy, ± 1 µm repeatability and 21 mm travel range.

The rotary table which is placed on the XY table provides 10 µ◦ resolution and it is used for orienting and aligning the samples. Both the processed and unfinished samples are stored in holders which are mounted on the rotary table. Holders are basically tiny containers which store the fibers in either wet or dry state. Although in Figure 3.3 all three micromanipulators have active microgrippers, the microrobotic platform can be modified easily according to the needs. For instance, the third micromanipulator can have a passive probe instead of an active microgripper.

In microrobotic bond breaking, a microdispenser, which is not shown in Figure 3.3, is needed. A passive probe and a dispenser are illustrated in Figure 3.4 where Items 1, 2, 3 are micromanipulators (Micromanipulator 3 is equipped with the passive probe), Item 4 is the dispenser, Item 5 is the rotary table and Item 6 is the XY table.

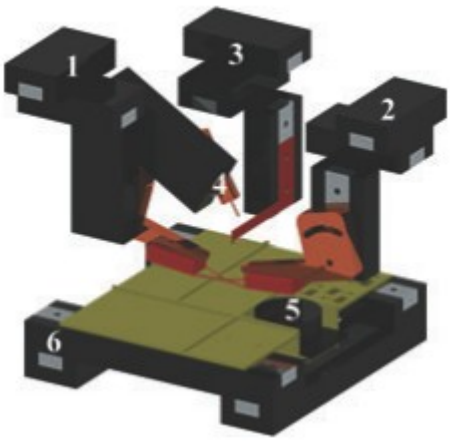

Figure 3.4 *Microrobotic platform with dispenser and passive probe [45]*

An additional linear positioner is added to Micromanipulator 1 in order to move the dispenser so that droplets can be dispensed on a desired place. The disperser is produced by Lee Co which is an American company and it can dispense droplets with a volume of 70 nL.

The microgrippers that are assembled to the end points of micromanipulators have exchangeable jaws which are also manufactured by SmarAct. The jaws have an opening gap of 1mm which is enough for fiber manipulation. The passive probe at the end of third micromanipulator is made of stainless steel and manufactured by laser machining. The passive probe is designed particularly for microscale fiber manipulation and it can handle both horizontal and inclined sample holders.

Linear and rotary micropositioners also both have position sensors except the micropositioner used for dispenser. The control and movement of the dispenser and rotary table are based on visual feedback.

Visualization function (F4) is provided by several equipments. Visual feedback from top is provided by Sony XCD-U100 CCD camera and an illumination system produced by Navitar Inc. which has 12 × zoom with 0.29–3.5 × magnification. The side view is provided by Sony XCD-X710 CCD camera and a 6 × macro–zoom-lens produced by Optem. The zoom of the top camera is controlled from computer whereas for side view manual control is compulsory. The top camera`s pixel size is 4.4 µm and the side camera`s pixel size is 4.65 µm.

As discussed previously while defining the control function, MP1 is controlled by human operator through user interface. The user interface is a part of the control software. Apart from providing the user interface, control software is used for controlling the devices on the platform and it ensures the acquisition of data from sensors and cameras.

An ordinary specimen handling is achieved as follows. The fibers are first placed in the sample holder by human operator. Then the fibers are observed through visual feedback thanks to the top camera. Once the most suitable fiber for handling is chosen, it is rotated according to the desired orientation by rotary table. After that, microgrippers are placed at the end points of the selected fiber by controlling the micromanipulators and

the gripper jaws are closed synchronously to pick the fiber. The picked fiber is then brought to the specimen holder and oriented properly. The release of the fiber is succeeded with the help of passive probe which is moved by micromanipulator too [45]. The signal flow diagram of specimen handling is shown in Figure 3.5.

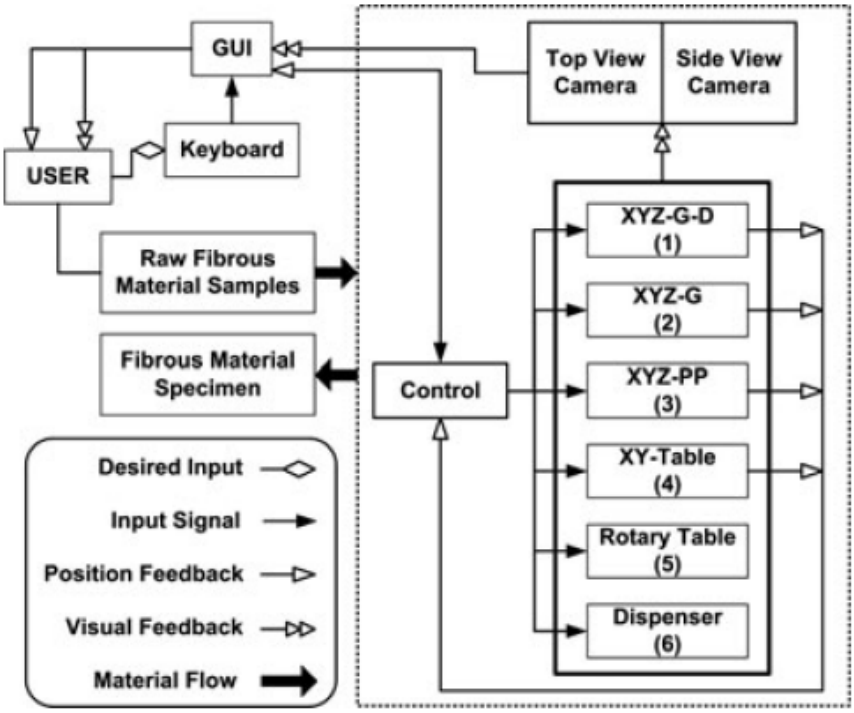

Figure 3.5 *Signal flow diagram. XYZ: Micromanipulator, G: Microgripper, D: Dispenser positioner, PP: Passive probe [45]*

Using the platform, there are two modes to break an IPFB which are Z-directional bond breaking and shear mode bond breaking. Section 3.2 will explain bond making, Section 3.2 and 3.3 introduces the two modes of IPFB breaking using MP1.

3.2 Bond Making

The process of IPFB strength measurement starts by preparing the bonds. In microrobotic bond making, separated IPFs are first placed on the rotary table with a pipette. Then the IPFs are detected by the operator using the visual feedback from cameras. The selected fiber is oriented with Micromanipulators 1 and 2 (Figure 3.3) using the rotary table. After that, Micromanipulators 1 and 2 grasp the fiber synchronously and place it on the fiber bank. This process is repeated until a sufficient amount of IPFs are placed and sorted on the fiber bank. Once there are enough dried IPFs on the fiber bank, IPFs are placed on top of each other as crosses on a Teflon plate. The main mechanism responsible for fiber bonds is hydrogen bonding. Water is crucial in fiber bond making since hydroxyl groups stands on the cellulose and hemicellulose of fiber walls. Water droplet is dispensed on the contact area of the fibers. Then the Teflon plate thus the crossed fibers are covered by another Teflon plate and they are placed in oven for 45 minutes at 70°C under 140 kN/m2 pressure [46]. The shooted droplet on crossed fibers and the fiber bond after taking it out from oven can be seen in Figure 3.6.

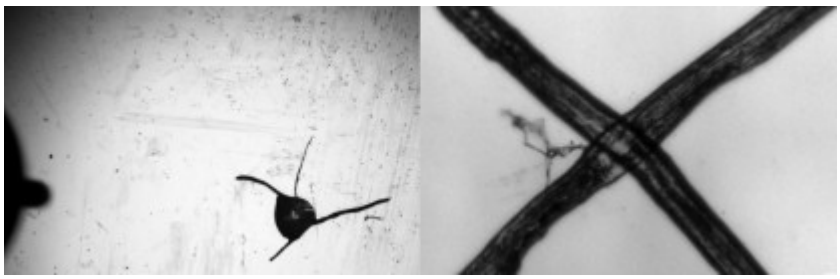

Figure 3.6 *Bond making process [46]*

Once the fiber bonds are ready on the Teflon plate, they are identified using the top camera and transferred to the rotary table using tweezers. Then XY table moves the rotary table under vision system where IPFBs are detected and oriented. Micromanipulators 1 and 2 pick the fiber bond synchronously and move at Z direction above from rotary table. In this phase, most of the bonds rotate 90 degrees and has the orientation shown in Figure 3.7.

Figure 3.7 *Vertical cross orientation of fiber bond [47]*

3.3 Bond Strength in Shear Mode

In shear mode measurements, grasping of one of the free ends of the fiber bond and bond breaking is done using a force sensor on the XY table. Grasping is achieved by gluing the force sensor to one of the free ends of the fiber bond. Firstly, the glue is placed on the edge of glass slide then the force sensor probe is dipped in this glue by using visual feedback. Once the probe is glued, the force sensor is aligned with the free end on both vertical and horizontal directions. The contact between glued probe and free end of fiber is not interrupted for 3 minutes so that the glue can dry. After 3 minutes, the XY table moves backwards continuously while Micromanipulators 1 and 2 stays at the same place, thus fiber bond breaks at some force which is measured by the sensor. When the experiment is done, the probe of the force sensor must be cleaned with acetone to be able to use the force sensor for the next measurement. Moreover, it must be calibrated again since acetone is an aggressive chemical and it may change the sensor's performance parameters. The application of acetone on sensor probe is done the same way as applying glue on it. Acetone is placed on the edge of the glass slide and force sensor is dipped in it [47].

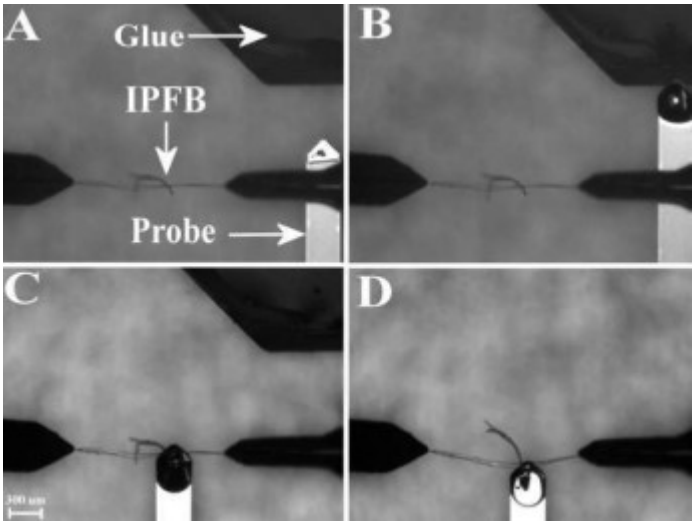

Figure 3.8 *Process of gluing fiber end to the sensor probe [47]*

The glue is prevented from contaminating the bonded area by the distance between the fiber end and contact area. This experiment is time consuming since gluing, cleaning and calibrating the force sensor probe takes redundant time. Micro- and Nanosystems Research Group of Tampere University of Technology is now working on developing another microgripper with an integrated force sensor which will be used for bond strength measurements. This new microgripper with force sensing functionality will save the operator from complex gluing process.

While the XY table moves backward, the force sensor measures different kind of forces at different displacement points which can be seen in Figure 3.9.

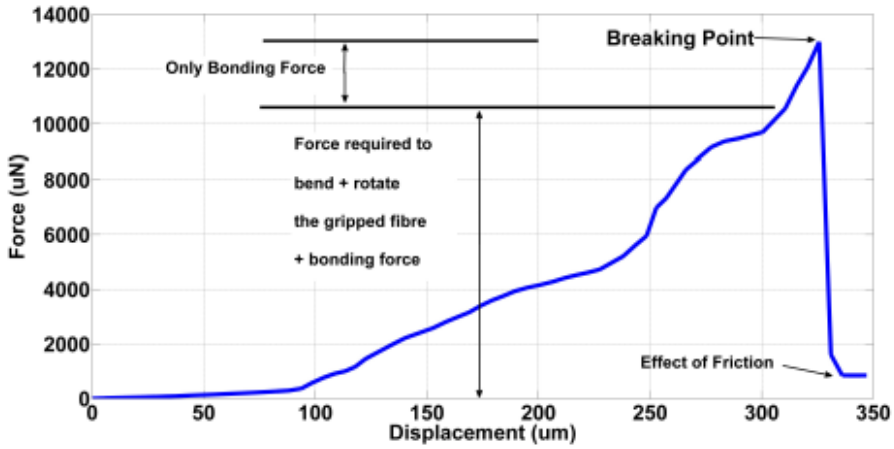

Figure 3.9*Force against displacement graph [48]*

As seen in the graph above, the first measured values are a combination of force required to bend, force required to rotate and bonding force thus the graph is not linear. Whereas the last part before breaking is linear since it represents just the bonding force. Moreover, the graph also shows that there is still friction force between the fibers after the breaking of the bond. In 2013, the method described above used to compare the bond strength measurement of aged and non-aged unrefined fibers from pine [48]. The results are given in Table 3.1.

Table 3.1 *Results of bond strength measurement (Aged fibers on the right) [48]*

Test No.	Force (μN)	Area (μm^2)	**Strength** (N/mm^2)	Force (μN)	Area (μm^2)	**Strength** (N/mm^2)
1	3181	2040	**1.56**	179	1318	**0.14**
2	2832	1444	**1.96**	478	1596	**0.30**
3	12995	2862	**4.54**	< 100	1824	**0.05**
4	12683	1642	**7.72**	< 100	924	**0.11**

As mentioned earlier, the fiber bond stands in a vertical cross and the free fiber is not aligned with the force sensor in parallel which means the measured value is a combination of normal and shear forces. This thesis intends to offer a solution to this problem particularly.

3.4 Z-Directional Bond Strength Measurement

Z-directional bond strength measurement is also significant for paper industry. There is a notable demand for Z-directional strength measurement of paper in both handsheet and IPFB levels. The Z-directional bond strength affects the paper properties directly. For instance, delamination and splitting in printing is caused by low bonding strength and reduction in opacity or in folding stiffness is caused by high bonding strength [49]. Thus, Z-directional bond strength is critical information that can help paper scientists to improve paper properties while lowering the costs. Although Z-directional bond strength is a valuable information, still all of the measurements are done with indirect measurements.

Micro- and Nanosystems Research Group of Tampere University of Technology has developed a novel method to measure the Z-directional bond strength of paper at individual fiber bond level. In this new method, a low-cost piezoelectric polymer material ployvinylidenefluoride (PVDF) is used since no commercial device is found in the market for Z-directional tensile testing at individual fiber bond level. The schematics of the new method are shown in Figure 3.10 where Item 1 is a PVDF element, Item 2 is a bond holder, Item 3 is a connecting element and Item 4 is the individual fiber bond.

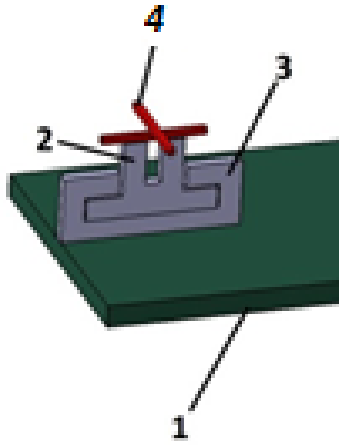

Figure 3.10 *Schematic design of method [49]*

The design shown in Figure 3.10 is assembled on the MP1 by using a mounting stage. The process of Z-directional bond strength measurement starts by picking a fiber bond and moving it over the bond holder. Then UV-curable glue is applied on one of the bond holder tips. After that, the Micromanipulator moves the fiber bond in a way that one of the ends of the fiber is placed in the glue. The Micromanipulator releases the bond as the glue is cured. Then, a passive probe that is attached to another XYZ Micromanipulator places the other end of the same fiber into the UV- curable glue and it is also cured. Once the bond is fixed on the bond holder, the bond holder is also mounted

on the place that is shown in Figure 3.10 by using tweezers. As its name suggests, connecting element connects the bond holder and the PVDF film which acts as a sensor.

Once the bond holder is placed on the connecting element, two microgrippers grasp the free ends of the fiber bond and synchronizedly move in the loading direction of PVDF film until the bond breaks. The microgrippers move with the same speed in each experiment for calibration issues. When an external load is applied to the PVDF film, the film bends and an electrical signal is produced according to the amplitude of the external force.

3.5 Summary

In this chapter, microrobotic platform is introduced. Its basic functions and components are presented by also providing their capabilities. Moreover, bond making procedure and two measurements which are shear mode bond strength and Z-directional bond strength are discussed.

There are 6 main functions that the platform presents which are sample storage (F1), micromanipulation (F2), force sensing (F3), visualization (F4), dispensing (F5) and control (F6).

Sample storage function (F1) provides suspension storage, dry storage and frame fixture.

The micromanipulation function (F2) is performed by five devices. There are three micromanipulators, each consists of three linear positioners SLC-1730 which are produced by SmarAct and provides traveling at X, Y and Z directions. A rotary table is used to rotate and orient the IPFB and XY table is used to position the IPFB according to the micromanipulators or to the force sensor.

The magnitude of the force that is generated during bending of IPF or the force that is required to break IPFB is measured by force sensing function (F3).

Sony XCD-U100 CCD camera and an illumination system produced by Navitar Inc. which has 12 × zoom with 0.29–3.5 × magnification provides the visual feedback from top and Sony XCD-X710 CCD camera and a 6 × macro–zoom-lens produced by Optem provides the side view for visual feedback for visualization function (F4).

Dispensing function (F5) is provided by a microdispenser (produced by Lee Co) which can dispense droplet with a volume of 70 nL.

Finally, control software provides the control function (F6). User interface is a part of control software and human operator uses it to control the microrobotic platform. Control software is used for controlling the devices on the platform and it ensures the acquisition of data from sensors and cameras.

4. DESIGN PROCESS

This chapter will explain the design process. The design process was mostly carried out together with the survey and selection of equipment. Engineering design approach is chased throughout the project. Section 4.1 introduces the engineering design concept and its steps. Sections 4.2, 4.3, 4.4, 4.5 and 4.6 examine the addition of two rotational degrees of freedom into microrobotics platform by going through the engineering design process step by step. Finally, Section 4.7 summaries the chapter.

4.1 Engineering Design Process

Engineering design can be defined as an iterative decision making process where scientific and mathematical principles are utilized creatively in order to fulfill desired requirements by using limited amount of resources [50]. Usually, the process includes several aspects such as design, manufacture, efficiency determination and economic availability. Although the main goal of engineering design is problem solving, it is clearly distinguished from other types of problem solving.

The most important feature of design problem is, it is open ended and it always has more than one possible solution, whereas analysis problems only has one specific solution. For instance, determining the distance covered by a bullet whose initial velocity and height are known is an analysis problem since it has just one answer. On the other side of the coin, devising a gun which will be able to shoot a bullet to a specific distance is a design problem since there can be numerous guns that can do the same job. The design process is iterative since as the project progresses, new problems arise which eventually force the engineer to go one or more steps back and modify the design [51] [52]. In contrast, once a step is completed correctly, there is no need to turn back in analysis problems since they are substantially sequential.

The iterative approach is a must in all design processes. One of the most well-known examples of this phenomenon is the Wright brothers' airplane. Before building a powered plane, they constructed over 700 kites and gliders in order to understand the air dynamics. With each new design, new questions and problems arised and forced them to renew their designs over and over again until they invented the first airplane. The reason why engineering design is iterative or cyclic is in each design new uncalculated problems occur. Thus, design process is also vague or open ended [51]. The engineering design process is divided into different steps by different authorities, however still most of them include the same content. In this project, the five steps approach is pursued. The five steps in engineering design process are, defining the problem, gathering pertinent

information, generating multiple solutions, analyzing and selecting a solution, testing and implementing the solution. The steps are also shown in Figure 4.1.

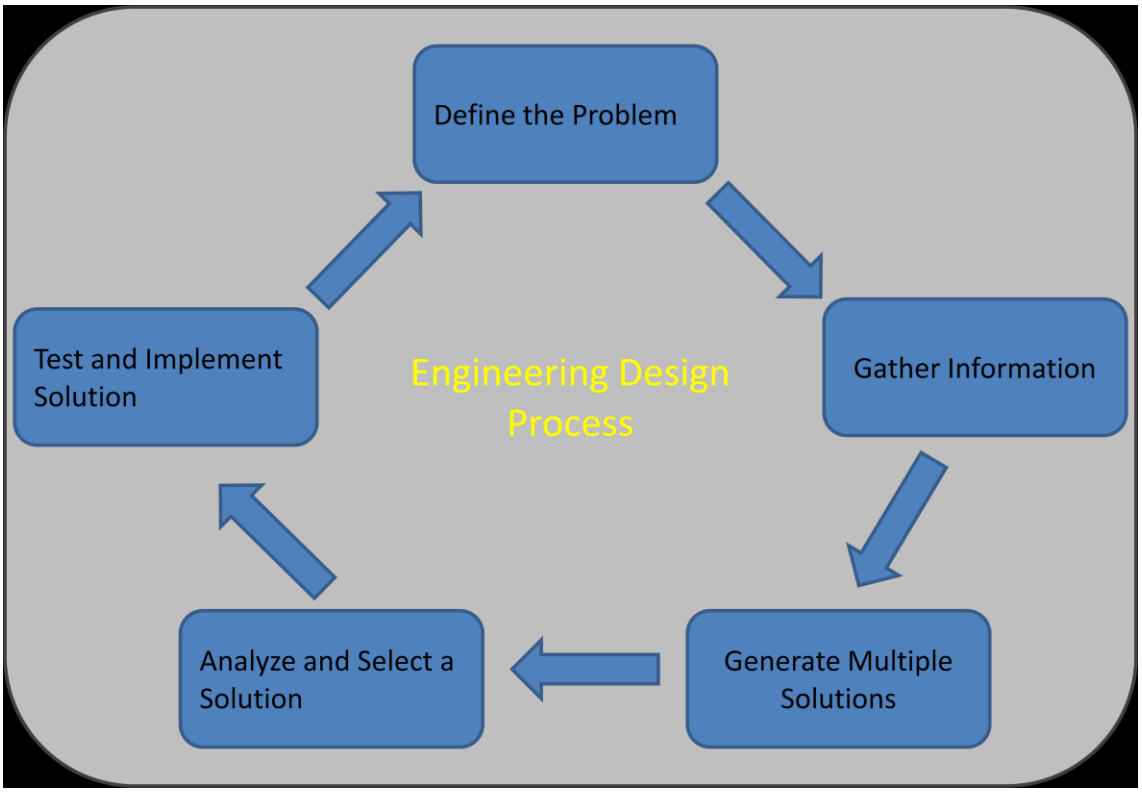

Figure 4.1 *Engineering design process steps [51]*

Although there is no strictly defined sequence of steps, still we can put them in order as illustrated in Figure 4.1. Defining the problem is the first step in design process. The problem statement must be clear and well understood. Moreover, there can also be some additional requirements which are desired to be met. The explicit definition of problem will provide the engineer to proceed in the right direction towards the goal and prevent wasting time on irrelevant matters.

Once the problem is clarified, information regarding the problem must be gathered. For instance, the previous works on the same field must be studied since there could be a solution to a similar problem. Moreover, scientific and mathematical principles that are included in the project must be covered.

With enough information on the problem and background of the problem, the engineer will be able to generate multiple solutions. In this phase, engineer must produce many solutions. Each of the solutions may have some advantages and disadvantages but these issues will be handled in the next step. In this step, the main idea is to consider all of the possible solutions in order to select the most appropriate one.

Analyses and selection of solution includes many aspects such as efficiency, sufficiency in terms of requirements, price and needed time to complete. The best solution is directly related to these factors. For example, a solution which fulfills all of the re-

quirements can be expensive so another solution which is cheaper and which will almost meet the requirements can be the best choice.

Finally, the selected approach must be tested before really building. This can be done by various methods such as prototyping and simulating. The tests will confirm the predicted performance of the solution. The tests may also reveal some unforeseen problems which would require the engineer to return to previous steps and correct them. If the tests also approve the selected design, then the solution can be implemented [51].

4.2 Define the Problem

The microrobotic platform is required to be modified in the pursuit of three goals which are i) improving the shear mode bond strength measurements by solving peeling mechanism problem, ii) facilitating the Z-directional bond strength measurement by revealing information on which fiber is on top and iii) allowing untwisting twisted fibers. These three goals and the problems which they include are discussed one by one.

4.2.1 Improving Shear Mode Bond Strength Measurement

The shear mode bond strength measurements cannot be done in pure shear mode with the current configuration of the platform. The force that is required to break the IPFB is a combination of normal force and shear force, which results in peeling mechanism. The problem of combined forces in bond strength measurement is shown in Figure 4.2.

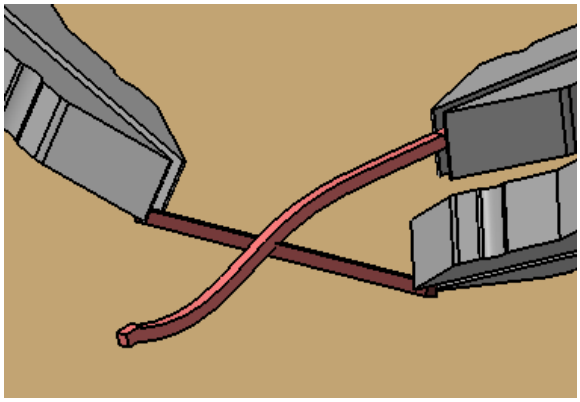

Figure 4.2 *Grasped IPFB with auxiliary angle*

In the auxiliary view the combination of the forces can be seen. The plane of the bonded area is not totally aligned with the gripper that will break the bond. When the microgripper will move backwards along a straight line, the force applied on the fiber at the bottom will be both upwards (Z) and in the movement direction of gripper (X). Thus, the measured force is a result of peeling mechanism. The same issue applies to every single bond, since fiber bonds are not strict cylindrical tubes but they are flexible and they can be found in many orientations.

Furthermore, although it is easy to realize IPFB orientation in Figure 4.2, in real situation, it is troublesome. This issue is shown in Figure 4.3. During shear force measurements the orientation of the fiber must be known so that it can be aligned with the gripper. Moreover, in order to prevent the peeling mechanism, the actual location of the grasped fiber must be known.

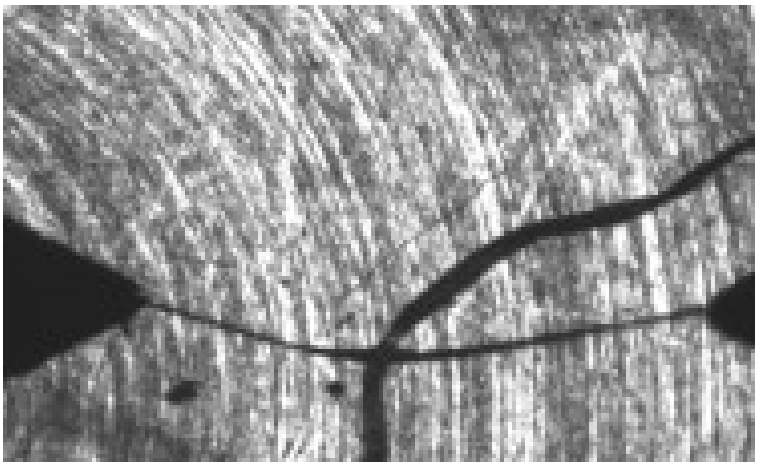

Figure 4.3 *IPFB from top view*

4.2.2 Facilitating the Z-Directional Bond Strength Measurement

The Z-directional bond strength measurement can be done more accurately and easily by providing two features. The first one is: it is troublesome to realize which fiber is on top. For instance although it is easy to see which fiber is on top in simulation (Figure 4.4), in reality it is hard, as can be understood from Figure 4.3. For this reason, sometimes the fiber bond is placed on the bond holder in a way that the fiber with free ends stays under the fixed fiber. Thus, when the microgrippers grasp the free ends of the fiber and move upwards simultaneously, not the bond between the fibers but the bond between bond holder and fixed fiber is broken.

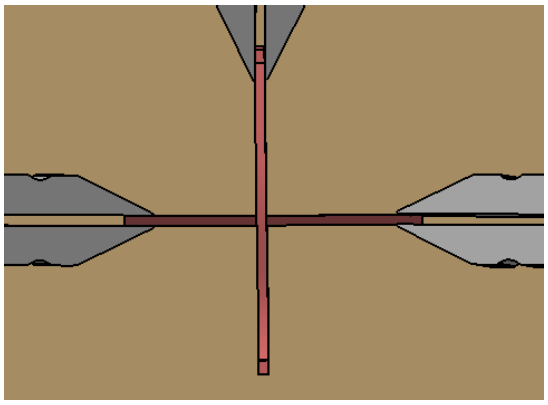

Figure 4.4 *IPFB from top view (Simulation)*

The second one is: in order to get more accurate results, it is important to have the ends of fiber with free ends parallel to the PVDF film. If the ends of the free fiber are

not aligned with the PVDF film, there will be an offset at Z-direction between the grasping grippers which will intervene with the pure Z-directional bond strength measurement.

4.2.3 Untwisting the Twisted Fibers

The microrobotics platform is not capable of untwisting the twisted fibers since it has no rotational degrees of freedom. Allowing untwisting twisting fibers can provide significant information regarding inside structure of fibers by measuring the torque that is required to untwist a fiber.

4.2.4 Theoretical Solution

The microrobotic platform must be modified in order to measure pure shear force which can be achieved by positioning and orienting the force sensor and the plane of the bonded area as parallels. This can be done by either orienting the force sensor (by actuators) or by adding a rotational degree of freedom to the microgripper. The addition of a rotational degree of freedom to the microgripper can be used in many applications whereas orienting force sensor can be utilized just when force measurement is required. For instance, during Z-directional bond strength measurement, rotation is required in order to understand which fiber is on top. Moreover, additional rotation can be also used for untwisting twisted fibers. Because of these reasons, the addition of a rotational degree of freedom to the microgripper approach is chosen.

The addition of rotation to one of the micromanipulators can be used with the following sequence of activities. First, the micromanipulator will take the fiber bond, then the micromanipulator with rotary DOF will take it from the first one and rotate it to achieve the desired orientation and to see which fiber is on top. Then the first micromanipulator will also grasp the fiber bond. As the fiber bond is fixed and oriented, the third microgripper will come, grasp the end of the free fiber and break the bond. Although, this addition of rotation to one micromanipulator seems like it solves the problem, in fact, it does not.

Two issues explained above can be addressed by adding at least two degrees of freedom to one of the micromanipulators. Not one but two rotational degrees of freedom are needed since just one rotation will cause circular motion of fiber. With just one rotation, the center of rotation will not be aligned with the fiber which will eventually results in circular motion. The obvious reason for this misalignment is, there are 3 linear positioners for each microgripper. Thus, one rotational degree of freedom around microgripper will not change the angle that the microgripper picks up the fiber which means there will always be an offset angle between them. Circular motion is not desired since it will both contribute to peeling mechanism and make grasping with both ends even harder. The circular motion of a single fiber with respect to the rotation of microgripper`s tip is illustrated in Figure 4.5 and the misalignment between microgripper and IPFB is shown in Figure 4.6.

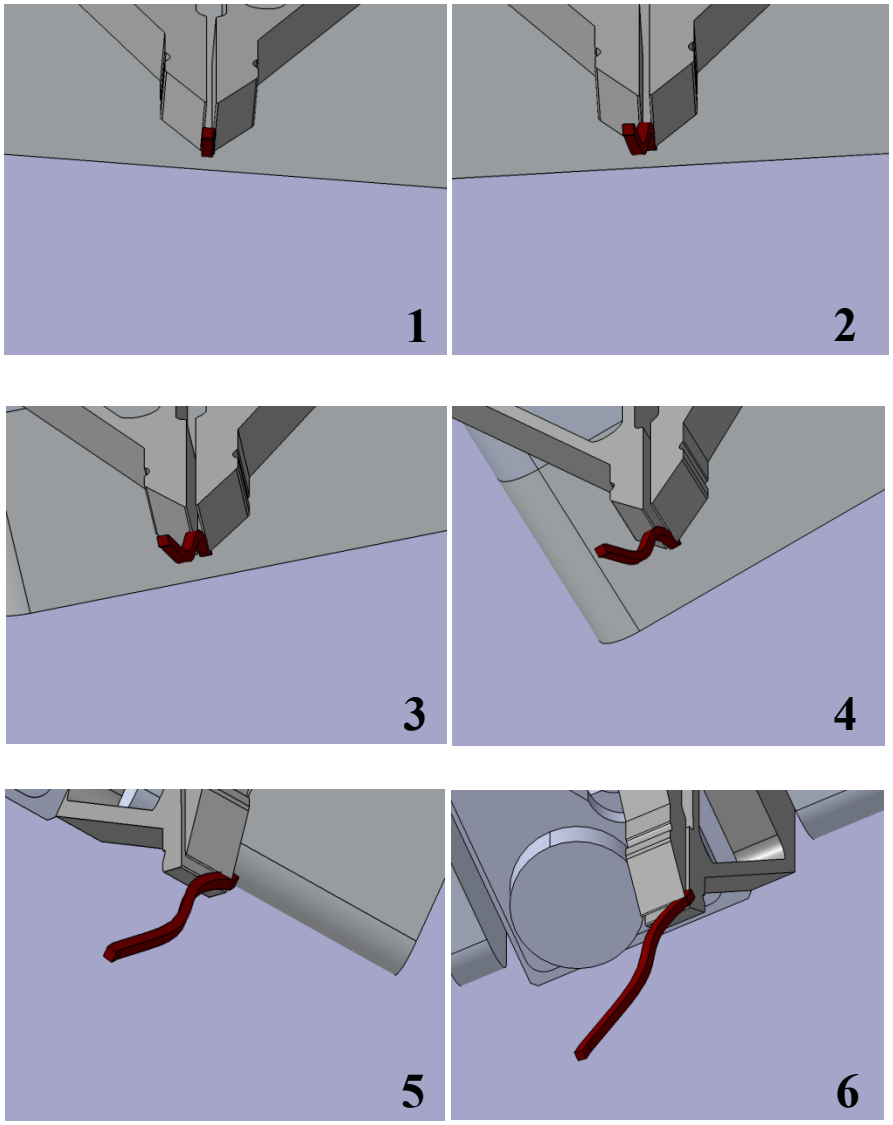

Figure 4.5 *Circular motion sequence of a single fiber with respect to rotation of microgripper tip*

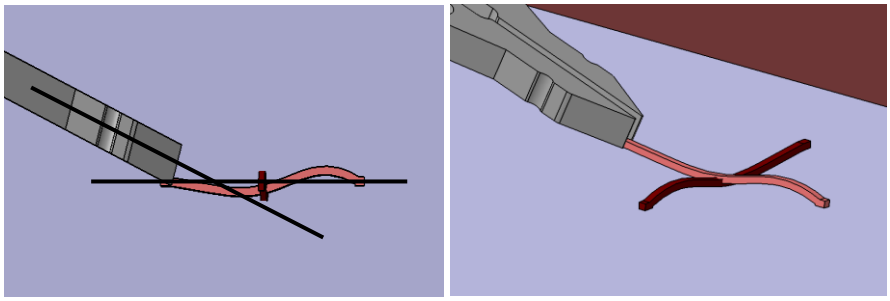

Figure 4.6 *Misalignment between IPFB and microgripper shown with two different angles*

The desired alignment of fiber bond and the jaw is shown in Figure 4.7.

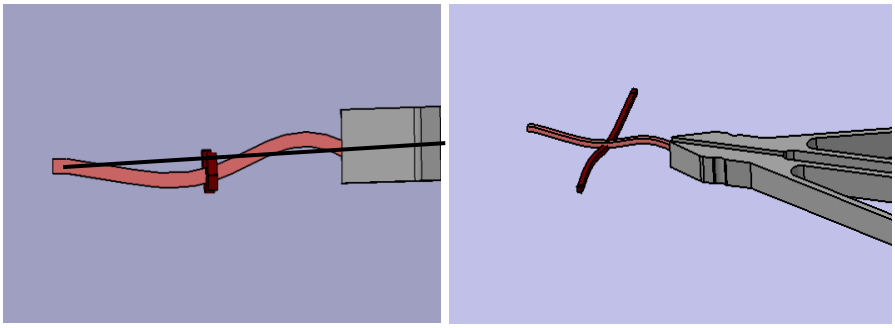

Figure 4.7 *Correct alignment between IPFB and microgripper with two different angles*

The black line in Figure 4.7 shows the alignment of the jaw and the fiber bond. Since fiber does not have a perfect cylindrical shape, the alignment is also not perfect. Another issue is, the fiber must be grasped with the jaw`s mid-point since the center of rotation is at the middle. If the fiber is not grasped with midpoint of jaws then even though it will be very small and negligible, circular motion will again occur. Figure 4.8 shows the rotation of fiber bond from top view when it is aligned correctly.

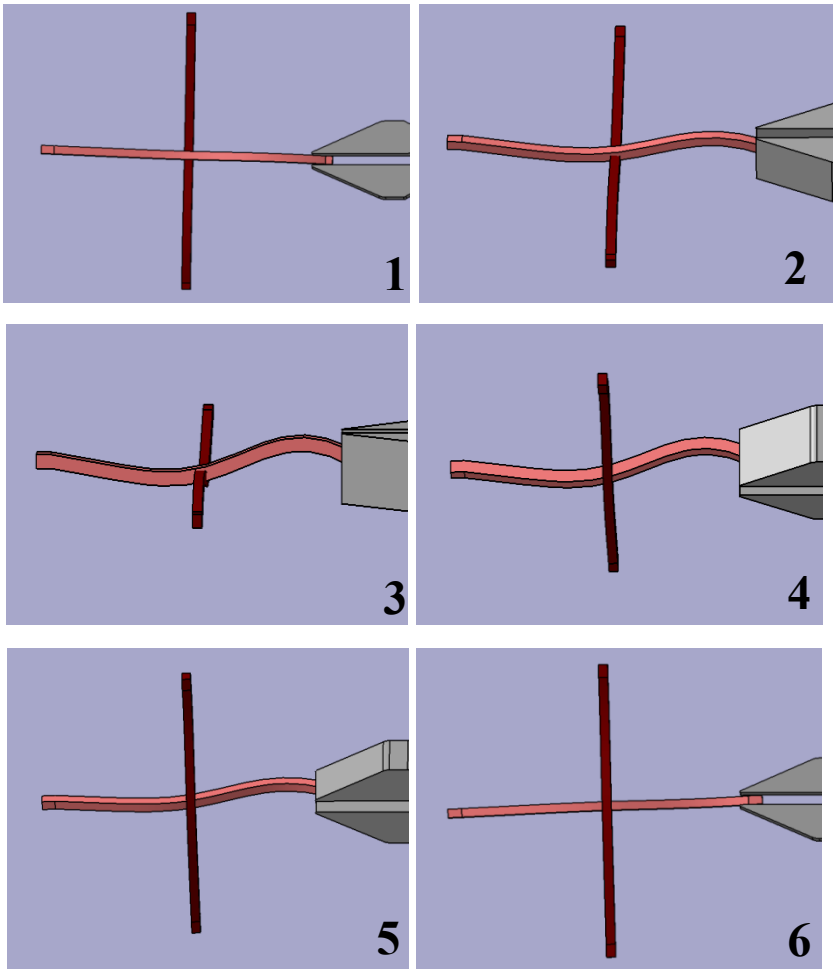

Figure 4.8 *180 degrees of rotation of IPFB with correctly aligned microgripper*

In Figure 4.8, the fiber bond is rotated with 180 degrees. Since the fiber bond is aligned correctly, the grasped fiber (pink one) just turns around on its own axis as gripper swivels.

With two rotational degrees of freedom, microgripper is capable of manipulating the fiber bond correspondingly. The non-fixed fiber can be oriented in such a way that the gripper that will break the bond can be perpendicular to the fixed fiber so that pure shear mode measurement can be performed. Also, although it is obvious which fiber is on top in Figure 4.8, in real life this information will be gained by rotating the fiber bond.

4.2.5 Technical Requirements

Apart from alignment problem, there are also some other important requirements that must be fulfilled in order to solve the previously discussed problems. Understanding the requirements is essential since they will facilitate the selection task when generating many solutions. These requirements may eliminate or promote a solution. The requirements for both rotations are listed as follows;

- Clockwise and counter clockwise rotation must be provided
- Speed: Maximum speed must be in minimum 18 deg/s
- Resolution maximum must be 0.1 deg or better
- Range must be in minimum 180 deg
- Closed-loop must be available
- The system must be integrated to both microrobotics platforms
- Maximum weight for overall system (new parts and microgripper) must be below 100 grams

As stated earlier two rotational degrees of freedom will be added to one of the micromanipulators. First, each of the rotations must be capable of both clockwise and counterclockwise rotation so that the alignment can be possible in all situations. Second, the speed of the rotation must be controllable and its maximum value must be 18 degrees per second in minimum which basically means a 180 degrees rotation will take 10 seconds at maximum speed. This requirement is not that strict (there will be no significant difference if it takes 11 seconds or 9 seconds to achieve 180 degrees rotation) but still it is significant since it will be too time consuming and inefficient if it is not met. Third, the resolution of each rotation must be 0,1 deg at maximum. This requirement is crucial because if it is not met then there is no point in modifiying the current platform. The alignment of fiber bond and the microgripper jaw will not be possible without this requirement. Fourth, each rotation must have a range of minimum 180 degrees so that all configuration of fiber bond in total 360 degrees is reachable with counter or counterclockwise rotation. Fifth, the control of new devices must be closed loop control so that desired accuracy and repeatibility can be achieved. Sixth, integrating the new devices to both microrobotich platforms should be fairly easy. Micro and Nanosystems research group of Tampere University of Technology currently

has two microrobotic platforms. Although they have too many features in common, some of the features are specially designed for performing different tasks. The problems stated before, apply for both systems and it will be wise if the modification could be utilized for both systems as well. Basically this requirement suggests a design whose assembly and interface to computer is easy for both of the microrobotic platforms. Last, the total weight of new devices and microgripper must not exceed 100 grams. This requirement is also substantial since otherwise the microrobotic platform will not work. As discussed in Chapter 3, there are three linear postioners that are connected perpendicularly. Thus, the last linear positioner which provides motion at Z-axis will carry the whole load of new devices and plus the microgripper. At Smaract`s catalogue, the allowable load for this linear positoner is stated as approximately 100 grams. Thus, while choosing new devices, the weight of each device plays a key role in terms of device selection.

4.3 Gather Information

In the previous section, the problems are defined and a theoretical solution is proposed. Once the problem is understood, background research is to be carried out since one cannot generate multiple solutions without enough knowledge on the topic. It is obligatory in engineering design process to investigate the previous studies and applications in the interest of finding a solution to the current problem. In Chapter 2 Section 2, previous studies have been discussed briefly. Although they showed several techniques for fiber bond measurements, still they are very different in terms of followed methods. The manipulation of fibers through microrobotic platform is novel and recently developed method, thus there are not much literature in this area.

In Chapter 3, the microrobotic platform is discussed, including the devices that are used and procedures of performing actions. Understanding the microrobotic platform and its features is crucial since every little detail of it might affect the design of new two rotational degrees of freedom. Although, published papers regarding the microrobotic platform was read, it was necessary to perform some experiments with the platform in order to understand how it works, how efficient and user friendly it is. Apart from the platform itself, side topics such as wood fiber and force modes are also examined since without having sufficient information about them, it is impossible to understand the problem.

After proposing the theoretical solution that is discussed in previous section, devices that can provide two rotational degrees of freedom are investigated. In Section 4.2.4, it is made clear that two rotational degrees of freedom are required to solve the problems by also fulfilling the side requirements. It is obvious that there must be some actuators which will provide the rotary motion eventually. There can be several approaches in order to provide two rotational degrees of freedom. This section aims just to reveal three main solution possibilities which are spherical actuators, rotary positioners and premade microrobots without analyzing them yet.

4.3.1 Spherical Actuators

The recent development in automation and robotics also lead to the advancement in actuators that can provide multiple degrees of freedom with high precision. Nowadays, multiple DOF are still mostly achieved by traditionally adding separate actuators for separate axis which results in heavier and more complex systems. The addition of separate actuators for each DOF causes many problems thanks to the impacts of inertia, backlash, nonlinear friction and elastic deformation of gears which decreases the dynamic performance [53]. Thus, spherical actuators which provide controllable several DOF in just one structure gains more importance day by day.

The spherical actuators were first invented in 1950`s and they were not developed appreciably since then. The major reason for this situation is the difficulties in controlling them which limited their competitiveness against other methods. However, recent developments in power electronics and digital signal processors allow the spherical actuators to be improved in the sense of performance, efficiency and accuracy [54]. Spherical actuators mainly use three types of driving methods which are mechanical, piezoelectricity and electromagnetic forces.

Mechanically driven spherical actuators utilize four or more wires whose one ends are connected to rotor and the other ends to the motors. The motors that are used for this purpose are usually step motors because of their precision and accuracy. The rotor orientation is controlled by the step motors which tighten or loose the wires that are connected to them. Mechanically driven spherical actuators still utilize many actuators. The motors change the orientation of the ball where wires act as connection elements and the output axis at the end of the ball is the ultimate orientation of the actuator. The ball is placed in a concave shell and its movement with respect to wires is sustained by the spherical sliding bearing. Figure 4.9 show the basic structure of a mechanically driven spherical actuator.

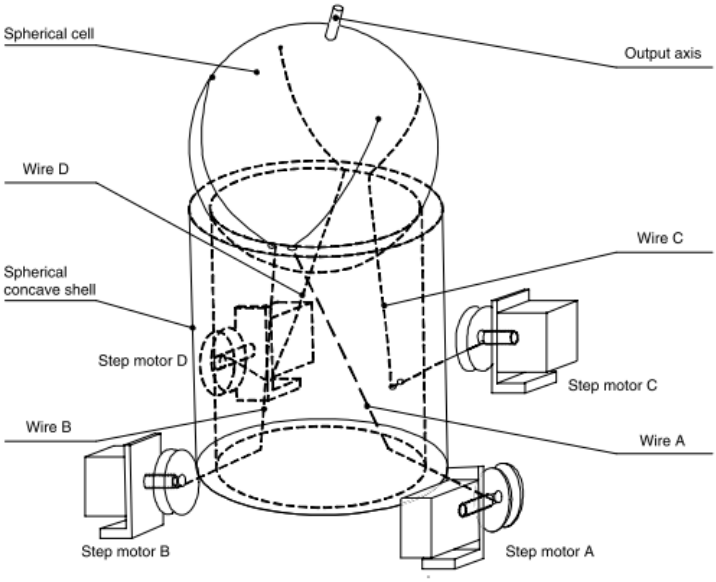

Figure 4.9 *Wire driven spherical actuator [55]*

Ultrasonic motors also work with a similar principle as the mechanically driven types. Ultrasonic motors use reverse piezoelectric effect of ceramics instead of the wires and motors. The dimensions of the piezoelectric materials are altered in desired ways by applying specific electric voltage on them. The working principle of ultrasonic motors is shown in Figure 4.10.

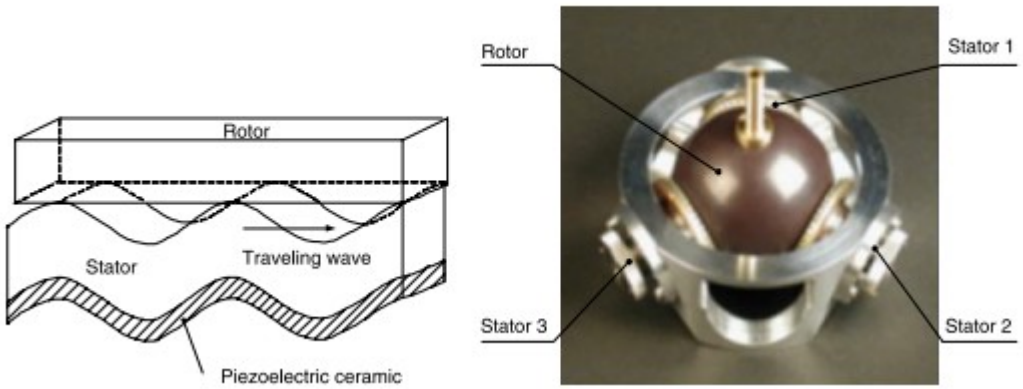

Figure 4.10 *Left; working principle, Right; structure of ultrasonic spherical actuator [55]*

The piezoelectric material (stator) whose surface is in touch with the ball expands or contracts with respect to electric voltage on it which produces travelling wave structure. This wave drives the rotor. By using three piezoelectric materials in different axis, 3 DOF are achieved.

Most spherical actuators are based on the principle of electromagnetism [55]. There are three different types which are permanent magnet, induction and variable reluctance. The induction and variable reluctance spherical motors do not have commercial application because of their complexity, difficulty in controlling and poor performances, thus just permanent magnet (PM) will be discussed [54].

Firstly, permanent magnet does not have the problem of excitation losses since field excitation system does not absorb electrical energy. There are many advantages of using electromagnetic motors such as high torque, moderate voltage operation and fast response. Thus PM spherical actuators are the mostly used ones among spherical actuator types. Nowadays there are several continuing studies on PM spherical actuators which aim to increase the working range and resolution of the actuator. Although the working principle of PM spherical actuator can differ slightly between different designs, still their major idea is the same. PM spherical actuator consists of "a ball-shaped rotor with a full circle of PM poles along the equator, and a spherical shell stator with multiple layers of circumferential air-core coils" [55]. PM is manufactured from elements which provide high flux density. The coils are energized in two longitudinal directions results in tilting of rotor and activating the other coils provides the spin of the ball around its own axis. The two tilts and the spinning motion with regards to activated coils are shown in Figure 4.11 (a) (b) and (c).

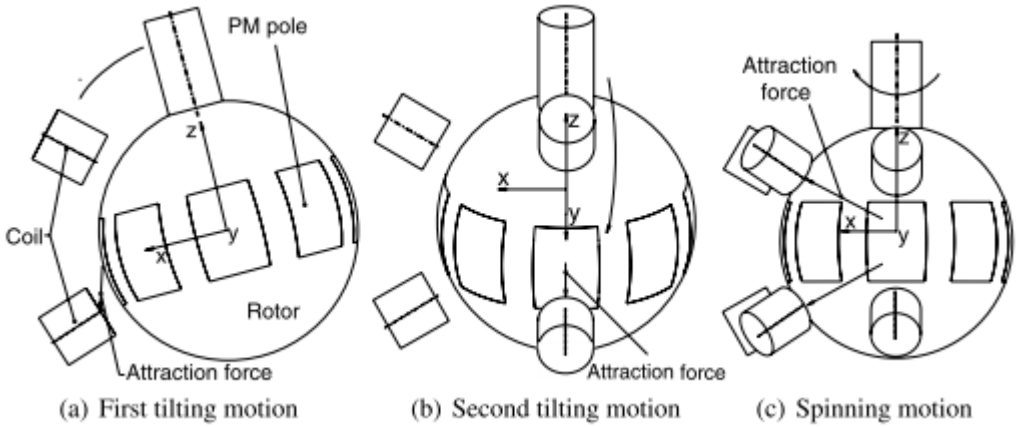

Figure 4.11 *(a) First tilting motion, (b) Second tilting motion, (c) Spinning motion [55]*

The activation or energizing of the coils is procured by feeding current to them, and the control of current provides the 3 DOF spherical motion [55].

Fuchiwaki, Ito, Misaki and Aoyama [56] used electromagnetic spherical Micromanipulator to provide motion to microtweezers in the Z direction. In their design they placed a steel ball on top of the four legs. The actuator can rotate the rotor in three axes. The rotation of movement is managed by the inchworm movement which is shown in Figure 4.12 and the structure of the actuator is shown in Figure 4.13.

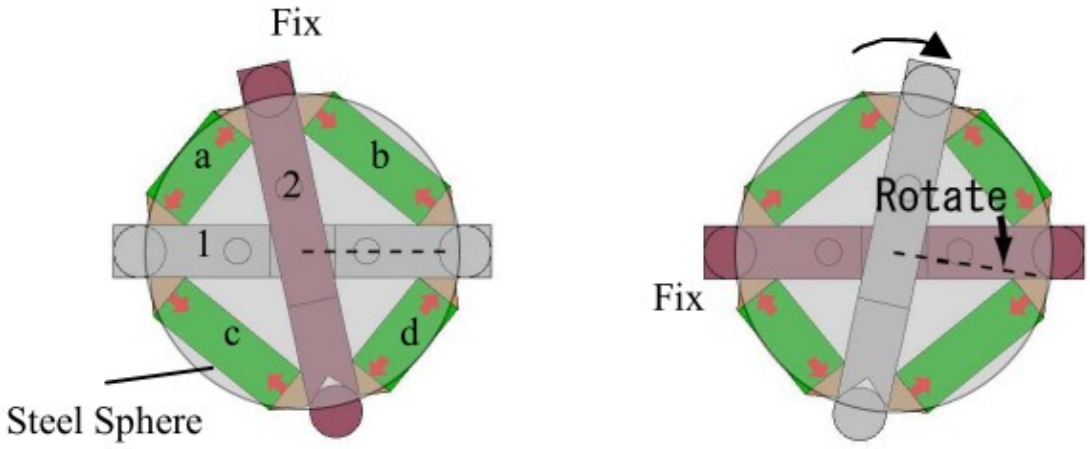

Figure 4.12 *Sequence of yaw direction [56]*

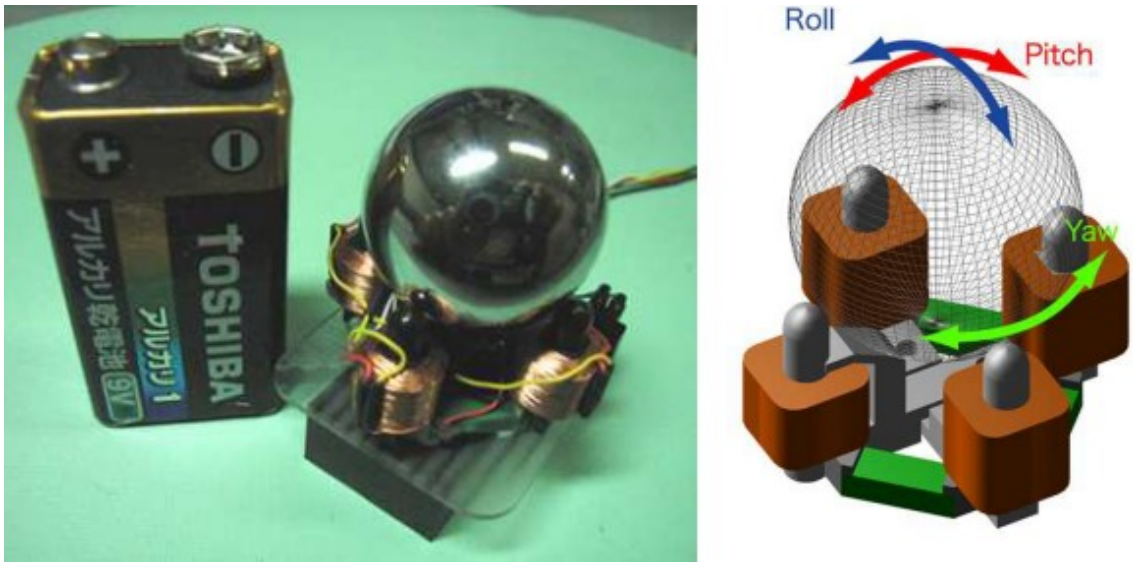

Figure 4.13 *Structure of electromagnetic spherical actuator [56]*

4.3.2 Rotary Positioners

Rotary positioners are much more developed and commercialized than the spherical actuators. With the required sizes, mostly there are two methods to drive rotary positioners which are stepper motors and piezo positioners. Since two degrees of freedom are needed, two rotary positioners are needed so sizes of each of them become more important. Moreover they must be assembled to the platform by connecting elements. The first rotary positioner must be able to carry both the second positioner and the gripper. Furthermore, they must be designed in such a way that they can be used by both of the systems.

One disadvantage of rotary positioners is, they are mostly designed as rotary tables or stages which are used to rotate just the samples. Mostly, they are not used as actuators that rotate other actuators like in robot arms. Because of this reason, commercialized products provide small forces and torque. Moreover, usually they are designed to be used horizontally like the rotary table in MP1 explained in Chapter 3. Rotary positioner is placed on a setup where it rotates the plate (sample holder) on it which stores the samples. The rotary positioner that is used in MP1 as rotary table is shown in Figure 4.14.

Figure 4.14 *Rotary positioner [57]*

4.3.3 Pre-made Microrobot

Kleindiek is a company which offers Micromanipulator robots with three degrees of freedom. The 3 DOF consists of 2 rotational and 1 linear motion. Linear motion is utilized just to provide forward and backward movements of the gripper. Kleindiek also provides the tool called Rotip-Em which can be integrated to achieve rotation around gripper's axis. Their product (MM3A-EM) has the specifications listed below and an image of the robot is given in Figure 4.15;

· Travel; 360 deg unlimited
· Maximum drive velocity; 45 degrees per second
· Resolution; 0.1 degree
· Size; 63*21*26 mm
· Weight; 45g+gripper
· Torque; 0.01 mNm

Figure 4.15 *MM3A-EM Micromanipulator robot [58]*

With the addition of plug in tool Rotip-Em, the micromanipulator robot can provide 4 DOF which is more than enough (2 DOF). MGS2-EM which is a microgripper can be also integrated with the Rotip-Em so that the gripped object can be rotated too. The tips

of the microgripper can be changed and customized according to needs but for this application standard tungsten probe tips will be sufficient.

4.3.4 Conclusion

Since two rotations are needed with the smallest size possible, the first consideration was using a spherical actuator in order to provide three degrees of freedom at once. Although they provide many benefits such as accurate position control with high motion resolution and low power consumption, their control algorithms are very complex, speed is low and they have hysteresis problems [54] [55].

Mechanically driven spherical actuators need again two actuators thus, while not having any advantages it also causes many control problems. Moreover, during the investigation of PM, and ultrasonic spherical actuators, it is realized that currently they are still on research progress and there are no commercial micro spherical actuators. Moreover, building one which will satisfy the requirements discussed previously is troublesome.

Most of the requirements are met by pre-made microrobot. Although torque is too low, it represents the torque at the end (it has its own gripper and specified torque is just meant for sample manipulation, thus it is enough). There are basically two problems with this product. The first one is, although the product provides very significant features, it is controlled by open loop which is not desired. The second one is the price. During a meeting at the TUT, the seller approximated the price of such manipulator as 20000 euros which is out of the budget limit.

Once spherical actuators and the pre-made microrobot (Kleindiek) were eliminated, rotary positioners market are to be investigated in details.

4.4 Generate Multiple Solutions

Since spherical actuators and micromanipulator robot from Kleindiek could not fulfill the requirements of this application, rotary positioners from numerous companies have been investigated and it has been realised that just few of the rotary positioners on the market satisfy the requirements.

Rotary positioners are mostly used for just rotating the sample so it is crucial to be sure that they will provide enough torque and force. Another issue about using rotary positioners is two of them are needed. Thus, each of them must be sufficiently small and light.

The possible basic configuration of system with two rotary positioners for the platforms is shown in Figure 4.16. In MP2, the gripper is around 20 grams and its connection element is 6 grams which means the second rotary positioner`s 0.50 Ncm torque capacity is more than enough to be safe. For the first rotary positioner it must be at least 0.70 Ncm depending on the secondary rotary positioner`s weight. Moreover, the overall weight of the rotary system including the microgripper must not exceed 100 grams since the linear positioner cannot handle more than 100 grams in vertical direction. The grip-

per (20 grams) and all other connection elements (30 grams) together weight approximately 50 grams which means, the total weight of two rotary positioners can be at maximum 100-50 = 50 grams. This configuration will be also suitable for the MP1 since its gripper is lighter (10 grams).

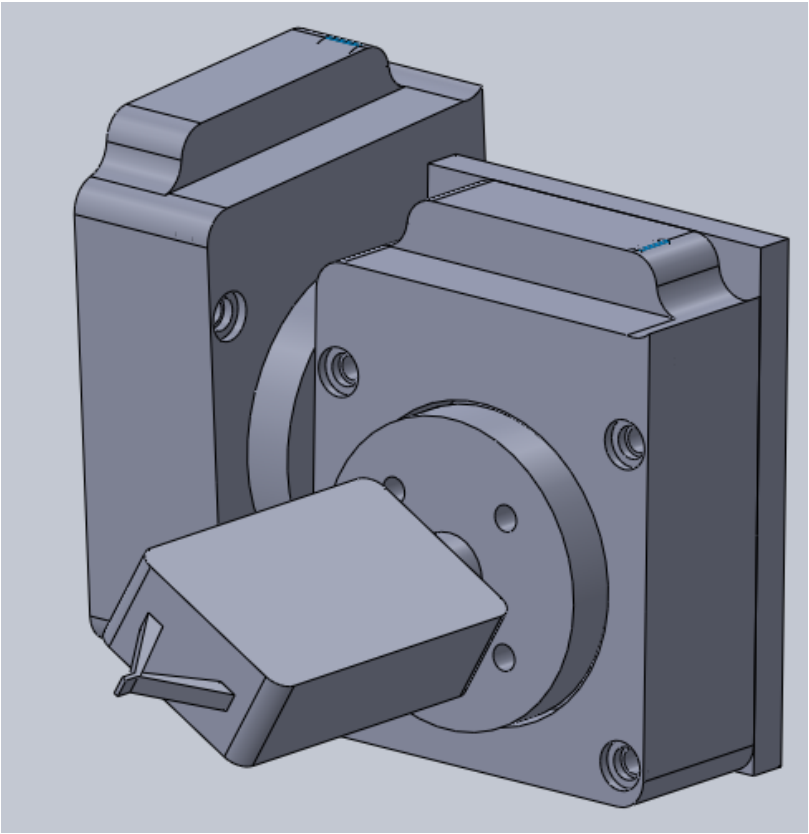

Figure 4.16 *Basic configuration with two rotary positioners*

Three companies (Attocube, Micronix and Smaract) are found to be the ones which provide products that satisfy the requirements.

4.4.1 Attocube

Attocube has a big portfolio of rotary positioners. The closed loop rotary positioners are shown below [59];

ANR51/RES;

- Clockwise and counterclockwise – 360 degrees endless in both directions
- Maximum drive velocity; 10 degrees per second
- Resolution; 6 μ degrees
- Size; 20*20*9.5 mm
- Weight; 10g
- Maximum load; 0.3N (30g) for mounting orientation axis vertical
- Maximum dynamic torque; 0.2 Ncm

ANRv51/RES**;**

- Clockwise and counterclockwise – 360 degrees endless in both directions
- Maximum drive velocity ; 10 degrees per second
- Resolution; 6 μ degrees
- Size; 20*21*10 mm
- Weight; 10 g
- Maximum load; 0.2N (20g) for mounting orientation axis vertical
- Maximum dynamic torque; 0.2 Ncm

ANR101/NUM**;**

- Clockwise and counterclockwise – 360 degrees endless in both directions
- Maximum drive velocity ; 30 degrees per second
- Resolution; 0.1 μ degrees
- Size; 30*30*18 mm
- Weight; 45.5g
- Maximum load; 1N (100g) for mounting orientation axis vertical
- Maximum dynamic torque; 0.8 Ncm

ANR101/RES**;**

- Clockwise and counterclockwise – 360 degrees endless in both directions
- Maximum drive velocity ; 30 degrees per second
- Resolution; 6 μ degrees
- Size; 30*30*17.5 mm
- Weight; 36g
- Maximum load; 1N (100g) for mounting orientation axis vertical
- Maximum dynamic torque; 0.8 Ncm

ANRv101/RES**;**

- Clockwise and counterclockwise – 360 degrees endless in both directions
- Maximum drive velocity ; 30 degrees per second
- Resolution; 6 μ degrees
- Size; 33 x 33 x 15.6 mm
- Weight; 37g
- Maximum load; 0.5N (50g) for mounting orientation axis vertical
- Maximum dynamic torque; 0.8 Ncm

ANRv220RES**;**

- Clockwise and counterclockwise – 360 degrees endless in both directions
- Maximum drive velocity ; 30 degrees per second

- Resolution; 6 µ degrees
- Size; 27 x 30 x 12 mm
- Weight; 38g
- Maximum load; 1N (100g) for mounting orientation axis vertical
- Maximum dynamic torque; 1 Ncm

/NUM ... closed-loop encoder based on an optoelectronic encoder
/RES ... closed-loop encoder based on a resistive encode

The configuration in Figure 4.16 can be sustained by selection of different positioners listed above. A quotation for two ANR101/NUM is requested from Attocube which is given in Figure 4.17.

Pos.	Item-No	Item Description	Quantity	Price	Amount
1	1002550	**ANR101/NUM/RT - rotator (360° endless)**	2,00 pcs.	2.430,00	4.860,00
2	1003063	**ANC350/3/NUM/RT Piezo Motion Controller** for closed loop control of up to 3 attocube positioners with /NUM encoders incl. 3 positioner connection cables, incl. 1 USB cable, incl. 1 country specific mains cable	1,00 pcs.	7.900,00	7.900,00
Optional Item (price not included in Grand Total)					
3	*1004201*	*ANC350 Ethernet interface activation code*	*1,00 pcs.*	*950,00*	*950,00*
					EUR 12.760,00

Figure 4.17 *Quotation from Attocube*

The overall package includes 2 rotary positioners and one piezo motion controller with total price of 12.760 euros without adding the optional Ethernet interface for controller which is 950 euros. Moreover, in this price the connecting elements were not covered since they just provide the positioners.

4.4.2 Micronix

Another firm which provides rotary positioners is Micronix. Their product PR-20 has the following properties;

- Rotation unlimited both clockwise and counter clockwise
- Maximum drive velocity ; 15 degrees per second
- Resolution; 500 µ degrees
- Size; 20*20*12 mm
- Weight; 13g

- *Fr*; 2N , *Fz*; 5N, *Mr*; 0.2 Nm, *Mz*; 0.01Nm

Where *Fr, Fz, Mr, Mz* stands for;

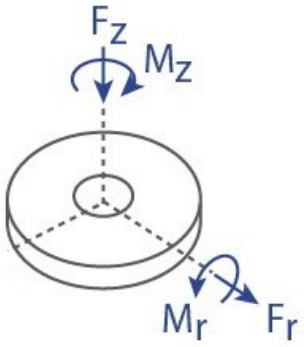

Figure 4.18 *Force and torque symbols on positioner [60]*

The offer that Micronix proposed was 1550 dollars for each rotary positioner and 4240 dollars for motion modular controller. Moreover, they requested 250 dollars per each connection element. With the PR20 rotary positioner 8 brackets are needed which meant 2000 dollars more. Furthermore, the needed torque and force for the first rotary positioner is not sufficient.

4.4.3 Smaract

The last candidate was Smaract which was also mentioned in previous chapter. They offer various rotary positioners with different features. Considering the force and torque limitations, two rotary positioners are found to be capable of forming the configuration in Figure 4.16. The features of SR-2013 and SR-2812 are given below [57];

SR-2013-S;

- Rotation unlimited
- Maximum drive velocity; 45 degrees per second
- Resolution; 25 µ degrees
- Size; 20*25*10.2 mm
- Weight; 10g
- Allowable load; 0.5N (50g)
- Blocking Torque; 0.5 Ncm

SR-2812-S;

- Rotation unlimited
- Maximum drive velocity; 45 degrees per second
- Resolution; 25 µ degrees
- Size; 37.5*30*12 mm
- Weight; 35g
- Blocking Torque; 3 Ncm

Both of the rotary positioners fulfill all of the requirements, one SR-2013-S and one SR-2812-S are proposed instead of selecting two of SR-2013-S since 0.5 Ncm blocking torque of SR-2013-S is smaller than 0.70 Ncm which is required for the first rotary positioner. The offer that is given by the Smaract is shown in Figure 4.19.

Pos.	Item	Description	Quantity	Unit Price [€]	Total Price [€]
1.	SR-2812-S	Rotary positioner with unlimited rotation and integrated sensor, precision ceramic bearing, hollow shaft (9 mm inner diameter), top plate electrically insulated from rest of positioner, Teflon-insulated wires in shielding braid	1 pcs.	2,380.00	2,380.00
2.	SR-2013-S	Rotary positioner with unlimited rotation, integrated nanosensor, precision ceramic bearing, top plate electrically insulated from rest of positioner,	1 pcs.	2,250.00	2,250.00
3.	SCE-CN	Planar connecting element between SLC-1730/SLC-1740 and first rotary positioner	1 pcs.	180.00	180.00
4.	SCE-RN	Rectangular connecting element between rotary positioners	1 pcs.	250.00	250.00
5.	SCE-F	Front connecting element holder for SG-06 gripper	1 pcs.	250.00	250.00
6.	SCE-F	Front connecting element holder for SG-1730 gripper	1 pcs.	250.00	250.00
7.	SCS	complete system configuration and assembly with cabling and final testing	1	500.00	500.00
				Intermediate sum of total prices	**€ 6,060.00**

Pos.	Item	Description	Quantity	Unit Price [€]	Total Price [€]
8.	CABLES	Cable lengths Positioner - Sensor Module: 60 cm	1	0.00	0.00
9.	PACKSHIP-FIN	packing and shipping (Finland, uninsured)	1	45.00	45.00
				Total net amount	**€ 6,105.00**
				VAT 0%	€ 0.00*
				Total gross amount	**€ 6,105.00**

Figure 4.19 *Quotation from Smaract*

As seen from the quotation the total price is 6105 euros which includes two rotary positioners, connection elements for both of the platforms, complete testing cables and shipping.

4.5 Analyze and Select a Solution

After generating multiple solutions, their features and prices are summed up in Table 4.1 where blue color means the feature fulfills the requirements and red color means the feature does not fulfill the requirements.

Table 4.1 *Possible commercial products with specifications*

Company-Product	**Travel**	**Maximum Drive velocity**	**Resolution**	**Size (mm)**	**Weight (grams)**	**Allowable load (N)**	**Price**
Requirements	180 deg CW and CCW rotation	18 (deg/s)	0.1 deg	-	50 grams without connecting elements	-	-
Attocube - ANR101/NUM (number of items; 2)	360 deg unlimited	30 (deg/sec)	0.1µ deg	30*30*18	45.5*2	1	12760 with controller
Micronix; PR-20 (number of items; 2)	360 deg unlimited	15(deg/sec)	500 µ deg	20*20*12	13*2	Insufficient	7790 dollars including connecting elements and controller
Smaract; SR 2013	360 deg unlimited	45 (deg/sec)	25 µ deg	20*25*10.2	10+(35)	0.5	6105 euros including connecting elements without controller
Smaract; SR-2812	360 deg unlimited	45 (deg/sec)	25 µ deg	37.5*30*12	35+(10)	3	

Attocube`s ANR101/NUM was eliminated since its price was higher than other rotary positioner producers. Micronix was not selected since PR-20 cannot provide enough torque and force for the first rotary positioner. Smaract`s SR-2013 and SR-2812 rotary positioners are selected as the best solution. Their specifications satisfy every requirement that are discussed previously. Moreover, many other components were bought from Smaract in the past and MST group is familiar with their product`s quality.

The new rotary positioners also require a MCS controller. Since there is no free space on the current MCS, a new one is needed. Thus a new controller is bought which

is second hand and cheaper than the controllers in the market. The channels of XY table is connected to the new controller which has 3 channels and the rotary positioners are connected to the old controller, to channels which became free after connecting XY table to the new controller.

4.6 Test and Implement Solution

After selecting the rotary positioners, the basic sketch in Figure 4.16 is modified with the help of Smaract according to the selected positioners and connecting elements. The modified versions can be seen in Figures 4.19 and 4.20.

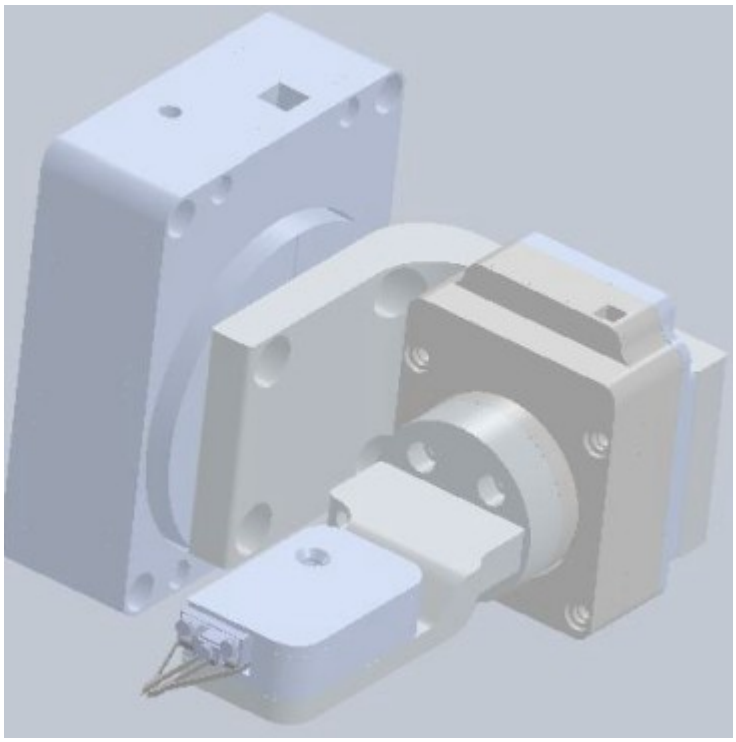

Figure 4.19 *Configuration of rotary positioners for Microrobotic Platform 1*

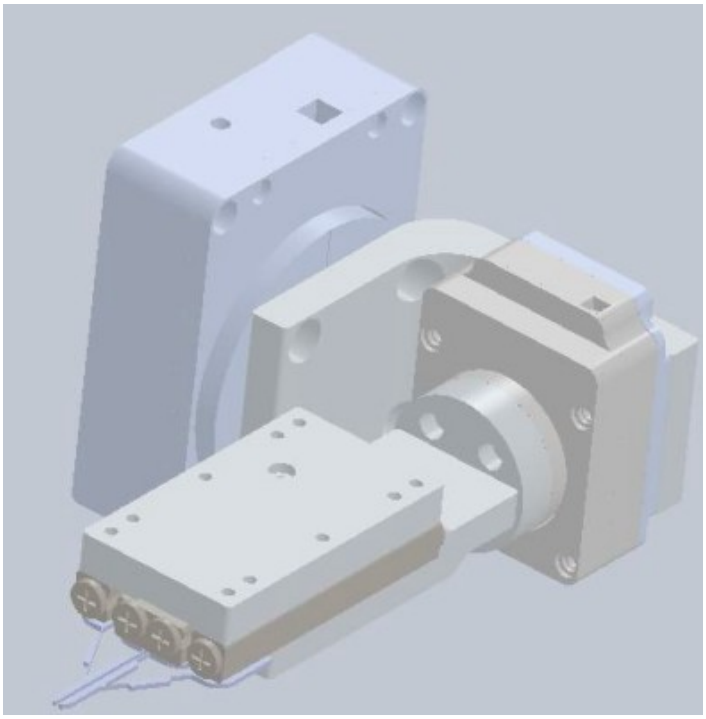

Figure 4.20 *Configuration of rotary positioners for Microrobotic platform 2*

In order to test and simulate the configuration, the whole MP1 is also modelled in Catia (Computer Aided Three-dimensional Interactive Application, multi-platform CAD/CAM/CAE commercial software) and the configuration in Figure 4.19 is added. Moreover, simulation using Delmia (digital manufacturing and production software) is done to see the actual movement capabilities of the system. Three applications of microrobotic platform which are flexibility measurement, IPF shear strength measurement and elongation of single fiber measurement are simulated from beginning to the end. The simulations showed that the solution can fulfill all the requirements defined before. One snapshot from the simulation is given in Figure 4.21.

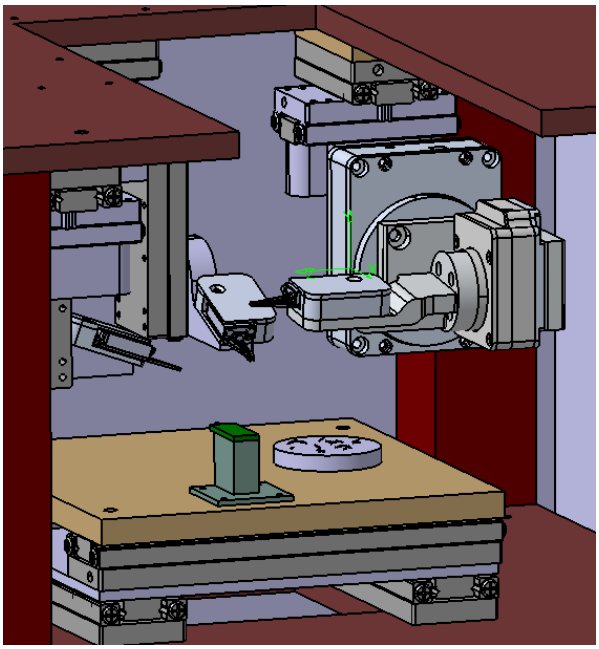

Figure 4.21 *Snapshot from simulation*

Although the simulation was done for the first microrobotic platform, the new devices are assembled to the second microrobotic platform. The addition of the new positioners and the connection elements between the gripper and the third linear positioner has changed the structure. At home position, the gripper must stay at the same place as before so that the workspace of the microgripper will not be changed. In order to preserve the workspace of the microgripper, a new attachment part is designed for the second microrobotic platform which can be seen at Figure 4.22.

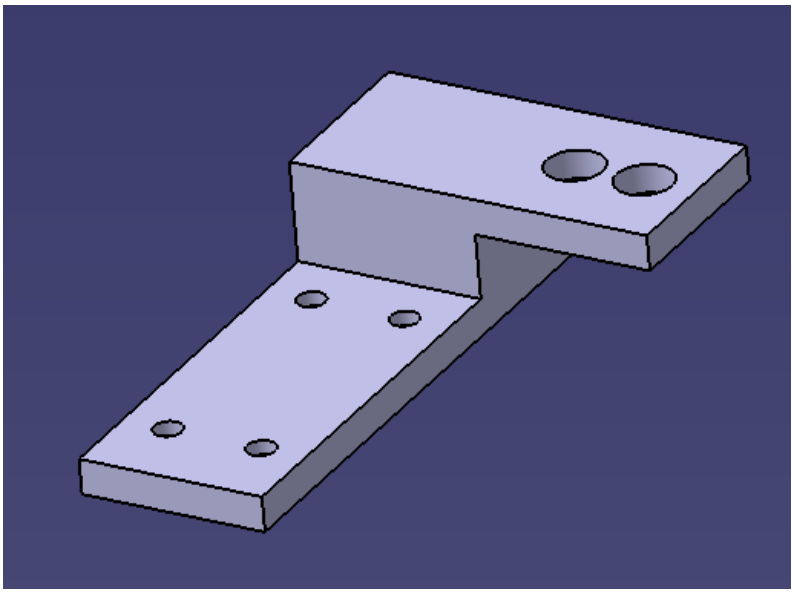

Figure 4.22 *New attachment part for second platform*

Once the designed attachment part is manufactured, the devices are assembled to the second microrobotic platform. The manufactured part (between the first linear positioner and the main frame that carries micromanipulator) can be seen in Figure 4.23 and the overall assembly can be seen in Figure 4.24.

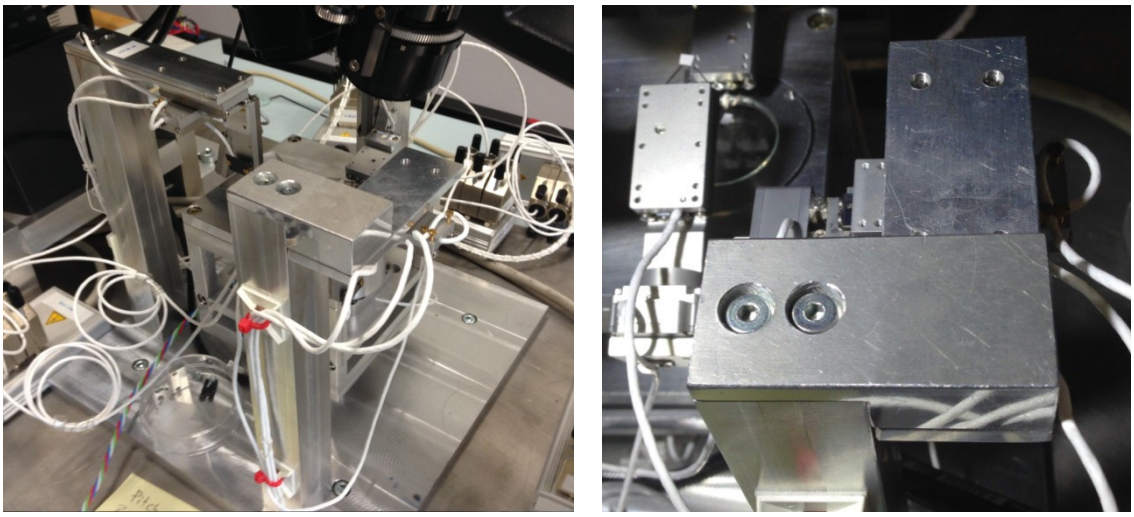

Figure 4.23 *Assembly of new devices*

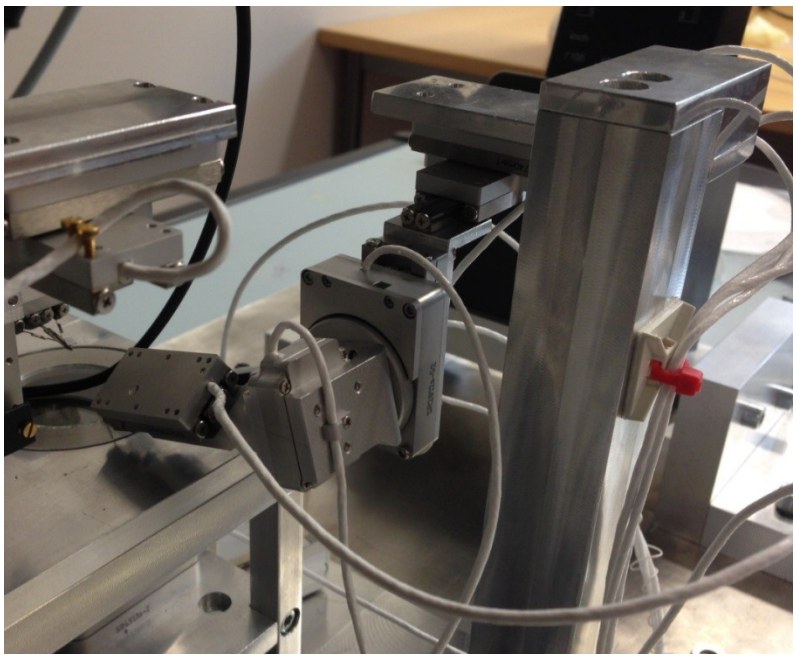

Figure 4.24 *Assembly of new devices*

The integration of new devices to control software and user interface is done by Mathias Von Essen. He also trained the thesis worker on how to use the system. The tests and implementation of the solution is also continued with the calculation of forward kinematics which will be discussed in Chapter 5.

4.7 Summary

In Chapter 4, the design process is explained in the concept of engineering design process. The EDP steps are walked through step by step. Firstly, the main problem is defined clearly and the side requirements are clarified. Then multiple solutions are generated in order to select the most suitable one. The generated solutions are analyzed and discussed in detail and the design with rotary positioners is selected as the best solution. After analyzing and selecting the solution, simulations are elucidated.

The microrobotic platform is required to be modified in the pursuit of three goals which are i) improving the shear mode bond strength measurements by solving peeling mechanism problem, ii) facilitating the Z-directional bond strength measurement by revealing information on which fiber is on top and iii) allowing untwisting twisted fibers. In order to achieve these three goals, several devices such as spherical actuators, pre-made microrobots or rotary positioners can be used but rotary positioners are the most suitable devices for this application. After selecting a solution, a basic sketch of the model is drawn. Out of many rotary positioner manufacturer companies, Smaract's offer is accepted and basic Catia model is redrawn. Moreover, simulation with Delmia is done in order to ensure the solution's capabilities. Finally, assembly of the devices is illustrated.

5. DEMONSTRATION OF COMPLETED SYSTEM

This chapter describes the implemented tests using the modified platform. Section 3.1 examines the forward kinematics, Section 3.2 compares the simulated forward kinematics with the real system and Section 3.3 encompasses the discussion.

5.1 Forward Kinematics

Forward kinematics of the system is calculated in order to compare the movements of the real system with the ideal system. The first step for calculating forward kinematics was to form the Denavit-Hartenberg (DH) table. The modified manipulator, shown in Figure 5.1, is modeled in Catia in order to find the DH parameters.

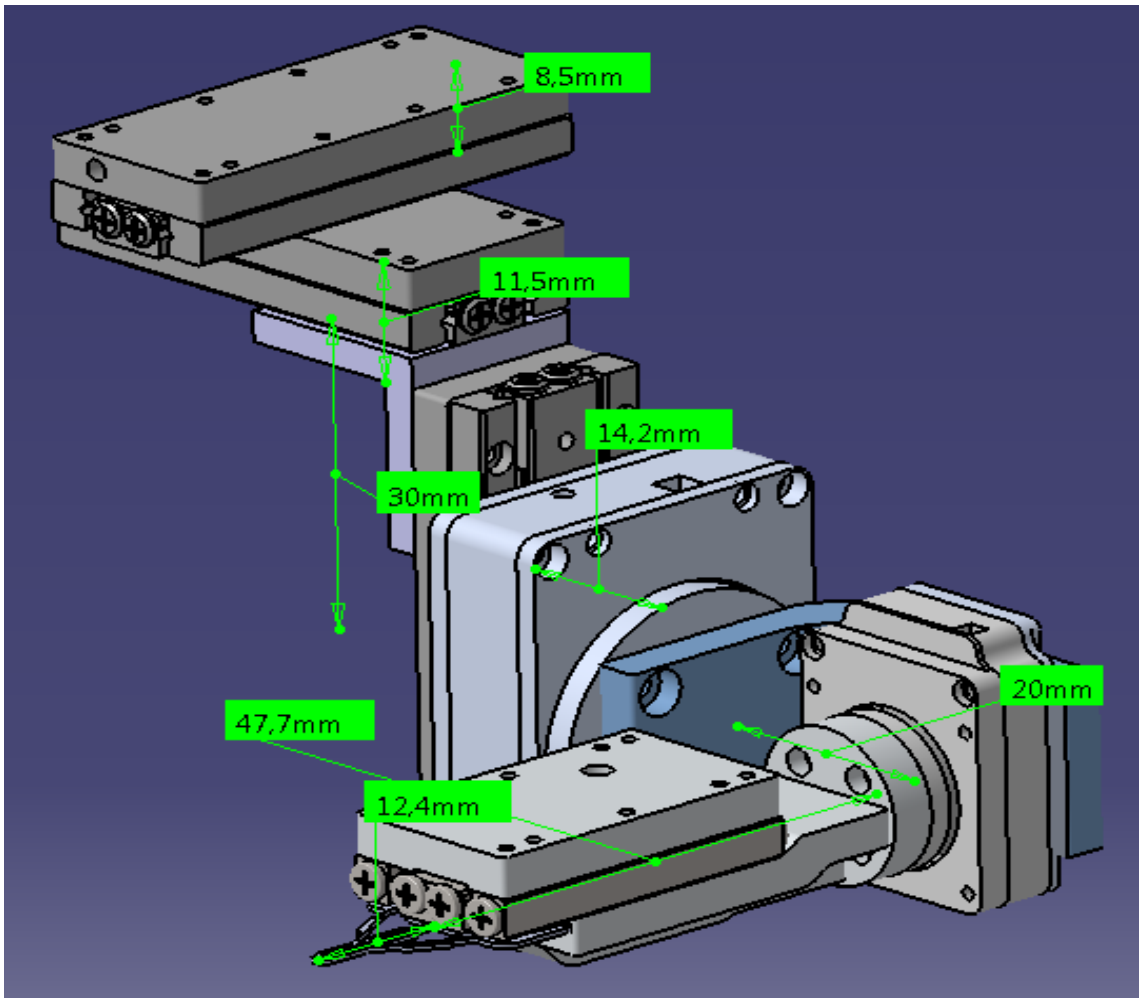

Figure 5.1 *Modified manipulator*

The link frame assignment can be seen in Figure 5.2.

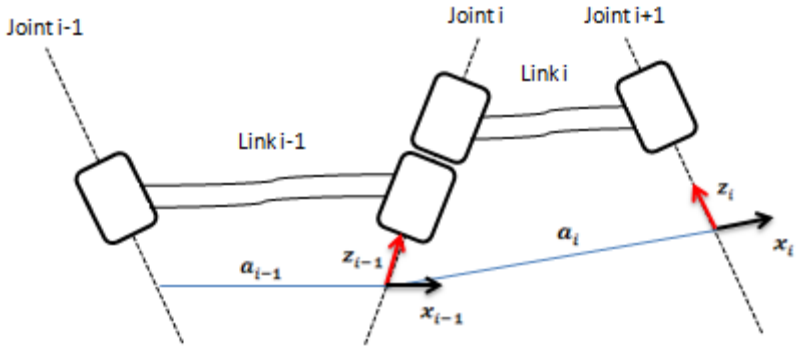

Figure 5.2 *Link frame assignment based on standard DH convention*

Four parameters are defined in Table 5.1 according to standard Denavit-Hartenberg notation.

Table 5.1 *Definition of four parameters [61]*

a_i	Distance from z_{i-1} to z_i along x_i
d_i	Distance from origin (i-1) to x_i along z_{i-1}
θ_i	Angle between x_{i-1} and x_i about z_{i-1}
α_i	Angle from z_{i-1} to z_i about x_i

The transformation matrix for each link can be found by using the defined parameters. The transformation matrix between two links can be found like;

$$ {}^{i-1}_{i}T = \begin{bmatrix} \cos\theta_i & -\sin\theta_i * \cos\alpha_i & \sin\theta_i * \sin\alpha_i & a_i * \cos\theta_i \\ \sin\theta_i & \cos\theta_i * \cos\alpha_i & -\cos\theta_i * \sin\alpha_i & a_i * \sin\theta_i \\ 0 & \sin\alpha_i & \cos\alpha_i & d_i \\ 0 & 0 & 0 & 1 \end{bmatrix} $$

Based on the transformation matrix above, transformation matrixes are formed like;

$$ {}^{Roll}T = \begin{bmatrix} \cos\theta_1 & -\sin\theta_1 * \cos\alpha_1 & \sin\theta_1 * \sin\alpha_1 & a_1 * \cos\theta_1 \\ \sin\theta_1 & \cos\theta_1 * \cos\alpha_1 & -\cos\theta_1 * \sin\alpha_1 & a_1 * \sin\theta_1 \\ 0 & \sin\alpha_1 & \cos\alpha_i & d_1 \\ 0 & 0 & 0 & 1 \end{bmatrix} $$

$$ {}^{Pitch}T = \begin{bmatrix} \cos\theta_2 & -\sin\theta_2 * \cos\alpha_2 & \sin\theta_2 * \sin\alpha_2 & a_2 * \cos\theta_2 \\ \sin\theta_2 & \cos\theta_2 * \cos\alpha_2 & -\cos\theta_2 * \sin\alpha_2 & a_2 * \sin\theta_2 \\ 0 & \sin\alpha_2 & \cos\alpha_2 & d_2 \\ 0 & 0 & 0 & 1 \end{bmatrix} $$

The ideal values of four parameters for both links are given in Table 5.2 which are obtained from Figure 5.1.

Table 5.2 *Ideal values of four parameters for roll and pitch links*

Parameter	**Value**	**Parameter**	**Value**
a_1	0	a_2	0
d_1	20	d_2	0
θ_1	Variable	θ_2	Variable
α_1	$\pi/2$	α_2	$-\pi/2$

Once transformation matrixes are formed for rotary positioners, a transformation matrix for base translation and rotation is formed.

$$^{Base}T = \begin{bmatrix} 1 & 0 & 0 & 0 \\ 0 & 1 & 0 & 20+8.5+14.2 \\ 0 & 0 & 1 & -(30+8.5+11.5) \\ 0 & 0 & 0 & 1 \end{bmatrix} * {}^{Mz}R * {}^{My}R * {}^{x}R * {}^{y}R * {}^{z}R$$

^{Base}T matrix firstly has a translation which moves all the system to a defined point. Then the overall system is rotated around Z-axis with ^{Mz}R rotation matrix and rotated around Y-axis with ^{My}R in order to provide proper orientation of the manipulator in Matlab. After setting the orientation and position of initial point of the system (center of rotation of the roll in this case) three more rotation matrixes are defined which are ^{x}R, ^{y}R, ^{z}R. ^{x}R defines how many degrees is the overall system rotated around X-axis, ^{y}R defines how many degrees is it rotated around Y-axis and ^{z}R defines how many degrees is it rotated around Z-axis. The rotation matrixes used to form base transformation matrix are shown below;

$$^{Mz}R = \begin{bmatrix} \cos\pi/2 & -\sin\pi/2 & 0 & 0 \\ \sin\pi/2 & \cos\pi/2 & 0 & 0 \\ 0 & 0 & 1 & 0 \\ 0 & 0 & 0 & 1 \end{bmatrix}$$

$$^{My}R = \begin{bmatrix} \cos\pi/2 & 0 & \sin\pi/2 & 0 \\ 0 & 1 & 0 & 0 \\ -\sin\pi/2 & 0 & \cos\pi/2 & 0 \\ 0 & 0 & 0 & 1 \end{bmatrix}$$

$$^{x}R = \begin{bmatrix} 1 & 0 & 0 & 0 \\ 0 & \cos\vartheta_1 & -\sin\vartheta_1 & 0 \\ 0 & \sin\vartheta_1 & \cos\vartheta_1 & 0 \\ 0 & 0 & 0 & 1 \end{bmatrix}$$

$$ {}^{y}R = \begin{bmatrix} \cos\vartheta_2 & 0 & \sin\vartheta_2 & 0 \\ 0 & 1 & 0 & 0 \\ -\sin\vartheta_2 & 0 & \cos\vartheta_2 & 0 \\ 0 & 0 & 0 & 1 \end{bmatrix} $$

$$ {}^{z}R = \begin{bmatrix} \cos\vartheta_3 & -\sin\vartheta_3 & 0 & 0 \\ \sin\vartheta_3 & \cos\vartheta_3 & 0 & 0 \\ 0 & 0 & 1 & 0 \\ 0 & 0 & 0 & 1 \end{bmatrix} $$

Where $\vartheta_1, \vartheta_2, \vartheta_3$are variables that are used for rotation of system around X,Y and Z axes. Lastly, another matrix is formed to define the end point of the gripper jaw.

$$ {}^{Gripper}T = \begin{bmatrix} 1 & 0 & 0 & x \\ 0 & 1 & 0 & y \\ 0 & 0 & 1 & z \\ 0 & 0 & 0 & 1 \end{bmatrix} $$

Gripper matrix defines the distance from the center point of pitch rotation to the midpoint of gripper jaw tip. In ideal case variables x and z are zero and y is 47.7 + 12.4 as can be seen from Figure 5.1.

Once transformation matrixes for base, rotations and gripper jaw tip are formed they are multiplied in order to get the overall transformation matrix as follows;

$$ {}^{Overall}T = {}^{Base}T * {}^{Roll}T * {}^{Pitch}T * {}^{Gripper}T $$

In the ideal case there are no offsets on θ_1 or θ_2, DH parameters remains exactly the same as in Table 5.2, midpoint of the gripper jaw has no offset on X or Z-axis but it has 60.1 mm on Y-axis, also the overall system has no rotation around X,Y or Z-axis. The ideal values for variables can be seen all together in Table 5.3.

Table 5.3 *Ideal values of all parameters in overall transformation matrix*

Parameter	**Ideal Value**
θ_1	Variable
θ_2	Variable
α_1	$\pi/2$
α_2	$-\pi/2$
a_1	0
a_2	0
d_1	20 mm
d_2	0
x	0
y	60.1 mm

z	0
ϑ_1	0
ϑ_2	0
ϑ_3	0

The calculation of forward kinematics is done in Matlab by using the robotic toolbox [61]. Once forward kinematics was calculated, manipulator is simulated at several points. These points are also checked with the Catia model. Moreover, the influences of alignment errors are simulated. In Figure 5.1, each positioner is perfectly aligned, however in reality there are some alignment errors between each positioner. Alignment errors add offsets to the ideal values of parameters which were given in Table 5.3. For instance, in ideal case the tip of the gripper jaw is perfectly aligned with the center of pitch rotation but in reality there are offsets in X and Z axes which results in totally different motion of the end point. In order to understand the sources of errors and their influence, offsets are added to the ideal parameters and their influences are analyzed. The analysis of alignment errors are shown in Table 5.4.

Table 5.4 *Influence of possible alignment errors*

<table>
<tr><td>Parameters</td><td>Ideal value</td><td>Offset in the ideal value</td><td colspan="3">Resultant Error</td></tr>
<tr><td rowspan="3">$\theta_1 = \theta_{1ideal} + \theta_{1offset}$</td><td rowspan="3">$\theta_{1ideal} = 0deg$</td><td rowspan="3">$\theta_{1offset} = 1\ deg$</td><td>X-axis</td><td>Y-axis</td><td>Z-axis</td></tr>
<tr><td>0 mm</td><td>0.0094 mm</td><td>1.0803 mm</td></tr>
<tr><td colspan="3">1 deg- rotation error around X-axis</td></tr>
<tr><td>$\theta_2 = \theta_{2ideal} + \theta_{2offset}$</td><td>$\theta_{2ideal} = 0deg$</td><td>$\theta_{2offset} = 1\ deg$</td><td colspan="3">1 degree rotation error around Y-axis (position unchanged)</td></tr>
<tr><td>$\alpha_1 = \alpha_{1ideal} + \alpha_{1offset}$</td><td>$\alpha_{1ideal} = \frac{\pi}{2}$</td><td>-</td><td colspan="3">Used just for creating the structure of the system in Matlab, thus it is not a source of error</td></tr>
<tr><td>$\alpha_2 = \alpha_{2ideal} + \alpha_{2offset}$</td><td>$\alpha_{2ideal} = -\frac{\pi}{2}$</td><td>$\alpha_{2offset} = 1\ deg$</td><td colspan="3">Defines the initial orientation of the gripper, 1 degree rotation error in pitch (position unchanged)</td></tr>
<tr><td rowspan="2">$a_1 = a_{1ideal} + a_{1offset}$</td><td rowspan="2">$a_{1ideal} = 0deg$</td><td rowspan="2">$a_{1offset} = 1\ deg$</td><td>X-axis</td><td>Y-axis</td><td>Z-axis</td></tr>
<tr><td>0 mm</td><td>0 mm</td><td>1 mm(constant)</td></tr>
</table>

<table>
<tr><td>a_2
$= a_{2ideal}$
$+ a_{2offset}$</td><td>a_{2ideal}
$= 0deg$</td><td>-</td><td colspan="3">Defines the distance from second rotation`s center to gripper`s end point on Z-axis which is already done by x, y, z variables, thus it is not changed</td></tr>
<tr><td rowspan="2">d_1
$= d_{1ideal}$
$+ d_{1offset}$</td><td rowspan="2">d_{1ideal}
$= 20mm$</td><td rowspan="2">$d_{1offset}$
$= 1\ mm$</td><td>X-axis</td><td>Y-axis</td><td>Z-axis</td></tr>
<tr><td>1
mm(constant)</td><td>0
mm</td><td>0
mm</td></tr>
<tr><td>d_2
$= d_{2ideal}$
$+ d_{2offset}$</td><td>d_{2ideal}
$= 0mm$</td><td>-</td><td colspan="3">Defines the distance from second rotation`s center to gripper`s end point on Y-axis which is already done by x, y, z variables, thus it is not changed</td></tr>
<tr><td>x
$= x_{ideal}$
$+ x_{offset}$</td><td>x_{ideal}
$= 0\ mm$</td><td>x_{offset}
$= 1mm$</td><td colspan="3">Circular motion error with 1 mm radius during pitch`s 360 degree motion-no rotation error</td></tr>
<tr><td rowspan="3">y
$= y_{ideal}$
$+ y_{offset}$</td><td rowspan="3">y_{ideal}
$= 60.1$</td><td rowspan="3">y_{offset}
$= 1mm$</td><td>X-axis</td><td>Y-axis</td><td>Z-axis</td></tr>
<tr><td>0
mm</td><td>1
mm</td><td>0
mm</td></tr>
<tr><td colspan="3">No rotation error- results in significant error in both X, Y and Z- axes when roll rotation changes, for the pitch, error in Y axis remain as offset</td></tr>
<tr><td>z
$= z_{ideal}$
$+ z_{offset}$</td><td>z_{ideal}
$= 0\ mm$</td><td>z_{offset}
$= 1\ mm$</td><td colspan="3">Circular motion error with 1 mm radius during pitch`s 360 degree motion-no rotation error</td></tr>
<tr><td rowspan="3">ϑ_1
$= \vartheta_{1ideal}$
$+ \vartheta_{1offset}$</td><td rowspan="3">ϑ_{1ideal}
$= 0\ mm$</td><td rowspan="3">$\vartheta_{1offset}$
$= 1\ deg$</td><td>X-axis</td><td>Y-axis</td><td>Z-axis</td></tr>
<tr><td>0
mm</td><td>0.0094
mm</td><td>1.0803
mm</td></tr>
<tr><td colspan="3">Has same effect as adding 1 deg offset to roll.</td></tr>
<tr><td rowspan="2">ϑ_2
$= \vartheta_{2ideal}$
$+ \vartheta_{2offset}$</td><td rowspan="2">ϑ_{2ideal}
$= 0\ mm$</td><td rowspan="2">$\vartheta_{2offset}$
$= 1\ deg$</td><td>X-axis</td><td>Y-axis</td><td>Z-axis</td></tr>
<tr><td>0.003
mm</td><td>0
mm</td><td>0.3490
mm</td></tr>
<tr><td rowspan="2">ϑ_3
$= \vartheta_{3ideal}$
$+ \vartheta_{3offset}$</td><td rowspan="2">ϑ_{3ideal}
$= 0\ mm$</td><td rowspan="2">$\vartheta_{3offset}$
$= 1\ deg$</td><td>X-axis</td><td>Y-axis</td><td>Z-axis</td></tr>
<tr><td>1.0834
mm</td><td>0.3396
mm</td><td>0
mm</td></tr>
</table>

5.2 Comparison of Ideal system and Real system

Three measurements are done in order to compare the behavior of the real system with the ideal system that is created in Matlab.

5.2.1 Image Processing

The measurements are done using image processing of recorded images with the help of Juha Hirvonen. As mentioned in Section 4.1.5, the rotary positioners are assembled to the second microrobotic platform. MP2 has two cameras (Manta GS-501, Allied Vision Technologies Inc.) which include motorized optics (12x Zoom, Zoom 7000, Navitar Inc.) [63]. Two cameras are used for visual feedback which can be seen in Figure 5.3.

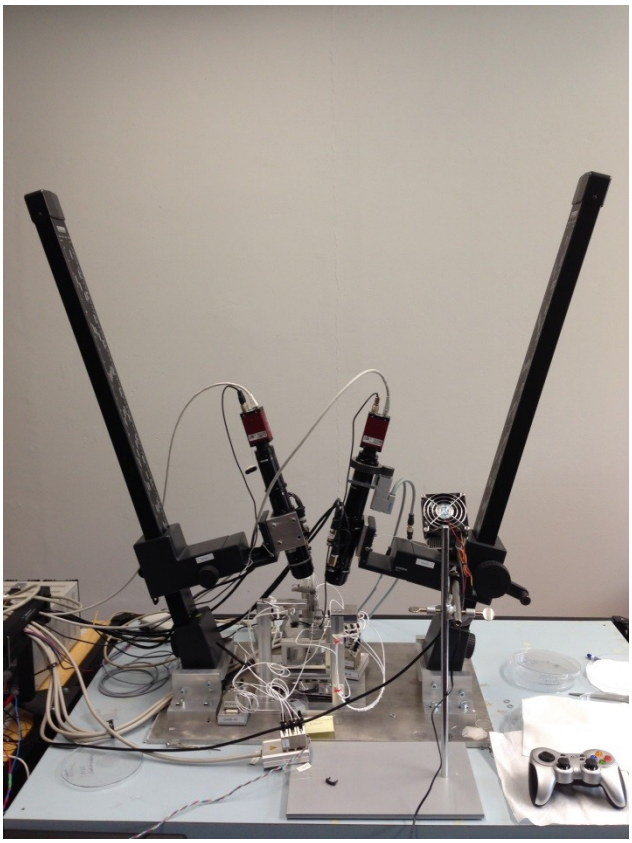

Figure 5.3 *Cameras of the second microrobotic platform*

Both of the cameras are inclined backwards with 15 degrees. Image processing starts with the calibration. For this purpose, a grid pattern is placed on the gripper jaw and proper illumination is achieved as well as the focus with both of the cameras. The image coordinates and the manipulator coordinates are related to each other by tracking the grid pattern along a trajectory which consists of 27 different positions. The location of the grid is realized in the trajectory points and then they are "mapped against the manipulator's position in its own coordinate system" [63]. Once the matrixes of the cameras are determined, the metric 3D coordinate system is formed from the image point-image point correspondences. After that, in order to assign the created coordinate sys-

tem to the tip of microgripper jaw, offsets on X, Y and Z axes which define the distance between grid pattern and the tip of the gripper jaw are added to the coordinates [63]. The grid pattern that is tracked can be seen in Figure 5.4.

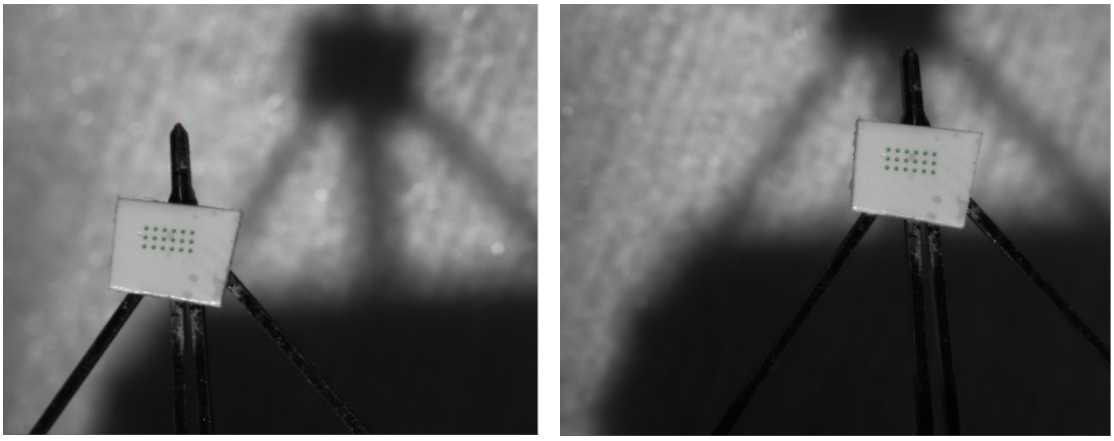

Figure 5.4 *Images from cameras, east camera on left and west camera on right*

Once the calibration is completed, human operator controls the positioners through user interface and achieves the desired position and orientation of the gripper. After that, images are obtained by using user interface. Finally, the image processing algorithm processes the obtained images and gives the X, Y and Z coordinates of the tip of the gripper jaw based on the coordinate system created during calibration.

5.2.2 Measurements

In the real system there are some sources of errors which are manufacturing tolerances, alignment errors due to torques that are applied while tightening the screws and the gripper jaw assembly. Firstly, the parameters in the transformation matrix for forward kinematics are determined from the Catia model which are perfect. Thus, the manufacturing tolerances cause errors by adding some offsets to these parameters. Secondly, the assembly is done by a human who tightens the screws. Since the screws are tightened with different torques again the real system differs from the ideal one and the ideal parameters changes. Lastly, the gripper jaw must be assembled in a way that it must be perfectly parallel to the microgripper but the holes for screws are not totally closed which means, achieving this parallel assembly depends totally on human skills. The gripper jaw assembly is shown in Figure 5.5.

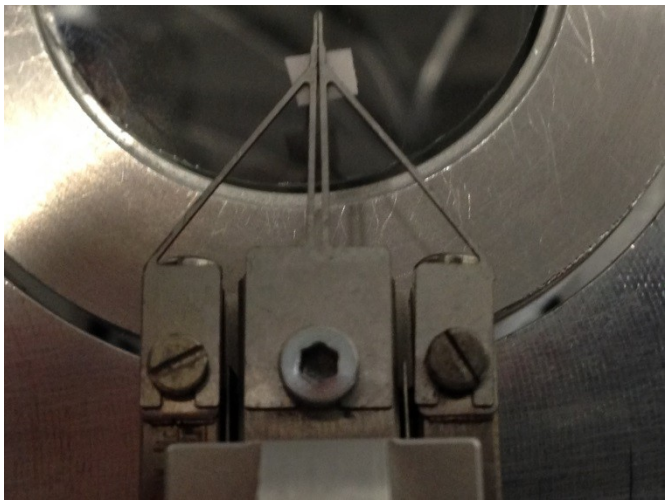

Figure 5.5 *Gripper jaw assembly*

After the 3D coordinate system creation using image processing, three measurements are done. In the first measurement, the first rotary positioner is remained unchanged and the second rotary positioner moved from -15 degrees to 15 degrees with 1 degree steps. First measurement is carried out in order to compare the pitch rotation of the real system with the ideal system. Roll rotation remained constant in this measurement so that the error in motion during pure pitch rotation can be seen. In the second measurement the first rotary positioner moved from -2 degrees to 2 degrees with 0.5 degree steps and the second rotary positioner is remained unchanged. Second measurement is carried out in order to compare the roll rotation of the real system with the ideal system. Pitch rotation remained constant in this measurement so that the error in motion during pure roll rotation can be seen. Finally in the third measurement, the first rotary positioner is moved from 0 degrees to 2 degrees and the second rotary positioner is moved from 0 degree to 10 degrees in one step. Third measurement is carried out in order to reveal the errors in motion when both roll and pitch rotations are changed. By changing one rotation at a time during first two measurements, revealing the sources of errors became easier.

In each step, the coordinates of the tip of the microgripper jaw is obtained by image processing as discussed in Section 5.2.1. After that, the same movements are also repeated with the ideal system in Matlab and the results are compared at axis level for each measurement. The detailed comparison of results for each axis and for each measurement can be seen in the appendix and a summary of the results can be seen in Table 5.5.

Table 5.5 *Comparison of measurements with ideal system*

All in micrometers		Measurements	
	Measurement 1	Measurement 2	Measurement 3
Average Error in X axis	52.6	9.75	39
Max Error in X axis	107	15	
Average Error in Y axis	0.43	55.625	63.6
Max Error in Y axis	2	97	
Average Error in Z axis	49.6	99.9	136.5
Max Error in Z axis	78	195	

The error is calculated as follows. First, the distance from the initial point to points at each step is calculated with image processing values and then the same calculations are done with ideal Matlab values. After that, these values at each step are subtracted from each other which are called the "error". In each step, depending on the distance covered, the error changes. Average errors and maximum errors can be also found in Table 5.5.

In order to estimate the errors, the ideal parameters were modified in the simulation model such that the behavior of the forward kinematics will match with the behavior of the real system. Each measurement is analyzed one by one in order to find the offsets in the parameters. In Table 5.6, the errors at the Y-axis in the second measurement (roll moves from -2 degrees to 2 degrees with 0.5 degrees step and pitch remains unchanged) is given.

Table 5.6 *Errors at Y-axis in Measurement 2.*

	All in micrometers		
Angle Change (deg)	Measured Displacement	Simulated Displacement	Error Displacement
-2 to -1.5	29	16	13
-2 to -1	52	27,4	24,6
-2 to -0.5	72	34,3	37,7
-2 to -0	87	36,6	50,4
-2 to 0.5	97	34,3	62,7
-2 to 1	101	27,4	73,6
-2 to 1.5	102	16	86
-2 to 2	97	0	97
		Average	55,625
		Max	97

With the ideal parameters in Matlab, after 4 degrees of rotation from -2 to 2, the tip of microgripper comes to its initial place at Y-axis as expected. This can be seen in Table 5.3 where "-2 to 2" is 0 at the "Simulated Displacement" column. However, if we check the real system values, it is not 0 at the end of the movement. The distance from

the initial point is increasing in every step except the last one. In the ideal case it starts to decrease on the half way when the rotation reaches to the positive side. Out of these results it is concluded that there must be an offset around the X-axis. After this point, an optimal value for offset is found iteratively. Because of this offset around the X-axis, the real system`s initial position is not at -2 degrees at the beginning of the measurement but it is at -3.453 degrees. Thus, the distance between the first point and last point starts to decrease at the last step where rotation reaches to the positive side. This offset around X-axis is illustrated at Figure 5.6 in an exaggerated way.

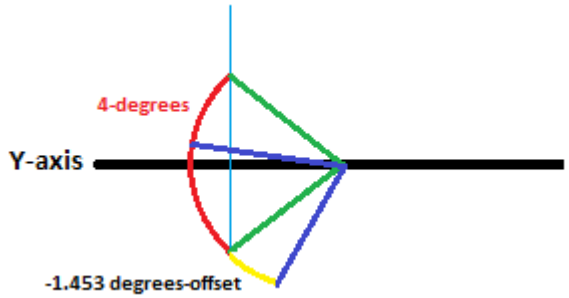

Figure 5.6 *Illustration of offset around X-axis*

After finding the -1.453 degrees offset, the comparison is made once more by also adding the offset to ideal forward kinematics. The results are shown in Table 5.7.

Table 5.7 *Errors at Y-axis in second measurement after adding offset*

	All in micrometers		
Angle Change (deg)	**Measured Displacement**	**Simulated Displacement**	**Error Displacement**
-2 to -1.5	29	28,8	0,2
-2 to -1	52	52,9	-0,9
-2 to -0.5	72	72,2	-0,2
-2 to -0	87	86,7	0,3
-2 to 0.5	97	96,5	0,5
-2 to 1	101	101,4	-0,4
-2 to 1.5	102	101,6	0,4
-2 to 2	97	97	0
		Average error	0,3625

As it is obvious from Table 5.7, the errors decreased significantly after the addition of rotation offset around X-axis. In the same manner, other measurements and the errors in each axis are analyzed and appropriate values for offsets are obtained iteratively. The modified parameters can be found in Table 5.8.;

Table 5.8 *Parameters with ideal and modified values*

Parameter	**Ideal Values**	**Modified Values**
θ_1	Variable	Variable
θ_2	Variable	Variable
α_1	$\pi/2$	$\pi/2$
α_2	$-\pi/2$	$-\pi/2$
a_1	0	0
a_2	0	0
d_1	20 mm	20 mm
d_2	0	0
x	0	-0.2 mm
y	60.1 mm	62.7
z	0	0.15
ϑ_1	0	-1.453 deg
ϑ_2	0	0.22 deg
ϑ_3	0	0

After predicting the offset values, measurement values are compared with the modified forward kinematics as it is done in Table 5.7. The results are shown in Table 5.9.

Table 5.9 *Comparison of measurements with ideal system after adding offsets*

		Measurements (Micron)	
	Measurement 1	**Measurement 2**	**Measurement 3**
Average Error in X axis	3.23	2.6	10.5
Max Error in X axis	8.25	3.9	
Average Error in Y axis	1.3	0	16.9
Max Error in Y axis	2.9	0.36	
Average Error in Z axis	7.17	9.8	22.4
Max Error in Z axis	24.9	19.8	

After the addition of offsets in different parameters, errors are decreased and reduction of errors in percentages are given in Table 5.10.

Table 5.10 *Reduction of errors in percentages*

	Measurement 1	Measurement 2	Measurement 3
Reduction in average error in X-axis	%93.85	%73.33	%73.07
Reduction in maximum error in X-axis	%92.28	%74	
Reduction in average error in Y-axis	-	%100	%73.42
Reduction in maximum error in Y-axis	-	%99.61	
Reduction in average error in Z-axis	%85.54	%90.19	%83.58
Reduction in maximum error in Z-axis	%68.07	%89.84	

5.3 Discussion

In order to understand the behavior of the real system, it has been compared with the behavior of the ideal system and the errors between them have been analyzed in this chapter. Then the sources of errors or offsets in parameters were estimated by analyzing the measurements and offsets were determined iteratively. The errors are reduced in three measurements at minimum %68.07. The errors in Y-axis of first measurement is not decreased but increased approximately 1 micrometers but since the difference is so little it is ignored. One possible explanation for this issue could be the image processing tolerance. The measurement setup and image processing algorithm are also not perfect, thus the measurements also include tolerances. The errors are decreased significantly but there are still other parameters that can be modified to decrease the errors further. For instance in the modified parameters, ϑ_3 remained unchanged in Table 5.8. However, there must be an offset also for it. Moreover, the predicted offsets are not the exact values but they are just approximations on real offsets.

The problems discussed above means, the errors can be decreased even more by applying proper kinematic calibration methods which use algorithms that approximates each parameter by analyzing the errors.

6. SUMMARY, CONCLUSIONS AND FUTURE WORK

In this chapter, summary, conclusion and future work regarding this thesis will be discussed.

6.1 Summary

Addition of two rotational degrees of freedom to microrobotics platform was required in order to solve problems and increase the platform`s performance during the shear mode and Z-directional mode bond strength measurements. Moreover, the modification was also needed to allow the system to untwist twisted fibers.

Firstly, previous studies and literature regarding the topic were reviewed in order to enhance the knowledge on the context. There was no previous study on Z-directional bond strength measurement at individual fiber bond level. Thus, previous studies regarding the shear mode bond strength were examined.

Wood fiber properties were also studied in order to understand the samples that were worked on. Before starting to select and design the new components and devices, microrobotic platform was examined. Its basic functions, used devices and two measurements were analyzed to be able to offer a proper design for new requirements.

The design process was iterative; it was mostly carried out together with survey and selection of equipment. The requirements were listed carefully and the problem was defined clearly in order to avoid missing any details. Without rushing into a solution, multiple solution options were generated and they were analyzed one by one.

The design that included two rotary positioners from SmartArt was chosen as the final design. The new design was modeled in Catia together with the microrobotic platform. Before implementing the solution, flexibility and shear mode bond breaking measurements were simulated using Delmia to ensure that the proposed solution will fulfill the requirements. As the simulation confirmed the solution, new devices with connection elements were ordered, assembled and integrated with the user interface of microrobotic platform.

Forward kinematics of the modified manipulator was calculated in Matlab. The data simulated with Matlab was compared with values obtained from the real system in order to ensure the capabilities of new devices and to find and eliminate offsets in the system.

6.2 Conclusion

Two rotational degrees of freedom are designed and implemented into microrobotics platform which enhance its capabilities as well as facilitating advanced fiber manipulation. Although modified platform has not been used to perform the shear mode bond strength measurement, Z-directional bond strength measurement or untwisting twisted fibers yet, experiments and measurements showed that rotational degrees of freedom will i) improve the shear mode bond strength measurements by solving peeling mechanism problem, ii) facilitate Z-directional bond strength measurement by revealing information on which fiber is on top and iii) allow untwisting twisted fibers. As expected, real system differed from the ideal one according to measurement results. Before modifying the parameters in the ideal transformation matrix, the errors were relatively high. In three measurements performed, the maximum errors were 107 micrometers at the X-axis, 97 micrometers at the Y-axis and 195 micrometers at the Z-axis. After modifying the parameters, the maximum errors were reduced to 10 micrometers at the X-axis, 17 micrometers at the Y-axis and 25 micrometers at the Z-axis, providing a reduction of 90.65%, 82.47% and 87.17% in errors, respectively.

6.3 Future Work and Development Proposals

First of all, shear mode bond strength and Z-directional both strength measurements must be done by also using the modified microrobotic platform in order to validate the simulation results.

Gripper jaw assembly must be modified since with the current configuration the orientation and positioning of the jaw mostly depends on human skills which is in sufficient in terms of micro-scale applications.

A sensor can be designed and implemented to the system in order to measure the torque required to untwist twisted fibers.

Lastly, although there is a clear reduction in errors discussed in Section 5.3, still proper calibration methods must be applied in order to eliminate all of the offsets.

Apart from future works related to this thesis topic, microrobotics platform and measurements can be also developed with several modifications. Two of them are given below.

A third microgripper with a force sensor must be designed and implemented since gluing process takes too much time during shear mode bond breaking measurements.

The first microrobotic platform`s user interface crashes and closes too often which delays the experiments. This problem is already solved in the second microrobotic platform and it needs to be solved with the first one too.

REFERENCES

[1] Franz J. Schmied, C. Teichert, L. Kappel, U. Hirn, W. Bauer, R. Schennach, "*What Holds Paper Together: Nanometre Scale Exploration of Bonding Between Paper Fibres*", Published at 22 August 2013, Nature Publishing Group, Retrieved from http://www.nature.com/srep/2013/130822/srep02432/full/srep02432.html

[2] Christopher J. Biermann, "*Handbook of Pulping and Papermaking"*, Second Edition, 1996, Elsevier Inc., Total pages 754, pp 1-10

[3] K. V. Joshi, "*A New Technique to Measure Shear Bond Strength*", Master thesis, Australian Pulp and Paper Institute, Department of Chemical Engineering Monash University Australia, 2007, Total pages 118, pp 1-50

[4] Baohua Shen, "*Variation in the Local Structure and Properties of Paper*", Master thesis of Applied Science, Department of Chemical Engineering and Applied Chemist- University of Toronto, June 30 2000, Total pages: 110, Retrieved from https://tspace.library.utoronto.ca/bitstream/1807/15585/1/MQ58719.pdf

[5] C. Ververis, K. Georghiou, N. Christodoulakis, P. Santas, R. Santas, "*Fiber dimensions, lignin and cellulose content of various plant materials and their suitability for paper production*", Industrial crops and products, Volume 19, Issue 3, May 2004, Pages 245–254.

[6] Mikael S. Magnusson, X. Zhang, S. Östlund, "*Experimental evaluation of the interfibre joint strength of papermaking fibres in terms of manufacturing parameters and in two different loading directions*", 2013, Report 523, BiMaC Innovation, KTH Engineering Sciences, Department of Solid Mechanics, SE-100-44 Stockholm, Sweden, Available at: http://www.diva-portal.org/smash/get/diva2:600375/FULLTEXT01.pdf

[7] Anna K. Vainio, H. Paulapuro, "*Interfiber Bonding and Fiber segment Activation in Paper*", Laboratory of Paper and Printing Technology, Helsinki University of Technology, Published on August 2007, BIO Sources 2(3), pp 442-458, Available at: http://www.ncsu.edu/bioresources/BioRes_02/BioRes_02_3_442_458_Vainio_Paulapuro_Interfiber_Bond_Activation.pdf

[8] Robert A. Stratton, Norman L. Colson, "*Dependence of fiber/fiber bonding on some papermaking variables*", Atlanta, June 1990, The Institute of Paper Science and Technology, Total pages 16, Retrieved from https://smartech.gatech.edu/bitstream/handle/1853/2136/tps-357.pdf;jsessionid=4FDE28AFD3935DA790D2020C9A25DB4D.smart2?sequence=1

[9] Mikael S. Magnusson, S. Ostlund, "*Numerical evaluation of interfibre joint strength measurements in terms of three-dimensional resultant forces and moments*", Cellulose (2013) 20:1691–1710, BiMaC Innovation, Department of Solid Mechanics, KTH Royal Institute of Technology, Sweden, Published online: 25 May 2013

[10] K. Hofstetter, E. Kristofer Gamstedt, "*Hierarchical modelling of microstructural effects on mechanical properties of wood. A review*", Holzforschung, Vol. 63, pp. 130–138, 2009 Copyright by Walter de Gruyter ,Berlin ,New York. DOI 10.1515/HF.2009.018

[11] P. Saketi, "*Microrobotics Platform for Manipulation and Flexibility Measurement of Individual Paper Fibers*", Master of Science Thesis, Tampere University of Technology master`s degree program in Machine Automation, January 2010, Total pages 81

[12] N. Chaillet, S. Regnier, "*Microrobotics for Micromanipulation*", June 2010, Wiley-ISTE, Total pages: 512, Foreword and Intro

[13] S. Fatikow, U. Rembold, "*Microsystem Technology and Microrobotics*", March 20 1997, Springer, 408 pages, pp 1-10

[14] K. Kim, X. Liu, Y. Zhang, Y. Sun, "*Nanonewton force-controlled manipulation of biological cells using a monolithic MEMS microgripper with two-axis force feedback*", Journal of Micromechanics and Microengineering 18 (2008) 055013 (8pp), IOP Publishing Ltd, Published 1 April 2008, University of Toronto

[15] Sakaki K., Dechev, Burke, Park, "*Development of a five degree of freedom biomanipulator for autonomous single cell electroporation*", Intelligent Robots and Systems, 2007. IROS 2007. IEEE/RSJ International Conference on Oct. 29 2007-Nov. 2 2007, Page(s): 3137 - 3143

[16] H. Matsuoka, T. Komazaki, Y. Mukai, M. Shibusawa, H. Akane, A. Chaki, N. Uetake, M. Saito, "*High throughput easy injection with a single-cell manipulation supporting robot*", Journal of Biotechnology, Elsevier, 16 March 2005, Volume 116, Issue 2, Pages 185–194, Retrieved from http://www.sciencedirect.com/science/article/pii/S016816560400519X

[17] F. Krohs, S. Hagemann, S. Fatikow, "*Automated cell characterization by a nanohandling robot station*", Published in Control & Automation, 2007. MED '07. Mediterranean Conference , University of Oldenburg

[18] Wang W, Liu X, Gelinas D, Ciruna B, Sun Y (2007),“ *A Fully Automated Robotic System for Microinjection of Zebrafish Embryos*”. PLoS ONE 2(9): e862. doi:10.1371/journal.pone.0000862

[19] Retrieved from http://www.tut.fi/en/about-tut/departments/automation-science-and-engineering/research/projects/powerbonds/index.htm

[20] Retrieved from http://www.tut.fi/en/about-tut/departments/automation-science-and-engineering/research/projects/fibam/index.htm

[21] D.H. Page, R.S. Seth, B.D. Jordan and M.C. Barbe, “*Curls, crimps, kinks and microcompressions in pulp fibres – their origin, measurement and significance*”. In Papermaking Raw Materials, Trans. VIIIth Fund. Res. Symp. Oxford, 1985, (V. Punton, ed.), *pp* 183–227, FRC, Manchester, 2003. ISBN: 0 9541126 8 7.

[22] Wolfgang J. Fischer, U. Hirn, W. Bauer and R. Schennach, “*Testing of individual fiber-fiber joints under biaxial load and simultaneous analysis of deformation*”. Nordic Pulp and Paper Research Journal Vol. 27 no.2/2012, Pages 237-244

[23] Gurnagul, N., Ju, S. & Page, D. S. “*Fibre-fibre bond strength of once-dried pulps. J. Pulp Paper Science*”.), Journal of Pulp and Paper Science (Impact Factor: 0.68). 03/2001; 27(3):88

[24] Kappel, L., Hirn, U., Bauer, W. and Schennach, R. (2009), “*A novel method for the determination of bonded area of individual fiber-fiber bonds*”. Nord. Pulp Paper Res. J. 24(2), 199

[25] Burgert, I. Frühmann, K., Keckes, J., Fratzl, P. and Stanzl-Tschegg, S.E. (2003), “*Microtensile Testing of Wood Fibers Combined with Video Extensometry for Efficient Strain Detection*”, Holzforschung, 57, 661.

[26] C. H. Mayhood, JR., O. J. Kallmes, and M. M. Cauley, “*The Mechanical Properties of Paper – Part II: Measured Shear Strength of Individual Fiber to Fiber contacts*”, Tappi J. 45(1):69-73 (1962)

[27] Mikael S. Magnusson and Sören Östlund, “*Inter-Fibre Bond Strength and Combined Normal and Shear Loading*”. 2011, BiMaC Innovation, Department of Solid Mechanics KTH, Royal Institute of Technology, Sweden, Available at http://www.diva-portal.org/smash/get/diva2:600406/FULLTEXT01.pdf

[28] Alan F. Button, "*Fiber-Fiber Bond Strength: A study of a linear elastic model structure*". Doctoral Dissertation, Publication Rights Reserved by the Institute of Paper Chemistry, June 1979, Total pages 235.

[29] Retrieved from http://www.oxforddictionaries.com/definition/english/wood

[30] Kaarlo Niskanen, "*Paper Physics",* 1998, Finland, Published by Fapet Oy, pp. 14-89

[31] McIntosh, "*Tensile and Bonding strengths of loblolly pine kraft fibers cooked to different yields*". Tappi, 1963. 46(5): p. 273-277.

[32] McIntosh, B. Leopold, "*Bonding Strength of Individual fibres*". 1962, BPBMA: London. p. 265-276.

[33] Thorpe, J.L., et al., "*Mechanical-Properties of Fiber Bonds"*. Tappi, 1976. 59(5): p. 96-100.

[34] Available at http://treescharlotte.org/wp-content/uploads/2013/11/How-A-Tree-Works.pdf

[35] Kellomaki S. Ed., "*Forest resources and sustainable management*". Fapet Oy, Helsinki, Finland 1998, pp.21 and 121.

[36] Christopher J. Biermann, "*Handbook of Pulping and Papermaking*". Second Edition, 1996, Pages 158–189.

[37] A. Vehniäinen, "*Single fiber properties – a key to the characteristic defibration patterns from wood to paper fibers*". Dissertation for the degree of Doctor of Science in Technology, Department of Forest Products Technology, Helsinki, University of Technology, October 17 2008, ISSN 1457-6252, Pages; 14-19, Available at http://www.ce.berkeley.edu/~paulmont/CE60New/wood.pdf

[38] Paulo Monteiro, "wood", The University of California Berkeley, Available at http://www.ce.berkeley.edu/~paulmont/CE60New/wood.pdf

[39] Gullichsen J., Fogelholm C.-J. Ed, "*Papermaking and Technology*", Book 6A and 6B, "Chemical pulping". ISBN: 952-5216-00-4, Fapet Oy, Helsinki, Finland 1999, pp A.22.

[40] Lorraine C. Vander Wielen, "*The Structure and Physical Properties of Pulpwood Fibers*", Ph.D. thesis, Available at http://ipst.gatech.edu/faculty/ragauskas_art/technical_reviews/Proerties%20of%20Pulpwood%20Fibers.pdf

[41] J. D. Mauseth, "*Botany-An Introduction to Plant Biology-3rd Edition*", ISBN: 0763721344, Jones and Bartlett Publishers Inc., 2003

[42] Retrieved from; School of Biological Sciences, University of Edinburgh Website, "http://www.biology.ed.ac.uk/research/groups/jdeacon/FungalBiology/woodrots.htm"

[43] Micky Rakotondrabe, Yassine Haddab, C´edric Cl´evy, Philippe Lutz, "*Automation of Assembly and Packaging at the Micro/Nano-scale"*. 2011, Conference on Automation Science and Engineering Trieste, Italy - August 24-27, 2011, Pages; 3-4

[44] Pooya Saketi, Pasi Kallio, "Microrobotic Platform for Manipulation and Mechanical Characterization of Individual Paper Fibers", Published; Intelligent Robots and Systems (IROS), 2010 IEEE/RSJ International Conference

[45] P. Saketi, M. Von Essen, M. Mikczinski, S. Heinemann, S. Fatikow, P. Kallio. "*A flexible microrobotic platform for handling microscale specimens of fibrous materials for microscopic studies*". Journal of Microscopy, 248 (2):163–171, 2012.

[46] Saketi, P. & Kallio, P. "*Microrobotic platform for making, manipulating and breaking individual paper fiber bonds"*. Assembly and Manufacturing (ISAM), 2011 IEEE International Symposium on (2011) 1–6.

[47] P. Saketi and P. Kallio. "*Measuring bond strengths of individual paper fibers using microrobotics*". In Progress in Paper Physics Seminar, pages 199–203, Sep. 5 - 8 2011b.

[48] P. Saketi, M. Mikczinski, S. Fatikow, P. Kallio, "*Method for investigation of aged fibre-fibre bonds with micro and nanorobotic tools*". The 15th Pulp and Paper Fundamental Research Symposium. 1 (2013) 125-142.

[49] P. Saketi, S. Kourosh Latifi, J. Hirvonen, S. Rajala, A. Vehkaoja, T. Salpavaara, J. Lekkala, P. Kallio, "*Bending PVDF Film Microforce Sensor for Z-directional Paper Fiber Bond Strenght Measurement*". 2014, Submitted for publication.

[50] Retrieved from http://www.me.unlv.edu/Undergraduate/coursenotes/meg497/ABETdefinition.htm

[51] Seyyed Khandani, "*Engineering Design Process*", August 2005, Available at http://www.saylor.org/site/wp-content/uploads/2012/09/ME101-4.1-Engineering-Design-Process.pdf

[52] J. Hirtz, Robert B. Stone, Daniel A. McAdams, S. Szykman, Kristin L. Wood, "*A Functional Basis for Engineering Design: Reconciling and Evolving Previous Efforts*". National Institute of Standards and Technology (NIST) Technical Note 1447, Available at http://www.mel.nist.gov/msidlibrary/doc/szykman_RED.pdf

[53] Jiabin Wang, Geraint W. Jewel1, David Howe, "*A Novel Spherical Actuator: Design and Control*". IEEE Transactions on magnetics, Vol.33, No. 5, September 1997. Pages; 4209-4211, Available at http://eprints.whiterose.ac.uk/854/1/wangjb17.pdf?origin=publication_detail

[54] David Martíiinez Muñnoz, "*Spherical machines:a literature review*". Department of Industrial Electrical Engineering and Automation Lund University, CODEN: LUTEDX/ (TEIE-7208)/1-14/ (2005), Available at http://www.iea.lth.se/publications/Reports/LTH-IEA-7208.pdf

[55] Liang Yan, I-Ming Chen, Chee Kian Lim, Guilin Yang, Wei Lin, Kok-Meng Lee, "*Design, Modelling and Experiments of 3-DOF Electromagnetic Spherical Actuators*". 2011, Springer, ISBN 978-94-007-1646-9 Pages; 5-17

[56] Ohmi Fuchiwaki, Akira Ito, Daigo Misaki, Hisayuki Aoyama, "*Multi-axial Micromanipulation Organized by Versatile Micro Robots and Micro Tweezers*". 2008 IEEE International Conference on Robotics and Automation Pasadena, CA, USA, May 19-23, 2008, Pages; 893-898

[57] Retrieved from http://smaract.de

[58] Retrieved from http://www.nanotechnik.com

[59] Retrieved from http://www.attocube.com/

[60] Retrieved from http://www.micronixusa.com

[61] P.I. Corke, "*Robotics, Vision & Control*", Springer 2011, ISBN 978-3-642-20143-1.

[62] Hyunchang Kim, Myeonghyeon Kim, Daegab Gweon, "*Design of a New Type Multi Degree of Freedom Spherical Actuator*". Available at http://www.aspe.net/publications/Short%20Abstracts%2013A/3797.pdf

[63] Mathias von Essen, Juha Hirvonen, Seppo Kuikka, Pasi Kallio, *"Robotic software frameworks and software component models in the development of automated handling of individual natural fibers,"* Accepted: 4 June 2014, Springer-Verlag Berlin Heidelberg, J Micro-Bio Robot, DOI 10.1007/s12213-014-0078-8

A.APPENDIX- COMPARISION WITH IDEAL VALUES

Comparison of ideal system with the real system in measurement 1 at X-axis.

		Measured(µm)	Simulated(µm)				
Measured(mm)	Simulated(mm)	Distance of one step	Distance of one step	Angle Change (deg)	Measured Displacement (µm)	Simulated Displacement(µm)	Error Displacement(µm)
1,189	62,7						
1,188	62,7	1	0	-15 to -14	1	0	1
1,184	62,7	4	0	-15 to -13	5	0	5
1,18	62,7	4	0	-15 to -12	9	0	9
1,178	62,7	2	0	-15 to -11	11	0	11
1,178	62,7	0	0	-15 to -10	11	0	11
1,172	62,7	6	0	-15 to -9	17	0	17
1,166	62,7	6	0	-15 to -8	23	0	23
1,163	62,7	3	0	-15 to -7	26	0	26
1,157	62,7	6	0	-15 to -6	32	0	32
1,159	62,7	-2	0	-15 to -5	30	0	30
1,157	62,7	2	0	-15 to -4	32	0	32
1,148	62,7	9	0	-15 to -3	41	0	41
1,145	62,7	3	0	-15 to -2	44	0	44
1,147	62,7	-2	0	-15 to -1	42	0	42
1,138	62,7	9	0	-15 to 0	51	0	51
1,134	62,7	4	0	-15 to 1	55	0	55
1,134	62,7	0	0	-15 to 2	55	0	55
1,133	62,7	1	0	-15 to 3	56	0	56
1,127	62,7	6	0	-15 to 4	62	0	62
1,122	62,7	5	0	-15 to 5	67	0	67
1,117	62,7	5	0	-15 to 6	72	0	72
1,113	62,7	4	0	-15 to 7	76	0	76
1,106	62,7	7	0	-15 to 8	83	0	83
1,101	62,7	5	0	-15 to 9	88	0	88
1,098	62,7	3	0	-15 to 10	91	0	91
1,097	62,7	1	0	-15 to 11	92	0	92
1,094	62,7	3	0	-15 to 12	95	0	95
1,09	62,7	4	0	-15 to 13	99	0	99
1,082	62,7	8	0	-15 to 14	107	0	107
1,082	62,7	0	0	-15 to 15	107	0	107
	Average step-Measured	3,566666667				Average error	52,66666667
	Average step-Simulated		0			Max error	107

Comparison of ideal system with the real system in measurement 1 at Y-axis.

Measured(mm)	Simulated(mm)	Measured(µm)	Simulated(µm)						
		Distance of one step	Distance of one step	Angle Change (deg)	Measured Displacement (µm)	Simulated Displacement(µm)	Error Displacement(µm)	Absolute error
2,838	60,1		0	-15 to -14	0	0	0	0
2,838	60,1	0	0	-15 to -13	0	0	0	0
2,838	60,1	0	0	-15 to -12	0	0	0	0
2,838	60,1	0	0	-15 to -11	0	0	0	0
2,839	60,1	-1	0	-15 to -10	-1	0	-1	1
2,838	60,1	1	0	-15 to -9	0	0	0	0
2,838	60,1	0	0	-15 to -8	0	0	0	0
2,838	60,1	0	0	-15 to -7	0	0	0	0
2,838	60,1	0	0	-15 to -6	0	0	0	0
2,838	60,1	0	0	-15 to -5	0	0	0	0
2,839	60,1	-1	0	-15 to -4	-1	0	-1	1
2,838	60,1	1	0	-15 to -3	0	0	0	0
2,838	60,1	0	0	-15 to -2	0	0	0	0
2,84	60,1	-2	0	-15 to -1	-2	0	-2	2
2,838	60,1	2	0	-15 to 0	0	0	0	0
2,837	60,1	1	0	-15 to 1	1	0	1	1
2,838	60,1	-1	0	-15 to 2	0	0	0	0
2,838	60,1	0	0	-15 to 3	0	0	0	0
2,838	60,1	0	0	-15 to 4	0	0	0	0
2,838	60,1	0	0	-15 to 5	0	0	0	0
2,837	60,1	1	0	-15 to 6	1	0	1	1
2,837	60,1	0	0	-15 to 7	1	0	1	1
2,837	60,1	0	0	-15 to 8	1	0	1	1
2,838	60,1	-1	0	-15 to 9	0	0	0	0
2,837	60,1	1	0	-15 to 10	1	0	1	1
2,837	60,1	0	0	-15 to 11	1	0	1	1
2,838	60,1	-1	0	-15 to 12	0	0	0	0
2,837	60,1	1	0	-15 to 13	1	0	1	1
2,837	60,1	0	0	-15 to 14	1	0	1	1
2,837	60,1	0	0	-15 to 15	1	0	1	1
Average step-Measured		0,034482759					Average error	0,433333333
Average step-Simulated			0				Max Error	2

Comparison of ideal system with the real system in measurement 1 at Z-axis.

		Measured(µm)	Simulated(µm)				
Measured(mm)	Simulated(mm)	Distance of one step	Distance of one step	Angle Change (deg)	Measured Displacement (µm)	Simulated Displacement(µm)	Error Displacement(µm)
-11,376	-50						
-11,362	-50	-14	0	-15 to -14	14	0	14
-11,362	-50	0	0	-15 to -13	14	0	14
-11,365	-50	3	0	-15 to -12	11	0	11
-11,357	-50	-8	0	-15 to -11	19	0	19
-11,345	-50	-12	0	-15 to -10	31	0	31
-11,357	-50	12	0	-15 to -9	19	0	19
-11,337	-50	-20	0	-15 to -8	39	0	39
-11,345	-50	8	0	-15 to -7	31	0	31
-11,341	-50	-4	0	-15 to -6	35	0	35
-11,333	-50	-8	0	-15 to -5	43	0	43
-11,326	-50	-7	0	-15 to -4	50	0	50
-11,33	-50	4	0	-15 to -3	46	0	46
-11,334	-50	4	0	-15 to -2	42	0	42
-11,308	-50	-26	0	-15 to -1	68	0	68
-11,32	-50	12	0	-15 to 0	56	0	56
-11,328	-50	8	0	-15 to 1	48	0	48
-11,321	-50	-7	0	-15 to 2	55	0	55
-11,314	-50	-7	0	-15 to 3	62	0	62
-11,314	-50	0	0	-15 to 4	62	0	62
-11,306	-50	-8	0	-15 to 5	70	0	70
-11,316	-50	10	0	-15 to 6	60	0	60
-11,317	-50	1	0	-15 to 7	59	0	59
-11,317	-50	0	0	-15 to 8	59	0	59
-11,298	-50	-19	0	-15 to 9	78	0	78
-11,31	-50	12	0	-15 to 10	66	0	66
-11,308	-50	-2	0	-15 to 11	68	0	68
-11,302	-50	-6	0	-15 to 12	74	0	74
-11,31	-50	8	0	-15 to 13	66	0	66
-11,303	-50	-7	0	-15 to 14	73	0	73
-11,304	-50	1	0	-15 to 15	72	0	72
	Average step-Measured	-2,4				Average error	49,66666667
Average step-Simulated			0			Max Error	78

Comparison of ideal system with the real system in measurement 2 at X-axis.

		Measured(µm)	Simulated(µm)					
Measured(mm)	Simulated(mm)	Distance of one step	Distance of one step	Angle Change (deg)	Measured Displacement (µm)	Simulated Displacement(µm)	Error Displacement(µm)
1,132	62,7						
1,138	62,7	-6	0	-2 to -1,5	6	0	6
1,139	62,7	-1	0	-2 to -1	7	0	7
1,142	62,7	-3	0	-2 to -0,5	10	0	10
1,14	62,7	2	0	-2 to -0	8	0	8
1,144	62,7	-4	0	-2 to 0,5	12	0	12
1,141	62,7	3	0	-2 to 1	9	0	9
1,143	62,7	-2	0	-2 to 1,5	11	0	11
1,147	62,7	-4	0	-2 to 2	15	0	15
	Average step-Measured	-1,875				Average error	9,75
Average step-Simulated			0			Max Error	15

Comparison of ideal system with the real system in measurement 2 at Y-axis.

Measured(mm)	Simulated(mm)	Measured(µm)	Simulated(µm)							
2,767	60,0634	Distance of one step	Distance of one step	Angle Change (deg)	Measured Displacement (µm)	Simulated Displacement(µm)	Error Displacement(µm)	Error absolute		
2,796	60,0794	-29	-16	-2 to -1.5	29	16	13	13		
2,819	60,0908	-23	-11,4	-2 to -1	52	27,4	24,6	24,6		
2,839	60,0977	-20	-6,9	-2 to -0.5	72	34,3	37,7	37,7		
2,854	60,1	-15	-2,3	-2 to -0	87	36,6	50,4	50,4		
2,864	60,0977	-10	2,3	-2 to 0.5	97	34,3	62,7	62,7		
2,868	60,0908	-4	6,9	-2 to 1	101	27,4	73,6	73,6		
2,869	60,0794	-1	11,4	-2 to 1.5	102	16	86	86		
2,864	60,0634	5	16	-2 to 2	97	0	97	97		
	Average step-Measured	-12,125				Average error	55,625			
Average step-Simulated		0				Max Error	97			

Comparison of ideal system with the real system in measurement 2 at Z-axis.

	Measured(mm)	Simulated(mm)	Measured(µm)	Simulated(µm)					
			Distance of one step	Distance of one step	Angle Change (deg)	Measured Displacement (µm)	Simulated Displacement(µm)	Error Displacement(µm)
	-12,96	-52,0975						
	-12,416	-51,5732	-544	-524,3	-2 to -1,5	544	524,3	19,7
	-11,882	-51,0489	-534	-524,3	-2 to -1	1078	1048,6	29,4
	-11,331	-50,5245	-551	-524,4	-2 to -0,5	1629	1573	56
	-10,784	-50	-547	-524,5	-2 to -0	2176	2097,5	78,5
	-10,23	-49,4755	-554	-524,5	-2 to 0,5	2730	2622	108
	-9,678	-48,9511	-552	-524,4	-2 to 1	3282	3146,4	135,6
	-9,112	-48,4268	-566	-524,3	-2 to 1,5	3848	3670,7	177,3
	-8,57	-47,9025	-542	-524,3	-2 to 2	4390	4195	195
Average step-Simulated		Average step-Measured	-548,75				Average error	99,9375
-524,375							Max Error	195

Comparison of ideal system with the real system in measurement 3 at X, Y and Z-axes.

	Measured(mm)	Simulated(mm)				
X	1,14	62,7		Measured Displacement (µm)	Simulated Displacement(µm)	Error Displacement(µm)
	1,101	62,7	Distance A to B	-39	0	-39
Y	2,84	60,1				
	2,867	60,0634	Distance A to B	-27	36,6	63,6
Z	-11,334	-50				
	-9,1	-47,9025	Distance A to B	2234	2097,5	136,5

B.APPENDIX- COMPARISION WITH MODİFİED VALUES

Comparison of modified system with the real system in measurement 1 at X-axis.

		Measured(µm)	Simulated(µm)						
Measured(mm)	Simulated(mm)	Distance of one step	Distance of one step	Angle Change (deg)	Measured Displacement (µm)	Simulated Displacement(µm)	Error Displacement(µm)	Absolute error
1,189	62,891							
1,188	62,8883	1	2,7	-15 to -14	1	2,7	-1,7	1,7
1,184	62,8855	4	2,8	-15 to -13	5	5,5	-0,5	0,5
1,18	62,8827	4	2,8	-15 to -12	9	8,3	0,7	0,7
1,178	62,8798	2	2,9	-15 to -11	11	11,2	-0,2	0,2
1,178	62,8769	0	2,9	-15 to -10	11	14,1	-3,1	3,1
1,172	62,8739	6	3	-15 to -9	17	17,1	-0,1	0,1
1,166	62,8708	6	3,1	-15 to -8	23	20,2	2,8	2,8
1,163	62,8677	3	3,1	-15 to -7	26	23,3	2,7	2,7
1,157	62,8645	6	3,2	-15 to -6	32	26,5	5,5	5,5
1,159	62,8613	-2	3,2	-15 to -5	30	29,7	0,3	0,3
1,157	62,8581	2	3,2	-15 to -4	32	32,9	-0,9	0,9
1,148	62,8547	9	3,4	-15 to -3	41	36,3	4,7	4,7
1,145	62,8514	3	3,3	-15 to -2	44	39,6	4,4	4,4
1,147	62,848	-2	3,4	-15 to -1	42	43	-1	1
1,138	62,8445	9	3,5	-15 to 0	51	46,5	4,5	4,5
1,134	62,841	4	3,5	-15 to 1	55	50	5	5
1,134	62,8375	0	3,5	-15 to 2	55	53,5	1,5	1,5
1,133	62,8339	1	3,6	-15 to 3	56	57,1	-1,1	1,1
1,127	62,8302	6	3,7	-15 to 4	62	60,8	1,2	1,2
1,122	62,8266	5	3,6	-15 to 5	67	64,4	2,6	2,6
1,117	62,8228	5	3,8	-15 to 6	72	68,2	3,8	3,8
1,113	62,8191	4	3,7	-15 to 7	76	71,9	4,1	4,1
1,106	62,8153	7	3,8	-15 to 8	83	75,7	7,3	7,3
1,101	62,8115	5	3,8	-15 to 9	88	79,5	8,5	8,5
1,098	62,8076	3	3,9	-15 to 10	91	83,4	7,6	7,6
1,097	62,8037	1	3,9	-15 to 11	92	87,3	4,7	4,7
1,094	62,7998	3	3,9	-15 to 12	95	91,2	3,8	3,8
1,09	62,7958	4	4	-15 to 13	99	95,2	3,8	3,8
1,082	62,7918	8	4	-15 to 14	107	99,2	7,8	7,8
1,082	62,7878	0	4	-15 to 15	107	103,2	3,8	3,8
	Average step-Measured	3,566666667					Average error	3,323333333
Average step-Simulated			3,44				Max Error	8,5

Comparison of modified system with the real system in measurement 1 at Y-axis.

		Measured(µm)	Simulated(µm)					
Measured(mm)	Simulated(mm)	Distance of one step	Distance of one step					
2,838	62,6838			Angle Change (deg)	Measured Displacement (µm)	Simulated Displacement(µm)	Error Displacement(µm)	Absolute error
2,838	62,6838	0	0	-15 to -14	0	0	0	0
2,838	62,6839	0	-0,1	-15 to -13	0	-0,1	0,1	0,1
2,838	62,684	0	-0,1	-15 to -12	0	-0,2	0,2	0,2
2,838	62,6841	0	-0,1	-15 to -11	0	-0,3	0,3	0,3
2,839	62,6842	-1	-0,1	-15 to -10	-1	-0,4	-0,6	0,6
2,838	62,6843	1	-0,1	-15 to -9	0	-0,5	0,5	0,5
2,838	62,6843	0	0	-15 to -8	0	-0,5	0,5	0,5
2,838	62,6844	0	-0,1	-15 to -7	0	-0,6	0,6	0,6
2,838	62,6845	0	-0,1	-15 to -6	0	-0,7	0,7	0,7
2,838	62,6846	0	-0,1	-15 to -5	0	-0,8	0,8	0,8
2,839	62,6846	-1	0	-15 to -4	-1	-0,8	-0,2	0,2
2,838	62,6847	1	-0,1	-15 to -3	0	-0,9	0,9	0,9
2,838	62,6848	0	-0,1	-15 to -2	0	-1	1	1
2,84	62,6848	-2	0	-15 to -1	-2	-1	-1	1
2,838	62,6849	2	-0,1	-15 to 0	0	-1,1	1,1	1,1
2,837	62,685	1	-0,1	-15 to 1	1	-1,2	2,2	2,2
2,838	62,685	-1	0	-15 to 2	0	-1,2	1,2	1,2
2,838	62,6851	0	-0,1	-15 to 3	0	-1,3	1,3	1,3
2,838	62,6852	0	-0,1	-15 to 4	0	-1,4	1,4	1,4
2,838	62,6852	0	0	-15 to 5	0	-1,4	1,4	1,4
2,837	62,6853	1	-0,1	-15 to 6	1	-1,5	2,5	2,5
2,837	62,6853	0	0	-15 to 7	1	-1,5	2,5	2,5
2,837	62,6854	0	-0,1	-15 to 8	1	-1,6	2,6	2,6
2,838	62,6854	-1	0	-15 to 9	0	-1,6	1,6	1,6
2,837	62,6855	1	-0,1	-15 to 10	1	-1,7	2,7	2,7
2,837	62,6855	0	0	-15 to 11	1	-1,7	2,7	2,7
2,838	62,6856	-1	-0,1	-15 to 12	0	-1,8	1,8	1,8
2,837	62,6856	1	0	-15 to 13	1	-1,8	2,8	2,8
2,837	62,6857	0	-0,1	-15 to 14	1	-1,9	2,9	2,9
2,837	62,6857	0	0	-15 to 15	1	-1,9	2,9	2,9
	Average step-Measured	0,034482759					Average error	1,366666667
	Average step-Simulated		-0,065517241				Max Error	2,9

Comparison of modified system with the real system in measurement 1 at Z-axis.

Measured(mm)	Simulated(mm)	Measured(µm) Distance of one step	Simulated(µm) Distance of one step	Angle Change (deg)	Measured Displacement (µm)	Simulated Displacement(µm)	Error Displacement(µm)	Absolute error
-11,376	-51,5131							
-11,362	-51,5097	-14	-3,4	-15 to -14	14	3,4	10,6	10,6
-11,362	-51,5063	0	-3,4	-15 to -13	14	6,8	7,2	7,2
-11,365	-51,503	3	-3,3	-15 to -12	11	10,1	0,9	0,9
-11,357	-51,4997	-8	-3,3	-15 to -11	19	13,4	5,6	5,6
-11,345	-51,4965	-12	-3,2	-15 to -10	31	16,6	14,4	14,4
-11,357	-51,4933	12	-3,2	-15 to -9	19	19,8	-0,8	0,8
-11,337	-51,4902	-20	-3,1	-15 to -8	39	22,9	16,1	16,1
-11,345	-51,4872	8	-3	-15 to -7	31	25,9	5,1	5,1
-11,341	-51,4841	-4	-3,1	-15 to -6	35	29	6	6
-11,333	-51,4812	-8	-2,9	-15 to -5	43	31,9	11,1	11,1
-11,326	-51,4783	-7	-2,9	-15 to -4	50	34,8	15,2	15,2
-11,33	-51,4755	4	-2,8	-15 to -3	46	37,6	8,4	8,4
-11,334	-51,4727	4	-2,8	-15 to -2	42	40,4	1,6	1,6
-11,308	-51,47	-26	-2,7	-15 to -1	68	43,1	24,9	24,9
-11,32	-51,4673	12	-2,7	-15 to 0	56	45,8	10,2	10,2
-11,328	-51,4647	8	-2,6	-15 to 1	48	48,4	-0,4	0,4
-11,321	-51,4622	-7	-2,5	-15 to 2	55	50,9	4,1	4,1
-11,314	-51,4597	-7	-2,5	-15 to 3	62	53,4	8,6	8,6
-11,314	-51,4573	0	-2,4	-15 to 4	62	55,8	6,2	6,2
-11,306	-51,4549	-8	-2,4	-15 to 5	70	58,2	11,8	11,8
-11,316	-51,4526	10	-2,3	-15 to 6	60	60,5	-0,5	0,5
-11,317	-51,4504	1	-2,2	-15 to 7	59	62,7	-3,7	3,7
-11,317	-51,4483	0	-2,1	-15 to 8	59	64,8	-5,8	5,8
-11,298	-51,4462	-19	-2,1	-15 to 9	78	66,9	11,1	11,1
-11,31	-51,4442	12	-2	-15 to 10	66	68,9	-2,9	2,9
-11,308	-51,4422	-2	-2	-15 to 11	68	70,9	-2,9	2,9
-11,302	-51,4403	-6	-1,9	-15 to 12	74	72,8	1,2	1,2
-11,31	-51,4385	8	-1,8	-15 to 13	66	74,6	-8,6	8,6
-11,303	-51,4368	-7	-1,7	-15 to 14	73	76,3	-3,3	3,3
-11,304	-51,4351	1	-1,7	-15 to 15	72	78	-6	6
	Average step-Measured	-2,4					Average error	7,173333333
Average step-Simulated			-2,6				Max Error	24,9

Comparison of modified system with the real system in measurement 2 at X-axis.

Measured(mm)	Simulated(mm)	Measured(µm) Distance of one step	Simulated(µm) Distance of one step	Angle Change (deg)	Measured Displacement (µm)	Simulated Displacement(µm)	Error Displacement(µm)	Absolute error
1,132	62,8361							
1,138	62,8362	-0,006	-0,0021	-3,45 to -2,95	6	2,1	3,9	3,9
1,139	62,8403	-0,001	-0,0021	-2,95 to -2,45	7	4,2	2,8	2,8
1,142	62,8424	-0,003	-0,0021	-2,45 to -1,95	10	6,3	3,7	3,7
1,14	62,8445	0,002	-0,0021	-1,95 to -1,45	8	8,4	-0,4	0,4
1,144	62,8466	-0,004	-0,0021	-1,45 to -0,95	12	10,5	1,5	1,5
1,141	62,8487	0,003	-0,0021	-0,95 to -0,45	9	12,6	-3,6	3,6
1,143	62,8508	-0,002	-0,0021	- 0,45 to 0,05	11	14,7	-3,7	3,7
1,147	62,8529	-0,004	-0,0021	0,05 to 0,55	15	16,8	-1,8	1,8
	Average step-Measured	-0,001875					Average error	2,675
Average step-Simulated			-0,0021				Max Error	3,9

Comparison of modified system with the real system in measurement 2 at Y-axis.

		Measured(µm)	Simulated(µm)					
Measured(mm)	Simulated(mm)	Distance of one step	Distance of one step	Angle Change (deg)	Measured Displacement (µm)	Simulated Displacement(µm)	Error Displacement(µm)	Error absolute
2,767	62,5982							
2,796	62,627	-29	-28,8	-3.45 to -2.95	29	28,8	0,2	0,2
2,819	62,6511	-23	-24,1	-2.95 to -2.45	52	52,9	-0,9	0,9
2,839	62,6704	-20	-19,3	-2.45 to -1.95	72	72,2	-0,2	0,2
2,854	62,6849	-15	-14,5	-1.95 to -1.45	87	86,7	0,3	0,3
2,864	62,6947	-10	-9,8	-1.45 to -0.95	97	96,5	0,5	0,5
2,868	62,6996	-4	-4,9	-0.95 to -0.45	101	101,4	-0,4	0,4
2,869	62,6998	-1	-0,2	-0.45 to 0.05	102	101,6	0,4	0,4
2,864	62,6952	5	4,6	0.05 to 0.55	97	97	0	0
	Average step-Measured	-12,125				Average error	0,3625	
Average step-Simulated			-12,125					

Comparison of modified system with the real system in measurement 2 at Z-axis.

Measured(mm)	Simulated(mm)	Measured(µm) Distance of one step	Simulated(µm) Distance of one step					
-12,96	-53,6541							
-12,416	-53,1077	-544	-546,4	-3,45 to -2,95	544	546,4	-2,4	2,4
-11,882	-52,5611	-534	-546,6	-2,95 to -2,45	1078	1093	-15	15
-11,331	-52,0143	-551	-546,8	-2,45 to -1,95	1629	1639,8	-10,8	10,8
-10,784	-51,4673	-547	-547	-1,95 to -1,45	2176	2186,8	-10,8	10,8
-10,23	-50,9202	-554	-547,1	-1,45 to -0,95	2730	2733,9	-3,9	3,9
-9,678	-50,3731	-552	-547,1	-0,95 to -0,45	3282	3281	1	1
-9,112	-49,8259	-566	-547,2	-0,45 to 0,05	3848	3828,2	19,8	19,8
-8,57	-49,2788	-542	-547,1	0,05 to 0,55	4390	4375,3	14,7	14,7
	Average step-Measured	-548,75					Average error	9,8
Average step-Simulated			-546,9125				Max Error	19,8

Comparison of modified system with the real system in measurement 3 at X, Y and Z-axes.

	Measured(mm)	Simulated(mm)				
X	1,14	62,8445				
	1,101	62,816	Distance A to B	0,039	0,0265	10,5
Y	2,84	62,6849				
	2,867	62,695	Distance A to B	-0,027	-0,0101	-16,9
Z	-11,334	-51,4673				
	-9,1	-49,2557	Distance A to B	2,234	2,2116	22,4